Fluid-structure interaction involving multiple structural layers: theory and numerics

S. Čanić   B. Muha   M. Bukač

Chapter 1

Fluid-Structure Interaction Involving Multiple Structural Layers: Theory and Numerics

S. Čanić, B. Muha, M. Bukač

Fluid-structure interaction (FSI) problems arise in many applications. They include multi-physics problems in engineering such as aeroelasticity and propeller turbines, as well as biofluidic application such as self-propulsion organisms, fluid-cell interactions, and the interaction between blood flow and cardiovascular tissue. A comprehensive study of these problems remains to be a challenge due to their strong nonlinearity and multi-physics nature. To make things worse, in many biological applications the structure is composed of several layers, each with different mechanical characteristics. This is, for example, the case with arterial walls, which are composed of three main layers: the intima, media and adventitia, separated by thin elastic laminae. A stable and efficient FSI solver that simulates the interaction between an incompressible, viscous fluid and a multi-layered structure would be an indispensable tool for the computational studies of solutions.

The multi-physics nature of this class of problems suggests the use of partitioned, modular algorithms based on an operator splitting approach that would separate the different physics in the problem. This chapter presents such a scheme, which can be used not only in computations, but also to prove existence of weak solutions to this class of problems. Particular attention will be payed to multi-physics FSI problems involving structures consisting of multiple layers.

1.1   Introduction

Fluid-structure interaction (FSI) problems arise in many applications. The widely known examples are aeroelasticity and biofluids. In aeroelasticity, where the structure (wing of an airplane) is much heavier than the fluid (air), it is sometimes of interest to study small vibrations of the structure in which case linear coupling between the fluid and the structure may be sufficient to capture the main features of the solutions. In that case the fluid domain remains fixed in the FSI model, and only the location of the structure is computed based on the fluid loading (one-way coupling). In biofluidic applications, such as the interaction between blood flow and cardiovascular tissue where the density of the structure (arterial walls) is roughly equal to the density of the fluid (blood), the coupling between the fluid and the relatively light structure is **highly nonlinear**. In that case the fluid domain is not fixed in the FSI model, and its location is determined by the location of the structure. The elastodynamics of the structure influences the motion of the fluid through the contact force exerted by the structure onto the fluid, while the structure location is computed based on the fluid loading expressed through the contact force exerted by the fluid onto the structure (two-way coupling). It has recently been shown that classical "partitioned" time-marching numerical algorithms, which are based on subsequent solutions of the fluid and structure sub-problems, are unconditionally unstable in problems in which the density of the structure and of the fluid are comparable [30]. The exchange of energy between the moving fluid and structure is so significant, that a mismatch between the energy of the discretized problem and the energy of the continuous problem causes instabilities in classical "loosely coupled" partitioned schemes. The difficulties associated with the significant energy exchange and the high geometric nonlinearity of the fluid-structure interface are reflected not only in the design of numerical schemes, but also in the theoretical studies of existence and stability of solutions to this class of problems. A comprehensive study of these problems remains to be a challenge due to their strong nonlinearity and multi-physics nature.

In the blood flow application, the problems are further exacerbated by the fact that arterial walls of major arteries are composed of several layers, each with different mechanical characteristics. The main layers are the tunica intima, media, and adventitia. They are separated by the thin elastic laminae, see Figure 1. Recent developments in ultrasound speckle tracking methods revealed significant shear strain between the different layers in high adrenaline situations [2, 41, 42]. It was noted that the consequences of this phenomenon on cardiovascular disease are yet to be explored! An example of a disease which is associated with a pathophysiology of the aortic wall layers is aortic dissection: tears in the intimal layer result in separation of the aortic wall layers causing blood to flow within the aortic wall.

Until recently, there have been no fluid-structure interaction models or computational solvers of arterial flow that take into account the multi-layered structure of arterial walls. In this chapter we take a first step in this direction by studying a benchmark problem in fluid-multi-layered-structure interaction in which the struc-
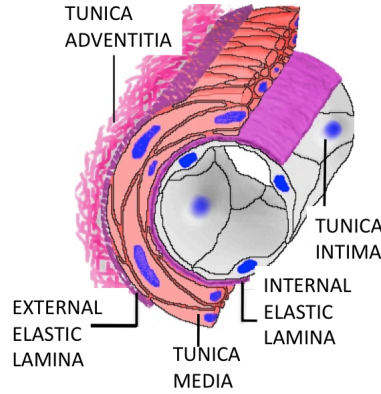
Figure 1.1: Arterial wall layers.

ture consists of two layers, a thin and a thick layer. See Figure 2. The fluid flow will be modeled by the Navier-Stokes equations for an incompressible, viscous, Newtonian fluid. This is a good approximation for blood flow in major arteries, such as the aorta or coronary arteries. The thin structural layer will be modeled by the cylindrical Koiter shell equations, and the thick structural layer will be modeled by the equations of linear elasticity. The thin structural layer located between the
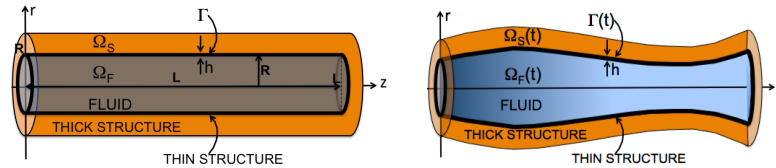
Figure 1.2: Left: Reference Domain. Right: Deformed Domain.

fluid and the thick structure, serves as a fluid-structure interface with mass. The proposed problem is a nonlinear moving-boundary problem of parabolic-hyperbolic type.

THE BENCHMARK PROBLEM

Fluid: Navier-Stokes equations for an incompressible, viscous fluid;

Thin Structure: Cylindrical Koiter shell equations;

Thick Structure: Classical equations of linear elasticity.

This is a **multi-physics problem** which constists of three different physical models: a model for fluid flow, a model describing the elastodynamics of the thin structure, and a model describing the elastodynamics of the thick structural layer. The multi-physics nature of the problem strongly suggests the use of a partitioned

algorithm that would solve the underlying coupled problem by splitting the problem into sub-problems determined by the different physics. This has the advantage of allowing modular implementations in both the numerical method development as well as in constructing the proof of existence for this class of problems. In this chapter we present a stable, convergent, modular scheme with precisely these properties, called the Kinematically-Coupled β-Scheme. This scheme was originally constructed to study fluid-structure interaction problems with a single structural layer modeled by the cylindrical Koiter shell equations in [85, 86], and then recently improved for higher accuracy in [19] (Kinematically-Coupled β-Scheme). Modifications of this scheme can be applied to a much larger class of multi-physics problems associated with FSI, such as FSI involving stent-artery-fluid interaction [123], FSI involving a multi-layered elastic porous medium [23], and FSI involving a non-Newtonian fluid [94, 95].

In this chapter we present a **general "recipe"** describing the construction of the main steps of such a scheme that can be used to:

- prove existence of weak solutions, and/or

- construct a numerical solver

to study a class of FSI problems that include:

- problems with viscoelastic and/or purely elastic structural models,

- problems with different coupling conditions (no-slip, slip),

- problems with nonlinear thin structure models,

- 2D and 3D scenarios.

An interesting new feature of the class of problems studied in this chapter is the fact that the presence of a thin fluid-structure interface with mass regularizes solutions of this class of FSI problems. More precisely, the energy estimates presented in this chapter will show that the thin structure inertia regularizes evolution of the thin structure, which affects the solution of the entire coupled FSI problem. Namely, if we were considering a problem in which the structure consisted of only one layer, modeled by the equations of linear elasticity, from the energy estimates we would not be able to conclude that the fluid-structure interface is even continuous. With the presence of a thin elastic fluid-structure interface with mass (modeled, e.g., by the linear wave equation), the energy estimates imply that the displacement of the thin interface is in $H^1(\Gamma)$, which, due to the Sobolev embeddings, implies that the interface is Hölder continuous $C^{0,1/2}(\Gamma)$. The inertia of the fluid-structure interface with mass serves as a regularizing mechanism for the entire FSI problem. It will be shown in Section 0.7 that numerical simulations confirm this behavior.

This is reminiscent of the results by Hansen and Zuazua [89] in which the presence of a point mass at the interface between two linearly elastic strings with solutions in asymmetric spaces (different regularity on each side) allowed the proof

of well-posedness due to the regularizing effects by the point mass. More precisely, they considered two elastic strings modeled by the linear wave equations, connected by a point mass, with initial data of different regularity on the left or right side of the point mass. They showed that the rough waves traveling through the point mass, which served as an interface with mass between the two elastic strings, were regularized due to the inertia effects of the point mass. See Section 0.7.7 for more details. For a reader with further interest in this area we also mention [90, 132, 143]. Further research in this direction, directly relevant to the FSI with multiple layers, is under way by the authors.

We begin by a review of models used in FSI studies to describe mechanical properties of arterial walls.

1.2 Mathematical Models of Arterial Walls

The walls of blood vessels are composed of three layers: the intima, media and adventitia. They are separated by thin elastic laminae. See Figure 1. The intima is the innermost layer and it is mainly composed of endothelial cells. The media is the middle layer and it is mainly composed of elongated smooth muscle cells, and also elastin and collagen. Most blood vessels contain smooth muscle arranged in either circular or spiral layers. The media gives rise to the majority of the vessel's viscoelastic behavior. The adventitia is the outermost layer, and it is manly composed of collagen fibrils, elastic sheets and elastic fibrils. The layers of smooth muscle and connective tissue surrounding the intima vary in thickness in different vessels.

The **aorta and major arteries** are characterized by walls that have a thick smooth muscle layer and large amounts of elastic and fibrous tissue. Because of the stiffness of the fibrous tissue, substantial amounts of energy are required to stretch the walls of an artery outward. This energy comes from the high blood pressure exerted onto the arterial walls during the systolic part of cardiac cycle, when the left ventricle of the heart contracts, and squeezes blood through the aortic valve on to the aorta. Once the artery is distended with blood, energy stored by stretching elastic fibers is released through elastic recoil. Elastic recoil takes place during the diastolic part of cardiac cycle, when the left ventricle relaxes and gets refilled by blood. During that time the elastic recoil of arteries helps propel blood to the far most parts of the cardiovascular system.

Downstream from the arteries, small vessels called **arterioles** create a high-resistance outlet for arterial blood flow. Arterioles direct distribution of blood flow to individual tissues by selectively constricting and dilating. Arteriolar diameter is regulated by both local factors, such as tissue oxygen, and by homeostatic control.

Downstream from the arterioles are **capillaries**. A leaky epithelium in the capillaries allows exchange of materials between the blood plasma, the interstitial fluid, and the cells of the body. At the distal end of the capillaries, blood flows into the venous side of the circulation and from there back to the right heart.

Depending on the types of questions one is trying to answer, and depending on the thickness of the vessel wall with respect to the diameter of the corresponding vessel, different arterial wall models can be used to describe the mechanical properties of arterial walls [72, 73, 87, 140]. Table 1 summarizes the mean diameter and wall thickness for arteries, arterioles, and capillaries [**?**].

	Artery	Arteriole	Capillary
Mean Diameter	4.0 mm	30.0 μm	8.0 μm
Mean Wall Thickness	1.0 mm	6.0 μm	0.5 μm

Table 1.1: Mean diameter and wall thickness for human vasculature.

In fluid-structure interaction studies, the coupling between blood flow and vascular tissue is so complicated that several simplifying assumptions have to be taken into account to make the computer simulations feasible. A common set of simplifying assumptions that captures only the most important physics in the description of the mechanical properties of arterial walls includes homogeneity and isotropy, capturing the average mechanical properties of arterial walls. Further simplifying assumptions that are often used in hemodynamics FSI literature are "small" displacements and "small" deformation gradients leading to the hypothesis of linear elasticity.

Depending on the relative thickness of the structure (arterial walls) with respect to the diameter of the cylindrical fluid domain (arterial lumen), different modes have been used to approximate the overall (average) mechanical behavior of arterial walls. Three-dimensional equations of elasticity have been used under the assumption that the thickness of arterial walls is comparable to the diameter of the vessel lumen, while reduced shell or membrane models have been used under the assumption that the ratio between the thickness of the vessel wall and the vessel radius is small ($\epsilon << 1$). In the latter case, most FSI hemodynamics literature assumes that only the radial component of displacement of the thin structural wall is non-negligible. Recent developments in ultrasound speckle tracking methods revealed, however, that the axial (longitudinal) component of displacement of arterial walls may be significant in certain situations. Moreover, it was revealed that there is significant axial shear strain between the different layers (the intima-media complex and the adventitia) in high adrenaline situations [41, 42, 129, 135]. It was noted that the consequences of this phenomenon on cardiovascular disease is yet to be explored. Motivated by these experimental findings, recent progress in designing a FSI solver capturing both longitudinal as well as radial displacement of a thin Koiter shell modeling arterial walls, was reported in [19, 20].

Finally, a further simplification that can be utilized in certain situations is axial symmetry of the loading exerted by the blood flow to the vessel walls in the approximately straight cylindrical sections, leading to the axially symmetric models with a potential of further reduction to 1D FSI models.

We give a brief review of these models next.

1.2.1 Elastodynamics of Thin Structures

The equations of shell theory have been derived by many authors, see [53] and the references therein. Due to variations in approach and rigor the variety of equations occurring in literature is overwhelming. Among all the equations of shell theory the Koiter shell equations appear to be the simplest consistent first approximation in the general theory of thin elastic shells, [97, 96]. In addition, they have been mathematically justified using asymptotic methods to be consistent with three-dimensional elasticity, [39]. Ciarlet and Lods showed in [39] that the Koiter shell model has the same asymptotic behavior as the three-dimensional membrane model, the bending model and the generalized membrane model in the respective regimes in which each of them holds. Motivated by these remarkable properties of the Koiter shell model, in [26, 27] Čanić et al. derived the Koiter shell equations for the cylindrical geometry with the purpose of using the equations as a model to study the mechanical behavior of arterial walls. The models in [26, 27], and a portion of the text presented in this section, were based on the derivations of the cylindrical Koiter shell equations, obtained by Tambača in [136]. The cylindrical Koiter shell equations are a generalization of several classes of models that have been used in modeling of arterial walls. They include the linear string model proposed by Quarteroni et al. in [140, 25] as a benchmark problem for testing numerical schemes for FSI in blood flow, the independent ring model [140], and the cylindrical membrane model.

In [26, 27] Čanić et al. have extended the linearly elastic cylindrical Koiter model to include the viscous effects of Kelvin-Voigt type, observed in the measurements of the mechanical properties of vessel walls, [3, 4, 11]. It was shown in [3, 4, 11] that the Kelvin-Voigt model approximates well the experimentally measured viscoelastic properties of the canine aorta and of the human femoral and carotid arteries. In [26, 27] it was shown that a reduced FSI model between the linearly elastic cylindrical Koiter shell and the flow of an incompressible, viscous fluid, approximates well the experimentally measured data presented in [3, 4, 11]. The Kelvin-Voight model was also used in [130] to model the arterial walls as a linearly viscoelastic membrane. We summarize the derivation of the **Koiter shell model** next.

The Cylindrical Koiter Shell Equations - General Framework

Consider a clamped cylindrical shell of thickness h, length L, and reference radius of the middle surface equal to R. See Figure 3. This reference configuration, which we denote by Γ, can be defined via the parameterization

$$\varphi : \omega \to \mathbb{R}^3, \quad \varphi(z, \theta) = (R\cos\theta, R\sin\theta, z)^t,$$
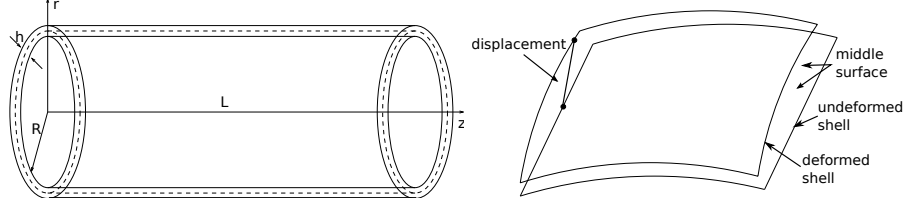
Figure 1.3: Left: Cylindrical shell in reference configuration with middle surface radius R and shell thickness h. Right: Deformed shell.

where $\omega = (0, L) \times (0, 2\pi)$ and $R > 0$. Therefore, the reference configuration is

$$\Gamma = \{\mathbf{x} = (R\cos\theta, R\sin\theta, z) \in \mathbb{R}^3 \; : \; \theta \in (0, 2\pi), z \in (0, L)\}. \qquad (1.1)$$

The associated covariant A_c and contravariant A^c metric tensors of this (non-deformed) cylinder are given by:

$$\mathbf{A}_c = \left(\begin{array}{cc} 1 & 0 \\ 0 & R^2 \end{array} \right), \; \mathbf{A}^c = \left(\begin{array}{cc} 1 & 0 \\ 0 & \frac{1}{R^2} \end{array} \right), \qquad (1.2)$$

and the area element along cylinder Γ is $dS = \sqrt{a}dy := \sqrt{\det A_c}dy = Rdy$. The corresponding curvature tensor in covariant components is given by

$$\mathbf{B}_c = \left(\begin{array}{cc} 0 & 0 \\ 0 & R \end{array} \right).$$

We define the elasticity properties of this cylindrical shell by the following elasticity tensor $\mathcal{A}$:

$$\mathcal{A}\mathbf{E} = \frac{4\lambda\mu}{\lambda + 2\mu}(\mathbf{A}^c \cdot \mathbf{E})\mathbf{A}^c + 4\mu\mathbf{A}^c\mathbf{E}\mathbf{A}^c, \quad \mathbf{E} \in \mathrm{Sym}(\mathcal{M}_2), \qquad (1.3)$$

where μ and λ are the Lamé coefficients.

Using the following relationships between the Lamé constants and the Young's modulus of elasticity E and Poisson ratio σ:

$$\frac{2\mu\lambda}{\lambda + 2\mu} + 2\mu = 4\mu\frac{\lambda + \mu}{\lambda + 2\mu} = \frac{E}{1 - \sigma^2}, \quad \frac{2\mu\lambda}{\lambda + 2\mu} = 4\mu\frac{\lambda + \mu}{\lambda + 2\mu}\frac{1}{2}\frac{\lambda}{\lambda + \mu} = \frac{E}{1 - \sigma^2}\sigma, \qquad (1.4)$$

the elasticity tensor $\mathcal{A}$ can also be written as:

$$\mathcal{A}\mathbf{E} = \frac{2E\sigma}{1 - \sigma^2}(\mathbf{A}^c \cdot \mathbf{E})\mathbf{A}^c + \frac{2E}{1 + \sigma}\mathbf{A}^c\mathbf{E}\mathbf{A}^c, \quad \mathbf{E} \in \mathrm{Sym}\left(\mathbb{R}^2\right).$$

A Koiter shell can undergo stretching of the middle surface, and flexure (bending). Namely, the Koiter shell model accounts for both the membrane effects

(stretching) and shell effects (flexure). Stretching of the middle surface is measured by the change of metric tensor, while flexure is measured by the change of curvature tensor. Consider an arbitrary displacement field $\boldsymbol{\eta} = (\eta_z, \eta_\theta, \eta_r)$ from the reference configuration Γ. Then, the corresponding change of metric, and change of curvature tensors for the deformed shell, in covariant components, are defined by:

$$\underbrace{\mathbf{G}(\boldsymbol{\eta}) = \frac{1}{2}\left(\mathbf{A}_c(\boldsymbol{\eta}) - \mathbf{A}_c\right),}_{\text{The Change of Metric Tensor}} \text{ and } \underbrace{\mathbf{R}(\boldsymbol{\eta}) = \frac{1}{2}\left(\mathbf{B}_c(\boldsymbol{\eta}) - \mathbf{B}_c\right),}_{\text{The Change of Curvature Tensor}} \tag{1.5}$$

where $\mathbf{A}_c(\boldsymbol{\eta})$ and $\mathbf{B}_c(\boldsymbol{\eta})$ are the covariant metric and curvature tensors, respectively, of the deformed shell. These will be specified below for the problem we consider in this chapter.

With the corresponding change of metric and change of curvature tensors we can now write formally the corresponding elastic energy of the deformed shell. The elastic energy of the cylindrical Koiter shell is given by [35, 36, 37, 97]:

$$E_{el}(\boldsymbol{\eta}) = \frac{h}{4}\int_\omega \mathcal{A}\mathbf{G}(\boldsymbol{\eta}) : \mathbf{G}(\boldsymbol{\eta})\sqrt{a} + \frac{h^3}{48}\int_\omega \mathcal{A}\mathbf{R}(\boldsymbol{\eta}) : \mathbf{R}(\boldsymbol{\eta})\sqrt{a}, \tag{1.6}$$

where : denotes the scalar product

$$\mathbf{A} : \mathbf{B} := \mathrm{Tr}\left(\mathbf{A}\mathbf{B}^T\right) \ \mathbf{A}, \mathbf{B} \in \mathbf{M}_2(\mathbb{R}) \cong \mathbb{R}^4. \tag{1.7}$$

Given a force with surface force density $\mathbf{f}$, the loaded shell deforms and the corresponding displacement $\boldsymbol{\eta}$ of the deformed shell is a minimizer of the energy functional [35, 36, 37, 97]:

$$\mathbf{J}(\boldsymbol{\eta}) = \frac{h}{4}\int_\omega \mathcal{A}\mathbf{G}(\boldsymbol{\eta}) : \mathbf{G}(\boldsymbol{\eta})\sqrt{a} + \frac{h^3}{48}\int_\omega \mathcal{A}\mathbf{R}(\boldsymbol{\eta}) : \mathbf{R}(\boldsymbol{\eta})\sqrt{a} - \int_\omega \mathbf{f}\cdot\boldsymbol{\eta}\sqrt{a}. \tag{1.8}$$

The corresponding weak formulation can be written as:

$$\frac{h}{2}\int_\omega \mathcal{A}\mathbf{G}(\boldsymbol{\eta}) : \mathbf{G}'(\boldsymbol{\eta})\boldsymbol{\psi}\sqrt{a} + \frac{h^3}{48}\int_\omega \mathcal{A}\mathbf{R}(\boldsymbol{\eta}) : \mathbf{R}'(\boldsymbol{\eta})\boldsymbol{\psi}\sqrt{a} = \int_\omega \mathbf{f}\cdot\boldsymbol{\psi}\sqrt{a}, \ \forall\boldsymbol{\psi} \in C_c^\infty, \tag{1.9}$$

where $\mathbf{G}'$ is the Gateux derivative of $\mathbf{G}$.

The weak formulation of the corresponding *elastodynamics problem* is given by the following:

$$\rho_K h \int_\omega \partial_t^2\boldsymbol{\eta}\boldsymbol{\psi}\sqrt{a} + \frac{h}{2}\int_\omega \mathcal{A}\mathbf{G}(\boldsymbol{\eta}) : \mathbf{G}'(\boldsymbol{\eta})\boldsymbol{\psi}\sqrt{a} + \frac{h^3}{48}\int_\omega \mathcal{A}\mathbf{R}(\boldsymbol{\eta}) : \mathbf{R}'(\boldsymbol{\eta})\boldsymbol{\psi}\sqrt{a}$$
$$= \int_\omega \mathbf{f}\cdot\boldsymbol{\psi}\sqrt{a}, \ \forall\boldsymbol{\psi} \in C_c^\infty, \tag{1.10}$$

where ρ_K and h are the Koiter shell density and thickness.

Associated with this problem are the following physical quantities:

- **Stress Resultant (Internal Force)**, which relates the internal force with the change of metric tensor, and is defined by

$$\boldsymbol{N} := \frac{h}{2}\mathcal{A}\mathbf{G}(\boldsymbol{\eta}), \tag{1.11}$$

and

- **Stress Couples (Bending Moment)**, which describe the bending moments in terms of the change of curvature tensor, and are defined by

$$\boldsymbol{M} := \frac{h^3}{24}\mathcal{A}\mathbf{R}(\boldsymbol{\eta}).$$

At this point we also introduce the effects of *prestress* by defining the stress resultant $\boldsymbol{N}_{ref}$ that relates the reference pressure p_{ref} with circumferential strain [47, 113, 114]

$$\frac{h}{2}\boldsymbol{N}_{\text{ref}} = hR\mathbf{A}^c \begin{bmatrix} 0 & 0 \\ 0 & p_{ref}\dfrac{R}{h}\eta_r \end{bmatrix} \mathbf{A}^c \tag{1.12}$$

so that the total stress resultant, including the effects of prestress, reads

- **Stress Resultant for a prestressed elastic Koiter shell**

$$\boldsymbol{N} = \frac{h}{2}\mathcal{A}\mathbf{G}(\boldsymbol{\eta}) + \frac{h}{2}\boldsymbol{N}_{ref}. \tag{1.13}$$

In what follows, we will be providing more specific details on a few concrete examples of the general framework described above.

Example1: The linearly elastic cylindrical Koiter shell with radial displacement.

We present the cylindrical Koiter shell equations *without the assumption of axial symmetry*. This means that the displacement $\boldsymbol{\eta}$ can be written as:

$$\boldsymbol{\eta}(t, z, \theta) = (\eta_z(t, z, \theta), \eta_\theta(t, z, \theta), \eta_r(t, z, \theta)).$$

However, as is common in the blood flow literature, we will be assuming that the azimuthal and longitudinal components of the displacement are negligible $\eta_\theta \approx 0, \eta_z \approx 0$, i.e., only the radial component of the displacement is different from zero, so that:

$$\boldsymbol{\eta}(t, z, \theta) = (0, 0, \eta_r(t, z, \theta),) = \eta(t, z, \theta)\mathbf{e}_r(\theta),$$

where $\mathbf{e}_r(\theta)$ is the unit vector pointing in the radial direction. Notice that this does not mean that the flow is axially symmetric, since the radial displacement is a function of both θ and z.

In this case, the corresponding *linearized* change of metric, and change of curvature tensors (5) take the following form:

$$\boldsymbol{G}(\boldsymbol{\eta}) = \begin{bmatrix} 0 & 0 \\ 0 & R\eta_r \end{bmatrix}, \quad \boldsymbol{R}(\boldsymbol{\eta}) = \begin{bmatrix} -\partial_z^2\eta & -\partial_{z\theta}^2\eta \\ -\partial_{z\theta}^2\eta & -\partial_\theta^2\eta + \eta \end{bmatrix}. \tag{1.14}$$

The elastic energy of the shell is defined by:

$$E_{el}(\eta) = \frac{h}{4}\int_\omega \mathcal{A}\boldsymbol{G}(\eta) : \boldsymbol{G}(\eta)\sqrt{a} + \frac{h^3}{48}\int_\omega \mathcal{A}\boldsymbol{R}(\eta) : \boldsymbol{R}(\eta)\sqrt{a}, \tag{1.15}$$

where η is the scalar displacement function. We will be assuming that the shell is clamped at the end points, satisfying the following boundary conditions:

$$\eta = \frac{\partial\eta}{\partial\mathbf{n}} = 0 \text{ on } \partial\omega.$$

The dynamics of the linearly elastic cylindrical Koiter shell is given by the following weak formulation: find $\eta \in H_0^2(\omega)$ such that

$$\rho_K h \int_\omega \partial_t^2\eta\psi\sqrt{a} + \frac{h}{2}\int_\omega \mathcal{A}\boldsymbol{G}(\eta) : \boldsymbol{G}(\psi)\sqrt{a} + \frac{h^3}{24}\int_\omega \mathcal{A}\boldsymbol{R}(\eta) : \boldsymbol{R}(\psi)\sqrt{a} = \int_\omega f\psi\sqrt{a} \tag{1.16}$$

for all $\psi \in H_0^2(\omega)$, where f is the radial component of the surface force density applied to the shell. Here, we have used the fact that for *linear problems*:

$$\mathbf{G}'(\eta)\psi = \mathbf{G}(\psi).$$

We define the corresponding linear elasticity operator $\mathcal{L}_{el}$:

$$\langle\mathcal{L}_{el}\eta, \psi\rangle = \frac{h}{2}\int_\omega \mathcal{A}\boldsymbol{G}(\eta) : \boldsymbol{G}(\psi)\sqrt{a} + \frac{h^3}{24}\int_\omega \mathcal{A}\boldsymbol{R}(\eta) : \boldsymbol{R}(\psi)\sqrt{a}, \ \forall\psi \in H_0^2(\omega).$$

A calculation shows that the operator $\mathcal{L}_{el}$ in differential form reads:

$$\mathcal{L}_{el}\eta = \frac{h^3\mu}{3R^4(\lambda+2\mu)}\Big((\lambda+\mu)\partial_\theta^4\eta + R^4(\lambda+\mu)\partial_z^4\eta + 2R^2(\lambda+\mu)\partial_z^2\partial_\theta^2\eta$$

$$-R^2\lambda\partial_z^2\eta - 2(\lambda+\mu)\partial_\theta^2\eta + (\lambda+\mu)\eta\Big) + \frac{4h}{R^2}\frac{(\lambda+\mu)\mu}{\lambda+2\mu}\eta.$$

By using the relationships between the Lamé constants and Young's modulus of elasticity E and Poisson ratio σ, given by (4), operator $\mathcal{L}_{el}$ can be written as:

$$\begin{aligned} \mathcal{L}_{el}\eta &= \frac{h^3E}{12R^4(1-\sigma^2)}\Big(\partial_\theta^4\eta + R^4\partial_z^4\eta + 2R^2\partial_z^2\partial_\theta^2\eta - 2\partial_\theta^2\eta + \eta\Big) \\ &+ \frac{h^3E\sigma}{6R^2(1-\sigma^2)}\partial_z^2\eta + \frac{hE}{R^2(1-\sigma^2)}\eta. \end{aligned} \tag{1.17}$$

Example 2: The axially-symmetric Koiter shell allowing both radial and longitudinal displacement.

Here, we assume that nothing in the problem depends on θ. The problem is axially symmetric, and the displacement $\boldsymbol{\eta}$ is given by

$$\boldsymbol{\eta}(t, z) = (\eta_z(r, z), \eta_r(t, z)).$$

The linearized change of metric tensor and the linearized change of curvature tensor are given, respectively by:

$$\boldsymbol{G}(\boldsymbol{\eta}) = \left[\begin{array}{cc} \partial_z \eta_z & 0 \\ 0 & R\eta_r \end{array} \right], \quad \boldsymbol{R}(\boldsymbol{\eta}) = \left[\begin{array}{cc} -\partial_{zz}\eta_r & 0 \\ 0 & \eta_r \end{array} \right]. \tag{1.18}$$

The elastic energy of the problem is given by:

$$E_{el}(\boldsymbol{\eta}) = \frac{h}{2} \int_0^L \mathcal{A}\boldsymbol{G}(\boldsymbol{\eta}) : \boldsymbol{G}(\boldsymbol{\eta}) R dz + \frac{h^3}{24} \int_0^L \mathcal{A}\boldsymbol{R}(\boldsymbol{\eta}) : \boldsymbol{R}(\boldsymbol{\eta}) R dz. \tag{1.19}$$

To define a weak formulation of the problem, introduce the following function space:

$$V_c = H_0^1(0, L) \times H_0^2(0, L) = \left\{ (\psi_z, \psi_r) \in H^1(0, L) \times H^2(0, L) : \right.$$
$$\left. \psi_z(0) = \psi_z(L) = \psi_r(0) = \psi_r(L) = 0, \partial_z \psi_r(0) = \partial_z \psi_r(L) = 0 \right\}.$$

Then the weak formulation of the linearly elastic cylindrical Koiter shell is given by the following: find $\boldsymbol{\eta} = (\eta_z, \eta_r) \in V_c$ such that

$$\frac{h}{2} \int_0^L \mathcal{A}\boldsymbol{G}(\boldsymbol{\eta}) : \boldsymbol{G}(\boldsymbol{\psi}) R dz + \frac{h^3}{24} \int_0^L \mathcal{A}\boldsymbol{R}(\boldsymbol{\eta}) : \boldsymbol{R}(\boldsymbol{\psi}) R dz = \int_0^L \boldsymbol{f} \cdot \boldsymbol{\psi} R dz, \quad \forall \boldsymbol{\psi} \in V_c, \tag{1.20}$$

Here $\boldsymbol{f}$ is the surface density of the force applied to the shell, and $\mathcal{A}$ is the elasticity tensor given by (3).

The weak formulation of the associated *elastodynamics problem* is given by:

$$\rho_K h \int_0^L \partial_t^2 \boldsymbol{\eta}\boldsymbol{\psi} R dz + \frac{h}{2} \int_0^L \mathcal{A}\boldsymbol{G}(\boldsymbol{\eta}) : \boldsymbol{G}(\boldsymbol{\psi}) R dz + \frac{h^3}{24} \int_0^L \mathcal{A}\boldsymbol{R}(\boldsymbol{\eta}) : \boldsymbol{R}(\boldsymbol{\psi}) R dz$$
$$= \int_0^L \boldsymbol{f} \cdot \boldsymbol{\psi} R dz, \quad \forall \boldsymbol{\psi} \in V_c, \tag{1.21}$$

To write the weak form explicitly in terms of displacement, we introduce a simpler notation for the spatial derivative with respect to z, and for the time derivative. Namely, in this section we will be using $'$ to denote the partial derivative with respect to z, and $\dot{}$ to denote the partial derivative with respect to time. Namely, for an arbitrary function f:

$$f' := \frac{\partial f}{\partial z}, \quad \dot{f} := \frac{\partial f}{\partial t}.$$

Using this notation, the weak formulation written explicitly in terms of the displacement now reads:

$$\rho_K h \int_0^L \ddot{\eta}_z \psi_z + \ddot{\eta}_r \psi_r$$

$$+\frac{h}{2} \int_0^L \left(\frac{4\mu\lambda}{\lambda+2\mu} \left(\eta'_z + \frac{1}{R}\eta_r \right) \cdot \left(\xi'_z + \frac{1}{R}\xi_r \right) + 4\mu \left(\eta'_z \xi'_z + \frac{1}{R^2}\eta_r\xi_r \right) \right) dz$$

$$+\frac{h^3}{24} \int_0^L \left(\frac{4\mu\lambda}{\lambda+2\mu} \left(-\eta''_r + \frac{1}{R^2}\eta_r \right) \cdot \left(-\xi''_r + \frac{1}{R^2}\xi_r \right) + 4\mu \left(\eta''_r \xi''_r + \frac{1}{R^4}\eta_r\xi_r \right) \right) dz$$

$$= \int_0^L (f_z\xi_z + f_r\xi_r)dz, \quad \forall(\xi_z, \xi_r) \in V_c.$$

By using the relationships between λ, μ and E, σ, given by (4), the weak formulation in terms of E and σ reads:

$$\rho_K h \int_0^L \ddot{\eta}_z \psi_z + \ddot{\eta}_r \psi_r$$

$$+h \int_0^L \left(\frac{E\sigma}{1-\sigma^2} \left(\eta'_z + \frac{1}{R}\eta_r \right) \left(\xi'_z + \frac{1}{R}\xi_r \right) + \frac{E}{1+\sigma} \left(\eta'_z \xi'_z + \frac{1}{R^2}\eta_r\xi_r \right) \right) dz \quad (1.22)$$

$$+\frac{h^3}{12} \int_0^L \left(\frac{E\sigma}{1-\sigma^2} \left(-\eta''_r + \frac{1}{R^2}\eta_r \right) \left(-\xi''_r + \frac{1}{R^2}\xi_r \right) + \frac{E}{1+\sigma} \left(\eta''_r \xi''_r + \frac{1}{R^4}\eta_r\xi_r \right) \right) dz$$

$$= \int_0^L (f_z\xi_z + f_r\xi_r)dz, \quad (\xi_z, \xi_r) \in V_c. \quad (1.23)$$

The terms multiplying $h/2$ account for the stored energy density due to stretching (membrane effects) and the terms multiplying $h^3/12$ account for the stored energy density due to bending (flexural shell effects). Integration by parts gives rise to the following dynamics equilibrium equations in differential form:

LINEARLY ELASTIC, AXIALLY SYMMETRIC CYLINDRICAL KOITER SHELL

$$\rho_K h \, \ddot{\eta}_z - \frac{hE}{1-\sigma^2} \left(\eta''_z + \sigma\frac{1}{R}\eta'_r \right) = f_z,$$

$$\rho_K h \, \ddot{\eta}_r + \frac{hE}{R(1-\sigma^2)} \left(\sigma\eta'_z + \frac{\eta_r}{R} \right) + \frac{h^3 E}{12(1-\sigma^2)} \left(\eta''''_r - 2\sigma\frac{1}{R^2}\eta''_r + \frac{1}{R^4}\eta_r \right) = f_r.$$

$$(1.24)$$

By ignoring the terms accounting for the bending energy (shell effects), the resulting equations representing a model for the linearly elastic, axially symmetric cylindrical Koiter membrane take the following form:

LINEARLY   ELASTIC,   AXIALLY   SYMMETRIC
CYLINDRICAL KOITER MEMBRANE

$$\rho_K h \, \ddot{\eta}_z - \frac{hE}{1-\sigma^2}\left(\eta_z'' + \sigma \frac{1}{R}\eta_r'\right) = f_z,$$
$$\rho_K h \, \ddot{\eta}_r + \frac{hE}{R(1-\sigma^2)}\left(\sigma\eta_z' + \frac{\eta_r}{R}\right) = f_r.$$

(1.25)

Example 3: A Nonlinearly Elastic, Axially Symmetric Koiter Membrane with Only Radial Displacement.

As in the previous example, we assume that nothing in the problem depends on θ. Also, for simplicity, we will be assuming that only the radial component of the displacement is different from zero, so that

$$\boldsymbol{\eta} = \boldsymbol{\eta}(t,z) = \eta \mathbf{e}_r.$$

Therefore, we consider axially symmetric deformations of a nonlinearly elastic Koiter membrane from the reference configuration Γ given by (1), with only the radial component of displacement different from zero. See Figure 4. The corresponding
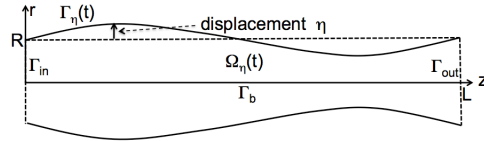
Figure 1.4: A sketch of an axially-symmetric fluid domain with radial displacement η.

change of metric tensor capturing membrane effects is given by

$$\mathbf{G}(\eta) = \frac{1}{2}\begin{pmatrix} (\partial_z\eta)^2 & 0 \\ 0 & 2R\eta + \eta^2 \end{pmatrix}.$$

(1.26)

The elastic energy of the Koiter membrane is given by the following:

$$E_{el}^{mem}(\eta) = \frac{h}{2}\int_0^L \mathcal{A}\mathbf{G}(\eta) \cdot \mathbf{G}(\eta) \; Rdz$$

(1.27)

We consider the dynamics of the Koiter membrane with fixed end points, modeled by the boundary conditions

$$\eta(0) = \eta(L) = 0.$$

Following (10), the variational formulation for the nonlinearly elastic Koiter membrane problem is given by the following:

$$\int_0^L \rho_K h \partial_t^2 \eta \xi \, Rdz + \frac{h}{2} \int_0^L \mathcal{A}\mathbf{G}(\eta) \cdot \mathbf{G}'(\eta)\xi \, Rdz = \int_0^L f\xi \, Rdz, \ \forall \xi \in H_0^2(0,L),$$
(1.28)

where $\mathbf{G}'$ is Gateux derivative of $\mathbf{G}$ given by:

$$\mathbf{G}'(\eta)\xi = \begin{pmatrix} \partial_z \eta \partial_z \xi & 0 \\ 0 & (R+\eta)\xi \end{pmatrix}.$$

This defines the following (nonlinear) differential operator $\mathcal{L}_{el}^{mem}$:

$$\langle \mathcal{L}_{el}^{mem}(\eta), \xi \rangle := \frac{h}{2} \int_0^L \mathcal{A}\mathbf{G}(\eta) \cdot \mathbf{G}'(\eta)\xi \, Rdz, \quad \forall \xi \in C_c^\infty(0,L).$$

Integration by parts yields the following formula:

$$\mathcal{L}_{el}^{mem}(\eta) = -\partial_z \Big[\Big(\frac{hE}{2(1-\nu^2)}(\partial_z\eta)^2 + \frac{hE\nu}{1-\nu^2}\Big(\frac{1}{R}\eta + \frac{1}{2R^2}\eta^2\Big)\Big)\partial_z\eta \Big]$$
$$+ \Big(\frac{hE}{1-\nu^2}\Big(\frac{1}{R}\eta + \frac{1}{2R^2}\eta^2\Big) + \frac{hE\nu}{2(1-\nu^2)}(\partial_z\eta)^2 \Big)\Big(\frac{1}{R} + \frac{1}{R^2}\eta\Big), \quad \eta \in W_0^{2,4}(0,L).$$
(1.29)

With this notation, the corresponding differential formulation of (28) can be written as:

$$\rho_K h \, \partial_t^2 \eta + \mathcal{L}_{el}^{mem}(\eta) = f.$$
(1.30)

Here, ρ_K is the structure density, h is the structure thickness, and f is the force density in the radial (vertical) $\mathbf{e}_r$ direction acting on the structure.

Example 4: A linearly viscoelastic Koiter shell

We introduce the viscoelastic effects to the linearly elastic Koiter shell by considering viscoelasticity of Kelvin-Voigt type in which the stress is linearly proportional to strain plus the time derivative of strain. For this purpose we introduce the following equivalent of the elasticity tensor $\mathcal{A}$ given by (3), which we denote by $\mathcal{B}$:

$$\mathcal{B}\mathbf{E} = \frac{4\lambda_v \mu_v}{\lambda_v + 2\mu_v}(\mathbf{A}^c \cdot \mathbf{E})\mathbf{A}^c + 4\mu_v \mathbf{A}^c \mathbf{E}\mathbf{A}^c, \quad \mathbf{E} \in \text{Sym}(\mathcal{M}_2),$$
(1.31)

where λ_v and μ_v are the viscoelastic counterparts of the Lamé constants of elasticity. Here $\mathbf{A}^c$ is the contra variant metric tensor of the reference configuration Γ, given in (2).

Given the force density $\mathbf{f}$, the displacement of the deformed *linearly viscoelastic* Koiter shell can be found by solving the following variational formulation for

$\boldsymbol{\eta}$:

$$\frac{h}{2}\int_\omega (\mathcal{A}\mathbf{G}(\boldsymbol{\eta}) + \mathcal{B}\mathbf{G}(\dot{\boldsymbol{\eta}})) : \mathbf{G}(\boldsymbol{\psi})\sqrt{a} + \frac{h^3}{48}\int_\omega (\mathcal{A}\mathbf{R}(\boldsymbol{\eta}) + \mathcal{B}\mathbf{R}(\dot{\boldsymbol{\eta}})) : \mathbf{R}(\boldsymbol{\psi})\sqrt{a}$$
$$= \int_\omega \mathbf{f} \cdot \boldsymbol{\psi}\sqrt{a}, \forall \boldsymbol{\psi} \in C_c^\infty, \tag{1.32}$$

where ρ_K and h are the Koiter shell density and thickness, respectively.

The energy of this problem is given by:

$$\begin{aligned} E(\boldsymbol{\eta}) \quad &= \frac{h}{2}\int_\omega \mathcal{A}\mathbf{G}(\boldsymbol{\eta}) : \mathbf{G}(\boldsymbol{\eta})\sqrt{a} + \frac{h^3}{48}\int_\omega \mathcal{A}\mathbf{R}(\boldsymbol{\eta}) : \mathbf{R}(\boldsymbol{\eta})\sqrt{a} \\ &+ \frac{h}{4}\frac{d}{dt}\int_\omega \mathcal{B}\mathbf{G}(\boldsymbol{\eta}) : \mathbf{G}(\boldsymbol{\eta})\sqrt{a} + \frac{h^3}{96}\frac{d}{dt}\int_\omega \mathcal{B}\mathbf{R}(\boldsymbol{\eta}) : \mathbf{R}(\boldsymbol{\eta})\sqrt{a} \\ &= E_{el}(\boldsymbol{\eta}) + \frac{1}{2}\frac{d}{dt}E_{vis}(\boldsymbol{\eta}), \end{aligned} \tag{1.33}$$

where

$$E_{el}(\boldsymbol{\eta}) = \frac{h}{2}\int_\omega \mathcal{A}\mathbf{G}(\boldsymbol{\eta}) : \mathbf{G}(\boldsymbol{\eta})\sqrt{a} + \frac{h^3}{48}\int_\omega \mathcal{A}\mathbf{R}(\boldsymbol{\eta}) : \mathbf{R}(\boldsymbol{\eta})\sqrt{a} \tag{1.34}$$

$$E_{vis}(\boldsymbol{\eta}) = \frac{h}{2}\int_\omega \mathcal{B}\mathbf{G}(\boldsymbol{\eta}) : \mathbf{G}(\boldsymbol{\eta})\sqrt{a} + \frac{h^3}{48}\int_\omega \mathcal{B}\mathbf{R}(\boldsymbol{\eta}) : \mathbf{R}(\boldsymbol{\eta})\sqrt{a} \tag{1.35}$$

The corresponding *elastodynamics problem* is given by:

$$\rho_K h\int_\omega \partial_t^2\boldsymbol{\eta}\boldsymbol{\psi}\sqrt{a} + \frac{h}{2}\int_\omega (\mathcal{A}\mathbf{G}(\boldsymbol{\eta}) + \mathcal{B}\mathbf{G}(\dot{\boldsymbol{\eta}})) : \mathbf{G}(\boldsymbol{\psi})\sqrt{a}$$
$$+ \frac{h^3}{48}\int_\omega (\mathcal{A}\mathbf{R}(\boldsymbol{\eta}) + \mathcal{B}\mathbf{R}(\dot{\boldsymbol{\eta}})) : \mathbf{R}(\boldsymbol{\psi})\sqrt{a} = \int_\omega \mathbf{f} \cdot \boldsymbol{\psi}\sqrt{a}, \forall \boldsymbol{\psi} \in C_c^\infty, \tag{1.36}$$

Introduce the following notation for the corresponding elastic and viscoelastic operators:

$$\langle \mathcal{L}_{el}\boldsymbol{\eta}, \boldsymbol{\psi}\rangle := \frac{h}{2}\int_\omega \mathcal{A}\mathbf{G}(\boldsymbol{\eta}) : \mathbf{G}(\boldsymbol{\psi})\sqrt{a} + \frac{h^3}{48}\int_\omega \mathcal{A}\mathbf{R}(\boldsymbol{\eta}) : \mathbf{R}(\boldsymbol{\psi})\sqrt{a}. \tag{1.37}$$

$$\langle \mathcal{L}_{vis}\dot{\boldsymbol{\eta}}, \boldsymbol{\psi}\rangle := \frac{h}{2}\int_\omega \mathcal{B}\mathbf{G}(\dot{\boldsymbol{\eta}}) : \mathbf{G}(\boldsymbol{\psi})\sqrt{a} + \frac{h^3}{48}\int_\omega \mathcal{B}\mathbf{R}(\dot{\boldsymbol{\eta}}) : \mathbf{R}(\boldsymbol{\psi})\sqrt{a}. \tag{1.38}$$

Then, we can write (36) as

$$\rho_K h\int_\omega \partial_t^2\boldsymbol{\eta}\boldsymbol{\psi}\sqrt{a} + \langle \mathcal{L}_{el}\boldsymbol{\eta}, \boldsymbol{\psi}\rangle + \langle \mathcal{L}_{vis}\dot{\boldsymbol{\eta}}, \boldsymbol{\psi}\rangle = \int_\omega \mathbf{f} \cdot \boldsymbol{\psi}\sqrt{a}, \forall \boldsymbol{\psi} \in C_c^\infty.$$

We now write the explicit form of these equations for the case when the structure displacement is independent on θ so that:

$$\boldsymbol{\eta}(t, z) = (\eta_z(t, z), \eta_r(t, z)),$$

and with the boundary conditions corresponding to a clamped shell

$$\eta(0) = \partial_z \eta(0) = \eta(L) = \partial_z \eta(L) = 0.$$

Therefore, to simplify the form of the explicit equations, we assume axial symmetry of the problem. In this case, we look for a weak solution which is in the space

$$V_c = H_0^1(0, L) \times H_0^2(0, L) = \left\{ (\psi_z, \psi_r) \in H^1(0, L) \times H^2(0, L) : \right.$$
$$\left. \psi_z(0) = \psi_z(L) = \psi_r(0) = \psi_r(L) = 0, \partial_z \psi_r(0) = \partial_z \psi_r(L) = 0 \right\}.$$

The corresponding weak formulation is given by (36), where we can replace the test space C_c^∞ by the space V_c. We write the differential form of the elastodynamics equations in terms of the Young's modulus of elasticity E and Poisson ratio σ, and the corresponding viscoelastic equivalents, which we denote be E_v and σ_v. The relationship between λ, μ and E, σ is given by (4). The same relationship holds between the corresponding viscoelastic constants λ_v, μ_v and E_v, σ_v.

After writing out the weak form (36), and after performing integration by parts, the corresponding dynamic equilibrium equations for the linearly viscoelastic Koiter shell in differential form are given by:

$$\rho_K h \frac{\partial^2 \eta_z}{\partial t^2} - C_2 \frac{\partial \eta_r}{\partial z} - C_3 \frac{\partial^2 \eta_z}{\partial z^2} - D_2 \frac{\partial^2 \eta_r}{\partial t \partial z} - D_3 \frac{\partial^3 \eta_z}{\partial t \partial z^2} = f_z, \quad (1.39)$$

$$\rho_K h \frac{\partial^2 \eta_r}{\partial t^2} + C_0 \eta_r - C_1 \frac{\partial^2 \eta_r}{\partial z^2} + C_2 \frac{\partial \eta_z}{\partial z} + C_4 \frac{\partial^4 \eta_r}{\partial z^4} + D_0 \frac{\partial \eta_r}{\partial t} - D_1 \frac{\partial^3 \eta_r}{\partial t \partial z^2}$$
$$+ D_2 \frac{\partial^2 \eta_z}{\partial t \partial z} + D_4 \frac{\partial^5 \eta_r}{\partial t \partial z^4} = f_r, \quad (1.40)$$

where

$$\begin{aligned}
C_0 &= \frac{hE}{R^2(1-\sigma^2)}\left(1 + \frac{h^2}{12R^2}\right), & C_1 &= \frac{h^3}{6}\frac{E\sigma}{R^2(1-\sigma^2)}, & C_2 &= \frac{h}{R}\frac{E\sigma}{1-\sigma^2}, \\
C_3 &= \frac{hE}{1-\sigma^2}, & C_4 &= \frac{h^3}{12}\frac{E}{1-\sigma^2}, & & \\
& & & & & (1.41) \\
D_0 &= \frac{h}{R^2}C_v\left(1 + \frac{h^2}{12R^2}\right), & D_1 &= \frac{h^3}{6}\frac{D_v}{R^2}, & D_2 &= \frac{hD_v}{R}, \\
D_3 &= hC_v, & D_4 &= \frac{h^3}{12}C_v,
\end{aligned}$$

and

$$C_v := \frac{E_v}{1-\sigma_v^2}, \quad D_v := \frac{E_v \sigma_v}{1-\sigma_v^2}.$$

We can write this problem using the operators $\mathcal{L}_{el}$ and $\mathcal{L}_{vis}$ as:

$$\rho_K h \frac{\partial^2 \boldsymbol{\eta}}{\partial t^2} + \mathcal{L}_{el}\boldsymbol{\eta} + \mathcal{L}_{vis}\frac{\partial \boldsymbol{\eta}}{\partial t} = \mathbf{f}, \quad (1.42)$$

where

$$\mathcal{L}_{el}\boldsymbol{\eta} = \begin{pmatrix} -C_2\dfrac{\partial \eta_r}{\partial z} - C_3\dfrac{\partial^2 \eta_z}{\partial z^2} \\[2mm] C_0\eta_r - C_1\dfrac{\partial^2 \eta_r}{\partial z^2} + C_2\dfrac{\partial \eta_z}{\partial z} + C_4\dfrac{\partial^4 \eta_r}{\partial z^4} \end{pmatrix}, \quad (1.43)$$

and

$$\mathcal{L}_{vis}\frac{\partial \boldsymbol{\eta}}{\partial t} = \begin{pmatrix} -D_2\dfrac{\partial^2 \eta_r}{\partial t \partial z} - D_3\dfrac{\partial^3 \eta_z}{\partial t \partial z^2} \\ D_0\dfrac{\partial \eta_r}{\partial t} - D_1\dfrac{\partial^3 \eta_r}{\partial t \partial z^2} + D_2\dfrac{\partial^2 \eta_z}{\partial t \partial z} + D_4\dfrac{\partial^5 \eta_r}{\partial t \partial z^4} \end{pmatrix}. \tag{1.44}$$

The typical values of the model parameters for the aorta and iliac arteries are given in Table 2

PARAMETERS	*AORTA/ILIACS*
Char. radius $R(m)$	0.006-0.012 [140]
Wall thickness $h(m)$	$1 - 2 \times 10^{-3}$[140]
Wall density $\rho_K(kg/m^3)$	1.1×10^3[140]
Young's modulus $E(Pa)$	$10^5 - 10^6$[140, 3, 11]
Wall viscosity coef. $hC_v/R(Pa \cdot s)$	$10^3 - 8 \times 10^3$[3, 4, 11]
Poisson's ratio σ	0.5

Table 1.2: Table with typical wall parameter values for the aorta and iliac arteries.

Example 5: The Linearly Elastic String Model

We present here a model which has been used by several authors to test numerical solvers for FSI in blood flow [9, 126, 8, 139, 85, 19]. This model problem was first introduced by Formaggia et al. in [71]. The structure model for this benchmark problem is of the form

$$\rho_s h\frac{\partial^2 \eta_r}{\partial t^2} - kGh\frac{\partial^2 \eta_r}{\partial z^2} + \frac{Eh}{1-\sigma^2}\frac{\eta_r}{R^2} - \gamma\frac{\partial^3 \eta_r}{\partial z^2 \partial t} = f. \tag{1.45}$$

Here $G = \frac{E}{2(1+\sigma)}$ is the *shear modulus* and k is the *Timoshenko shear correction factor*. The values of the model parameters used in [71] are given in Table 3.

PARAMETERS	*VALUES FOR MODEL PROBLEM*
Shear mod. G(dynes/cm^2)	0.25×10^6
Timoshenko factor k	1
Viscoelasticity γ (poise cm)	0.01
Radius R (cm)	0.5
Wall density ρ_s (g/cm^3)	1.1
Wall thickness h_s (cm)	0.1
Young's mod. E(dynes/cm^2)	0.75×10^6
Poisson's ratio σ	0.5

Table 1.3: Structure parameters for Example 5.

Notice that this model can be recovered from the linearly viscoelastic Koiter shell model (42) by taking the longitudinal component of displacement to be equal to zero, and by choosing the following values for the coefficients in (43), (44):

$$C_0 = \frac{Eh}{R^2(1-\sigma^2)}, \ C_1 = -kGh, \ D_2 = -\gamma,$$

with all the other coefficients equal to zero. The typical values of the parameters in this model are given in Table 3 [71]. The Young's modulus E and viscoelasticity γ are smaller than the physiological values. This means that the arterial wall in this example is rather elastic. The relatively large value of the coefficient in front of the second-order derivative with respect to z (describing bending rigidity), minimizes the oscillations that would normally appear in such structures. For the typical physiological values of these parameters see Table 2.

Example 6: The Independent Ring Model

The independent ring model has been extensively used in modeling elastic properties of arterial walls. See e.g., [140, 25], and the references therein. The model is particularly suitable to study blood flow in compliant arteries using a reduced, 1D model, studied in, e.g., [25].

The independent ring model reads

$$p - p_{ref} = \frac{hE}{R^2(1-\sigma^2)}\eta, \tag{1.46}$$

where p_{ref} is the reference pressure, i.e., the pressure at which the displacement from the reference configuration is equal to zero.

Notice that this model is included in the Koiter shell equations (182), (183). Indeed, if we ignore the longitudinal displacement and take only the terms that follow from the *membrane effects* ($\frac{h}{2}\int \mathcal{A}\mathbf{G}(\eta) : \mathbf{G}(\eta)$) we obtain exactly the Independent Ring Model:

$$f_r = C_0\eta_r = \frac{hE}{R^2(1-\sigma^2)}\eta. \tag{1.47}$$

We conclude this example by proposing a **Nonlinear Independent Ring model** consistent with the Koiter membrane theory. To obtain this model, consider the nonlinearly elastic Koiter membrane model (29), (30), which assumes axial symmetry, and only the radial component of displacement to be different from zero. By assuming, additionally, that the gradient of the radial displacement $\partial_z\eta$ is negligible, one obtains the following Nonlinear Independent Ring Model:

$$p - p_{ref} = \frac{hE}{(1-\sigma^2)R}\left(\frac{\eta}{R} + \frac{3}{2}\frac{\eta^2}{R^2} + \frac{1}{2}\frac{\eta^3}{R^3}\right). \tag{1.48}$$

For the parameter values given in Table 2, we calculated the pressure-displacement relationship for this model, which is depicted in Figure 5. This figure also shows the pressure-displacement relationship for the Linear Independent Ring model.
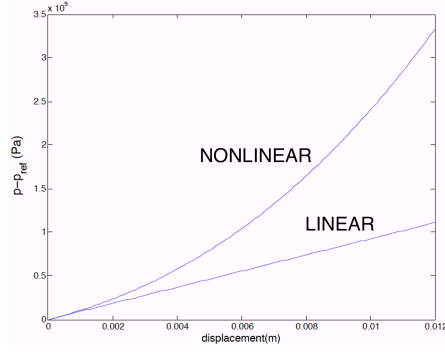
Figure 1.5: The pressure-displacement relationship for the nonlinear Independent Ring Model (48), and the linear Independent Ring Model (46).

We conclude this section by a remark on the nonlinearly elastic independent ring model of the form

$$p - p_{ref} = \frac{hE}{R(1 - \sigma^2)} \left(\left(\frac{R + \eta}{R} \right)^\beta - 1 \right), \tag{1.49}$$

which was used by certain authors to model the nonlinearly elastic properties of arterial walls. For $\beta > 1$, this model is **not** consistent with the linearly elas-
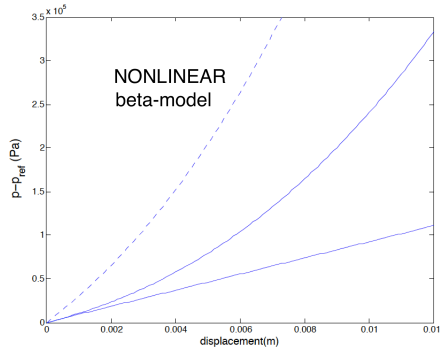
Figure 1.6: The pressure-displacement relationship for the nonlinear Independent Ring Model (49), shown in dashed line, superimposed over the plots of the linearly elastic and nonlinearly elastic Independent Ring models (46) and (48). Notice how the slope at zero for the nonlinear Independent beta-model (49) does not coincide with that of (46) and (48).

tic Independent Ring model, since its linearization does not coincide with the

linearly elastic Independent Ring model. Figure 6 shows the plot of the pressure-displacement relationship given by (49) with $\beta = 3$, for the same values of the parameter, given in Table 2 as the plot shown in Figure 5. Notice how the slope of the pressure-displacement curve for model (49), evaluated at $\eta = 0$, differs from the slope of the linearly elastic and nonlinearly elastic Independent Ring models given by (46) and (48). This means, in particular, that the leading-order coefficient modeling the stiffness of arterial walls for small displacements, is different for the β-model (49), and cannot be approximated for small displacements by the physically reasonable one stated in the linearly elastic Independent Ring model.

Example 6: A Koiter shell model with prestress

We follow the general description provided in (13) and calculate the differential form of the linearly elastic Koiter shell. The only difference with the examples presented above is in the coefficient multiplying the non-differentiated term, which will now have an extra term p_{ref}/R. Therefore, in Example 1, the linear operator $\mathcal{L}_{el}$ given by equation (17) now becomes

$$
\begin{aligned}
\mathcal{L}_{el}\eta &= \frac{h^3 E}{12R^4(1-\sigma^2)}\left(\partial_\theta^4 \eta + R^4\partial_z^4\eta + 2R^2\partial_z^2\partial_\theta^2\eta - 2\partial_\theta^2\eta + \eta\right) \\
&+ \frac{h^3 E\sigma}{6R^2(1-\sigma^2)}\partial_z^2\eta + \left(\frac{hE}{R^2(1-\sigma^2)} + \frac{p_{ref}}{R}\right)\eta.
\end{aligned}
$$

In Example 2, this gives rise to the following linearly elastic Koiter membrane equations with prestress:

$$
\begin{aligned}
\rho_K h\,\ddot\eta_z - \frac{hE}{1-\sigma^2}\left(\eta_z'' + \sigma\frac{1}{R}\eta_r'\right) &= f_z, \\
\rho_K h\,\ddot\eta_z + \frac{hE\sigma}{R(1-\sigma^2)}\eta_z' + \left(\frac{hE}{R(1-\sigma^2)} + p_{ref}\right)\frac{\eta_r}{R} &= f_r.
\end{aligned}
\tag{1.50}
$$

In Example 4, the prestress changes the constant C_0 in (41) , which now becomes

$$
C_0 = \frac{hE}{R^2(1-\sigma^2)}(1 + \frac{h^2}{12R^2}) + \frac{p_{ref}}{R}.
$$

1.2.2 Elastodynamics of Structures with Finite Thickness ("Thick Structures")

The equations modeling elastodynamics of a structure are typically given in terms of the displacement vector field $\boldsymbol{d} = \boldsymbol{d}(t, \boldsymbol{x})$. Vector field $\boldsymbol{d}$ denotes the displacement from a given reference configuration Ω_S. We will be assuming that the reference configuration of the thick structure is given by a straight cylinder of radius R, length L and thickness H. See Figure 2. The elastodynamics equations describe the second Newton's law of motion

$$
\rho_s\,\partial_{tt}\mathbf{d} = \nabla\cdot\mathbf{S} \quad \text{in } \Omega_S,\ t\in(0,T),
\tag{1.51}
$$

where ρ_s denotes density of the thick structure, and $\mathbf{S}$ is the *first Piola-Kirchhoff stress tensor*.

To close the system, we need to specify the dependence of $\mathbf{S}$ on $\boldsymbol{d}$. The relationship between $\mathbf{S}$ and $\boldsymbol{d}$ depends on the material under consideration. In this chapter will be assuming that our thick elastic structure is

- *homogeneous*, i.e., the material properties do not depend on $\boldsymbol{x}$, and

- *isotropic*, i.e., the response of the material deformation is the same in all directions.

Additionally, we will be assuming that

- *the displacement gradient* is small (i.e., $\nabla \boldsymbol{d} << 1$).

Under these assumptions, one of the simplest constitutive models for the mechanical behavior of linearly elastic structures, called the *linearized Saint-Venant Kirchhoff model*, takes the following form:

$$\mathbf{S} = \mu \left(\nabla \mathbf{d} + (\nabla \mathbf{d})^T \right) + \lambda (\nabla \cdot \mathbf{d}) \mathbf{I}, \tag{1.52}$$

Here, λ and μ are the Lamé constants, accounting the compression and distortion of the structure, respectively,

Writing a constitutive model for the behavior or elastic structures in general is a bit more involving. Arterial walls are, in fact, nonlinear. The linear approximation written above is good as long as the displacement gradient and displacement are not too large, which in the blood flow application means displacement not larger than roughly 5% of the reference radius of an artery. A typical displacement in a healthy artery under normal physiological conditions is between 5% and 10%. Thus, many physiological and pathophysiological situations can exceed the linearly elastic regime. Depending on what types of questions is one trying to answer, linear or nonlinear models may be appropriate.

A typical assumption in biomedical literature on soft tissue mechanics is that arterial walls behave as a *hyperelastic material*. This means that the relationship between stress and strain in the structure can be written as the derivative of the energy density function with respect to strain. More precisely, if we denote by

- $\boldsymbol{\Pi}$– *the second Piola-Kirchhoff stress tensor*,

- $\boldsymbol{E}$– *the Green-Lagrange strain tensor*, and

- W– *the energy density function*,

then, for a *hyperelastic material*

$$\boldsymbol{\Pi}(\boldsymbol{E}) = \frac{\partial W}{\partial \boldsymbol{E}}(\boldsymbol{E}).$$

What is the relationship between the first and second Piola-Kirchhoff stress tensors $\mathbf{S}$ and $\boldsymbol{\Pi}$, and between the Green-Lagrange strain tensor $\boldsymbol{E}$ and displacement $\boldsymbol{d}$? To explain these relationships we need to recall the notion of *deformation*. For each point $\boldsymbol{x} \in \Omega_S$ belonging to an undeformed, reference configuration

Ω_S, *deformation* is a mapping $\boldsymbol{\varphi}$ which to each point $\boldsymbol{x} \in \Omega_S$ associates a point $\boldsymbol{\varphi}(\boldsymbol{x}) = \boldsymbol{x} + \boldsymbol{d}(\boldsymbol{x})$, where $\boldsymbol{d}$ denotes the displacement of $\boldsymbol{x}$. Deformation gradient will be denoted by $\boldsymbol{F} = \nabla\boldsymbol{\varphi}$. Namely,

$$\boldsymbol{F} = \nabla\boldsymbol{\varphi} = \frac{\partial\boldsymbol{\varphi}_i}{\partial\boldsymbol{x}_j} = \boldsymbol{I} + \nabla\boldsymbol{d} = \boldsymbol{I} + \frac{\partial\boldsymbol{d}_i}{\partial\boldsymbol{x}_j}. \tag{1.53}$$

$\boldsymbol{F}$ plays a key role in specifying the relationship between the first and second Piola-Kirchhoff stress tensors, and in the relationship between strain and displacement. The first and second Piola-Kirchhoff stress tensors are related through the gradient of deformation as follows:

$$\boldsymbol{S} = \boldsymbol{F}\boldsymbol{\Pi}. \tag{1.54}$$

While the first Piola-Kirchhoff stress tensor is not generally symmetric, the second Piola-Kirchoff stress tensor is, and is, therefore, more suited for the description of physical properties of materials in terms of constitutive relations.

Constitutive relations, which specify the material properties of a structure, typically express a relationship between stress and strain, more precisely, between the second Piola-Kirchhoff stress tensor $\boldsymbol{\Pi}$ and the Green-Lagrange strain tensor $\boldsymbol{E}$:

$$\boldsymbol{\Pi} = \boldsymbol{\Pi}(\boldsymbol{E}),$$

where the Green-Lagrange strain tensor is defined via deformation gradient as

$$\boldsymbol{E} := \frac{1}{2}\left(\boldsymbol{F}^T\boldsymbol{F} - I\right). \tag{1.55}$$

A calculation shows that in terms of the displacement gradient, $\boldsymbol{E}$ is given by:

$$\boldsymbol{E} := \frac{1}{2}\left(\nabla\boldsymbol{d} + \nabla\boldsymbol{d}^T + \nabla\boldsymbol{d}\nabla\boldsymbol{d}^T\right). \tag{1.56}$$

Therefore, a general relationship between strain and displacement gradient is quadratic. For small displacement gradients, the quadratic term can be neglected, and the relationship becomes linear:

$$\boldsymbol{E} \approx \boldsymbol{\varepsilon} := \frac{1}{2}\left(\nabla\boldsymbol{d} + \nabla\boldsymbol{d}^T\right) = \boldsymbol{D}(\boldsymbol{d}), \tag{1.57}$$

where $\boldsymbol{D}$ is known as the symmetrized gradient of displacement.

Therefore, in summary, the **elastodynamics** of elastic structures is described by the second Newton's law of motion

$$\boxed{\rho_s\; \partial_{tt}\mathbf{d} = \nabla \cdot \mathbf{S}} \quad \text{in } \Omega_S \times (0, T),$$

where

- $\boldsymbol{S} = \boldsymbol{F}\boldsymbol{\Pi}$ is the first Piola-Kirchhoff stress tensor,

- $\boldsymbol{\Pi}$ is the second Piola-Kirchhoff stress tensor,
- $\boldsymbol{F} = \nabla\boldsymbol{\varphi} = I + \nabla\boldsymbol{d}$ is the deformation gradient,
- $\boldsymbol{\varphi}(\boldsymbol{x}) = \boldsymbol{x} + \boldsymbol{d}(\boldsymbol{x}), \boldsymbol{x} \in \Omega_S$ is deformation of Ω_S, and
- $\boldsymbol{d}$ is displacement from the reference configuration.

To close the system, a **constitutive relation** needs to be specified:

$$\boxed{\boldsymbol{\Pi} = \boldsymbol{\Pi}(\boldsymbol{E})},$$

where

- $\boldsymbol{E} = \frac{1}{2}\left(\boldsymbol{F}^T\boldsymbol{F} - I\right)$ is the Green-Lagrange strain tensor, also expressed as
- $\boldsymbol{E} = \frac{1}{2}\left(\nabla\boldsymbol{d} + \nabla\boldsymbol{d}^T + \nabla\boldsymbol{d}\nabla\boldsymbol{d}^T\right)$ in terms of displacement gradient.

Therefore, the elastodynamics equations in closed form can be written as

$$\rho_s\,\partial_{tt}\mathbf{d} = \nabla\cdot[(I + \nabla\boldsymbol{d})\boldsymbol{\Pi}(\underbrace{(\nabla\boldsymbol{d} + \nabla\boldsymbol{d}^T)/2 + \nabla\boldsymbol{d}\nabla\boldsymbol{d}^T/2}_{\boldsymbol{E}})],$$

where $\boldsymbol{\Pi}$ is a given function via a constitutive relation.

For *hyperelastic materials* we have

$$\boldsymbol{\Pi}(\boldsymbol{E}) = \partial W/\partial\boldsymbol{E}.$$

Examples of hyperelastic materials include:

- *The Saint-Venant Kirchhoff model* for which

$$W(\boldsymbol{E}) = \frac{\lambda}{2}[\mathrm{tr}\boldsymbol{E}]^2 + \mu[\mathrm{tr}(\boldsymbol{E}^2)], \quad \text{and so} \quad \boldsymbol{\Pi}(\boldsymbol{E}) = \lambda[\mathrm{tr}\boldsymbol{E}]I + 2\mu\boldsymbol{E}.$$

- *The linearized Saint-Venant Kirchhoff model* for which

$$\boldsymbol{E} \approx \boldsymbol{D}(\boldsymbol{d}) = (\nabla\boldsymbol{d} + \nabla\boldsymbol{d}^T)/2$$

  and so

$$\boldsymbol{\Pi} \approx \boldsymbol{\Pi}(\boldsymbol{D}(\boldsymbol{d})) = \lambda[\mathrm{tr}\boldsymbol{D}(\boldsymbol{d})]I + 2\mu\boldsymbol{D}(\boldsymbol{d}), \text{ and } \mathbf{S} \approx \mu\left(\nabla\mathbf{d} + (\nabla\mathbf{d})^T\right) + \lambda(\nabla\cdot\mathbf{d})\mathbf{I},$$

  where $\boldsymbol{D}(\boldsymbol{d})$ is the symmetrized gradient of displacement.

- *The exponential stiffening stress-strain law* of Fung [72, 73], providing a more realistic model of the mechanical properties of arterial walls, for which

$$W(\boldsymbol{E}) = C\exp(a_1 E_{\theta\theta}^2 + a_2 E_{zz}^2 + a_3 E_{\theta\theta}E_{zz}),$$

  where $E_{\theta\theta}$ and E_{zz} are strains in the circumferential direction (θ) and longitudinal direction (z), respectively, and C, a_1, a_2, a_3 are constants.

In the rest of this chapter we will be working with the linearized Saint-Venant Kirchhoff model.

1.3 The Benchmark Problem

In this section we focus on a benchmark problem in fluid-multi-layered structure interaction. The problem consists of studying FSI between an incompressible, viscous fluid, and a structure consisting of two layers: a thin layer modeled by the Koiter shell equations, and a thick layer modeled by the equations of linear elasticity. The methods presented in this chapter work for an entire class of problems in which the thin structural layer can be described by either the full cylindrical linearly elastic Koiter shell model, described in Examples 1 and 2 of Section 92, the linearly elastic membrane equations, presented in Example 2 of Section 92, the *nonlinearly* elastic Koiter membrane/shell model, described in Example 3 of Section 92, the cylindrical linearly *viscoelastic* Koiter shell model, presented in Example 4 of Section 92, or the elastic string model described in Example 5 of Section 92,

1.3.1 The Model Equations

The thin structural layer is modeled by the reduced equations of linear (visco)elasticity, discussed in Section 0.2.1, which take the general form:

$$\textbf{THIN STRUCTURE}: \quad \rho_K h \frac{\partial^2 \boldsymbol{\eta}}{\partial t^2} + \mathcal{L}_{el}(\boldsymbol{\eta}) + \mathcal{L}_{vis} \frac{\partial \boldsymbol{\eta}}{\partial t} = \boldsymbol{f}, \quad \text{on } \Gamma \times (0,T),$$

(1.58)

These equations are defined on the reference domain which is a cylinder of radius R:

$$\Gamma = \{(R\cos\theta, R\sin\theta, z) \in \mathbb{R}^3 : z \in (0,L), \ \theta \in (0, 2\pi)\}.$$

As discussed in Section 92, $\mathcal{L}_{el}$ may be a linear or a non-linear operator modeling the elastic properties of shells or membranes, and $\mathcal{L}_{visc}$ denotes a linear operator modeling their viscoelastic properties. Operator $\mathcal{L}_{vis}$ may be equal to the zero operator. The methodology presented in this chapter is robust in the sense that it can be applied to solving both the viscoelastic and purely elastic thin structure models.

The thick structural layer is modeled by the equations of linear elasticity, discussed in Section 0.2.2:

$$\textbf{THICK STRUCTURE}: \left\{ \begin{array}{rcl} \rho_s \ \partial_{tt}\mathbf{d} & = & \nabla \cdot \mathbf{S}, \quad \text{on } \Omega_S \times (0,T), \text{ where} \\ \mathbf{S} & = & \mu \ (\nabla \mathbf{d} + (\nabla \mathbf{d})^T) + \lambda(\nabla \cdot \mathbf{d})\mathbf{I}. \end{array} \right.$$

(1.59)

These equations are defined on the reference domain

$$\Omega_S = \{(x, y, z) \in \mathbb{R}^3 : z \in (0,L), \ R < \sqrt{x^2 + y^2} < R + H)\}.$$

The flow of an incompressible, viscous fluid is modeled by the Navier-Stokes equations. They are defined on a time-dependent cylindrical fluid domain $\Omega_F(t)$,

which is not known *a priori*:

$$\textbf{FLUID}: \qquad \left.\begin{array}{rcl} \rho_F(\partial_t \mathbf{u} + \mathbf{u}\cdot\nabla\mathbf{u}) & = & \nabla\cdot\boldsymbol{\sigma}, \\ \nabla\cdot\mathbf{u} & = & 0, \end{array}\right\} \text{ in } \Omega_F(t), \ t\in(0,T), \qquad (1.60)$$

where ρ_F denotes the fluid density; $\mathbf{u}$ the fluid velocity; $\boldsymbol{\sigma} = -p\mathbf{I} + 2\mu_F \mathbf{D}(\mathbf{u})$ is the fluid Cauchy stress tensor; p is the fluid pressure; μ_F is the dynamic viscosity coefficient; and $\mathbf{D}(\mathbf{u}) = \frac{1}{2}(\nabla\mathbf{u} + \nabla^\tau\mathbf{u})$ is the symmetrized gradient of $\mathbf{u}$. The typical values of the parameters ρ_F and μ_F for blood are given in Table 4.

Blood density $\rho_F(\frac{kg}{m^3})$	1.1×10^3 [140]
Blood dynamic viscosity $\mu_F(\frac{kg}{ms})$	1050 [140]

Table 1.4: Blood density and dynamics viscosity coefficients.

We will be working with the fluid equations written in Cartesian coordinates (x,y,z), while the structure equations will be written in cylindrical coordinates (r,θ,z). For any function f given in Cartesian coordinates, we define $\tilde{f}$ to be the corresponding function given in cylindrical coordinates:

$$\tilde{f}(r,\theta,z) := f(x,y,z).$$

For simplicity, in the rest of this chapter, we drop the tilde notation.
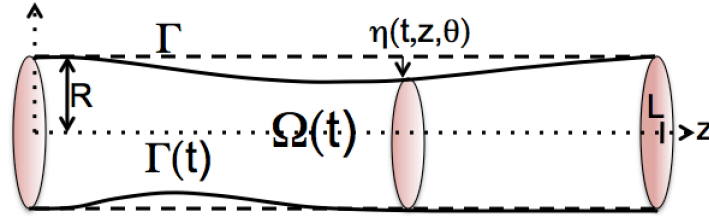
Figure 1.7: Domain sketch and notation.

The cylindrical fluid domain is of length L, with reference radius $r = R$. See Figure 7. The thin structure, described by equation (58), serves as a fluid-structure interface. The non-zero inertia term $\rho_K h \partial^2 \boldsymbol{\eta}/\partial t^2$ indicates that our fluid-structure interface has mass. This has important implications for the analysis and numerical simulation of FSI problems, discussed in Section 0.7.7.

For simplicity, in the rest of this chapter, we will be assuming that only the radial component of the displacement of the thin structure is different from zero, i.e., we will be assuming

$$\textbf{ASSUMPTION}: \qquad \boldsymbol{\eta} = (\eta_r, \eta_\theta, \eta_z) = (\eta_r, 0, 0) =: \eta\mathbf{e}_r, \qquad (1.61)$$

where $\mathbf{e}_r = \mathbf{e}_r(\theta, z)$ is the unit vector in the r-direction. This is a common assumption in the literature on FSI in blood flow. For problems with non-zero radial and longitudinal displacement $\eta_r, \eta_z \neq 0$, please see [19, 20].

The radius of the deformed domain is equal to $R + \eta(t, \theta, z)$. Thus, the fluid domain, sketched in Figure 7, is given by

$$\Omega_F(t) = \{(x, y, z) \in \mathbb{R}^3 : z \in (0, L), \ \sqrt{x^2 + y^2} < (0, R + \eta(t, \theta, z))\},$$

where the lateral boundary of the cylinder corresponds to fluid-structure interface, denoted by

$$\Gamma(t) = \{(x, y, z) \in \mathbb{R}^3 : z \in (0, L), \ \sqrt{x^2 + y^2} < (0, R + \eta(t, \theta, z))\}.$$

The inlet and outlet boundary of the fluid domain will be denoted by Γ_{in} and Γ_{out}, respectively.

1.3.2   The Coupling Conditions

Since we have three different physical models describing three different physical processes which are coupled, we need to describe the physics of the coupling between all of them. This includes prescribing coupling conditions between the fluid and structure, and prescribing coupling conditions between the thin and thick structure.

The coupling between the fluid, the thin structural layer, and the thick structural layer is achieved via two sets of coupling conditions: the kinematic coupling condition and the dynamic coupling condition. The kinematic coupling condition addresses the coupling of kinematic quantities, such as velocity. The dynamic coupling condition describes balance of forces that occurs at the interface between different physical models. These two sets of conditions give rise to a well-defined mathematical problem, while, at the same time, they capture the basic physical laws of the coupling.

In our problem, the thin structure serves both as a fluid-structure interface, and as a structure-structure interface. In this chapter we will be assuming that the kinematic coupling condition is the **no-slip** boundary condition between both the fluid and thin structure, as well as between the thin and thick structural layers.

Concerning the dynamic coupling condition, since $\Gamma(t)$ is a fluid-structure interface with mass, the dynamic coupling condition is simply the second Newton's Law of motion. It states that mass times acceleration of the interface is balanced by the sum of total forces acting on, or within, $\Gamma(t)$. This includes the contribution due to the elastic energy of the structure, and the balance of contact forces exerted by the fluid and the thick structure onto $\Gamma(t)$. More precisely, we have the following set of coupling conditions written in Lagrangian framework:

- **KINEMATIC COUPLING CONDITION:**

$$\partial_t\eta(t,\theta,z)\mathbf{e}_r(\theta,z) = \boldsymbol{u}(t,R+\eta(t,\theta,z),\theta,z), \quad \text{(continuity of velocity)}$$
$$\eta(t,\theta,z)\mathbf{e}_r(\theta,z) = \mathbf{d}(t,R,\theta,z), \qquad \text{(continuity of displacement)}$$
$$\tag{1.62}$$

  where $\mathbf{e}_r(\theta,z)$ is the unit vector in the r-direction.

- **DYNAMIC COUPLING CONDITION:**

$$\rho_K h\partial_{tt}\eta + \mathcal{L}_{el}(\eta) + \mathcal{L}_{vis}\frac{\partial\eta}{\partial t} = -J(\sigma\mathbf{n})|_{(t,R+\eta,\theta,z)}\cdot\mathbf{e}_r + R\mathbf{S}|_{(t,R,\theta,z)}\mathbf{e}_r\cdot\mathbf{e}_r. \tag{1.63}$$

  Here $J = J(t,\theta,z) = \sqrt{[1+(\partial_z\eta)^2][R+\eta]^2 + \partial_\theta\eta^2}$ denotes the Jacobian of the composit function which includes the transformation from Eulerian to Lagrangian coordinates, and the transformation from cylindrical to Cartesian coordinates; the R in front of $\mathbf{S}$ in (63) denotes the Jacobian of the transformation from cylindrical to Cartesian coordinates evaluated at $r = R$, and $\mathbf{n}$ evaluated at $(t,R+\eta,\theta,z)$ is the outward unit normal vector to the deformed fluid-structure interface $\Gamma(t)$. As before, $\eta = \eta(t,\theta,z)$, and $\mathbf{e}_r = \mathbf{e}_r(\theta,z)$ is the unit vector in the r-direction.

  If we did not have the thin structure with mass present, i.e., if we only had the fluid and thick structure interacting with each other, the dynamic coupling condition would look slightly different. The balance of contact forces at the fluid-structure interface would be given by the following:

$$-J(\sigma\mathbf{n})|_{(t,R+\eta,\theta,z)} \cdot \mathbf{e}_r + R\mathbf{S}|_{(t,R,\theta,z)}\mathbf{e}_r \cdot \mathbf{e}_r = 0, \text{ on } \Gamma \times (0,T).$$

Namely, the dynamic coupling condition in this case reads that the normal stress exerted by the fluid onto the thick structure is balanced the normal stress exerted by the thick structure onto the fluid.

1.3.3   The Boundary and Initial Conditions

To get to a well-defined mathematical problem, equations (58)-(63) need to be supplemented with initial and boundary conditions.

Fluid inlet and outlet boundary conditions: Examples of the inlet and outlet boundary conditions for the *fluid* include the following:

- *Dynamic pressure data:* In the existence proof presented later in the chapter, we will be working with the following inlet/outlet data:

$$\left.\begin{aligned} p + \frac{\rho_F}{2}|\mathbf{u}|^2 &= P_{in/out}(t), \\ \mathbf{u} &= u_z\mathbf{e}_z, \end{aligned}\right\} \quad \text{on } \Gamma_{in/out}, \tag{1.64}$$

  where $P_{in/out} \in L^2_{loc}(0,\infty)$ are given, and $\mathbf{e}_z$ is the outer unit normal to $\Gamma_{in/out}$. Therefore, the fluid flow is driven by a prescribed dynamic pressure

drop, and the flow enters and leaves the fluid domain orthogonally to the inlet and outlet boundary.

- *Normal stress data:* In the section on numerical simulations, presented later in this chapter, we will be using the following inlet/outlet data:

$$
\begin{aligned}
\boldsymbol{\sigma}\mathbf{n}|_{\Gamma_{in}} &= P_{in}(t), \\
\boldsymbol{\sigma}\mathbf{n}|_{\Gamma_{out}} &= P_{out}(T).
\end{aligned}
\tag{1.65}
$$

Structure inlet and outlet boundary conditions: Examples of the boundary conditions for the *structure* at the inlet and outlet ends of the tube include the following:

- *The thin structure data.* At the end points of the thin structure we prescribe zero displacement:

$$
\eta(t, r, \theta, 0) = \eta(t, r, \theta, L) = 0, \ r \in (0, R), \ \theta \in (0, 2\pi), t \in (0, T). \tag{1.66}
$$

If 4-th order derivative terms with respect to z appear in the model (i.e., if bending rigidity is included in the model), we consider a clamped Kotier shell with the additional boundary conditions

$$
\eta_z(t, r, \theta, 0) = \eta_z(t, r, \theta, L) = 0, \ r \in (0, R), \ \theta \in (0, 2\pi), t \in (0, T). \tag{1.67}
$$

- *The thick structure data.* At the end points of the annular sections of the thick structure we prescribe zero displacement:

$$
\mathbf{d}(t, r, \theta, 0) = \mathbf{d}(t, r, \theta, L) = 0, \quad \text{for } r \in (R, R + H), \theta \in (0, 2\pi).
$$

The external boundary condition. We will be assuming that the external boundary of the thick structure

$$
\Gamma_{ext} = \{(x, y, z) \in \mathbb{R}^3 : z \in (0, L), x^2 + y^2 = (R + H)^2\}
$$

is exposed to an external ambient pressure P_e:

$$
\mathbf{S}\mathbf{e}_r = -P_e\mathbf{e}_r, \quad \text{on } \Gamma_{ext}. \tag{1.68}
$$

Initial data. The initial fluid and structure velocities, and the initial displacements, are given by

$$
\mathbf{u}(0, .) = \mathbf{u}_0, \ \eta(0, .) = \eta_0, \ \partial_t \eta(0, .) = v_0, \ \mathbf{d}(0, .) = \mathbf{d}_0, \ \partial_t \mathbf{d}(0, .) = \mathbf{V}_0, \tag{1.69}
$$

and are assumed to belong to the following spaces: $\mathbf{u}_0 \in L^2(\Omega_F(0))$, $\eta_0 \in H_0^1(0, 1)$, $v_0 \in L^2(0, 1)$, $\boldsymbol{V}_0 \in L^2(\Omega_S)$, $\boldsymbol{d}_0 \in H^1(\Omega_S)$.

A summary of the benchmark problem. The benchmark problem in fluid-multi-layered-structure interaction that we are interested in studying is given by the following:

Find $\mathbf{u}$, p, η and $\mathbf{d}$ such that:

$$\left.\begin{array}{rcl} \rho_F \left(\partial_t \mathbf{u} + (\mathbf{u} \cdot \nabla)\mathbf{u}\right) & = & \nabla \cdot \boldsymbol{\sigma} \\ \nabla \cdot \mathbf{u} & = & 0 \end{array}\right\} \text{ in } \Omega_F(t), \ t \in (0,T),$$

$$\rho_S \partial_{tt}\mathbf{d} = \nabla \cdot \mathbf{S} \quad \text{in } \Omega_S \times (0,T),$$

$$\left.\begin{array}{l} \partial_t \eta \mathbf{e}_r = \boldsymbol{u}|_{R+\eta}, \\ \eta \mathbf{e}_r = \mathbf{d}|_R, \\ \rho_K h \partial_{tt}\eta + \mathcal{L}_{el}(\eta) + \mathcal{L}_{vis}\frac{\partial \eta}{\partial t} = -J(\sigma\mathbf{n})|_{R+\eta} \cdot \mathbf{e}_r + R\mathbf{S}|_R\mathbf{e}_r \cdot \mathbf{e}_r \end{array}\right\} \text{ on } \Gamma \times (0,T).$$

---

where $\boldsymbol{\sigma}$, $\mathbf{S}$, $\mathcal{L}_{el}$ and $\mathcal{L}_{vis}$ are defined above. In this formulation, the fluid and thick structure equations are defined in Cartesian coordinates, while the thin structure model is given in cylindrical coordinates. Furthermore, the fluid equations are given in Eulerian framework, while the structure equations are given in Lagrangian framework. To account for the different coordinates, J in the dynamic coupling condition denotes the Jacobian of the transformation from the Eulerian to the Lagrangian framework, and from Cartesian to cylindrical coordinates. Similarly, the factor R in front of the first Piola-Kirchhoff stress tensor $\mathbf{S}$ is the Jacobian of the transformation between the Cartesian and cylindrical coordinates. While the coupling conditions are calculated at the deformed interface $\Gamma(t)$, they are written in terms of the reference configuration of the fluid-structure interface, namely, they are written in terms of points on Γ.

Supplemented with initial and boundary conditions, this problem defines a nonlinear, moving boundary problem of mixed, parabolic-hyperbolic type. Hyperbolicity is associated with the thick structure problem and with the thin structure problem when no viscoelastic effects are taken into account, i.e., when $\mathcal{L}_{vis} = 0$. Parabolicity describes the properties of the fluid problem.

We will be studying this class of problems from both numerical, as well as theoretical point of view. Numerical method development for this class of problems will be presented in Section 0.7, while existence of solutions will be studied in Section 0.6. In those sections, concrete examples of this class of problems will be presented and studied. A simplified version of these equations in 2D will be presented.

1.4   FSI Literature Review

Fluid-structure interaction problems have been extensively studied for the past 20 years by many authors. The focus has been exclusively on FSI problems with structures consisting of a single material, except for the numerical simulations us-

ing the Immersted Boundary Method which is particularly suitable to deal with structures composed of fibers. The field has evolved from first studying FSI between an incompressible, viscous fluid and a rigid structure immersed in a fluid, to considering compliant (elastic/viscoelastic) structures interacting with a fluid. Concerning compliant structures, the coupling between the structure and fluid was first assumed to take place along a fixed fluid domain boundary (linear coupling). This was then extended to FSI problems in which the coupling was evaluated at a deformed fluid-structure interface, giving rise to an additional nonlinearity in the problem (nonlinear coupling).

1.4.1 Analysis Literature

Well-posedness results in which the structure was assumed to be a rigid body immersed in a fluid, or described by a finite number of modal functions, were studied in [18, 43, 48, 51, 52, 61, 74, 133]. FSI problems coupling the Navier-Stokes equations with linear elasticity where the coupling was calculated at a fixed fluid domain boundary, were considered in [55], and in [12, 13, 100] where an additional nonlinear coupling term was added at the interface. A study of well-posedness for FSI problems between an incompressible, viscous fluid and an elastic/viscoelastic structure with nonlinear coupling evaluated at a moving interface started with the result by daVeiga [17], where existence of a strong solution was obtained locally in time for an interaction between a $2D$ fluid and a $1D$ viscoelastic string, assuming periodic boundary conditions. This result was extended by Lequeurre in [109, 110], where the existence of a unique, local in time, strong solution for any data, and the existence of a global strong solution for small data, was proved in the case when the structure was modeled as a clamped viscoelastic beam. D. Coutand and S. Shkoller proved existence, locally in time, of a unique, regular solution for an interaction between a viscous, incompressible fluid in $3D$ and a $3D$ structure, immersed in the fluid, where the structure was modeled by the equations of linear [45], or quasi-linear [46] elasticity. In the case when the structure (solid) is modeled by a linear wave equation, I. Kukavica and A. Tufahha proved the existence, locally in time, of a strong solution, assuming lower regularity for the initial data [101]. A similar result for compressible flows can be found in [102]. A fluid-structure interaction between a viscous, incompressible fluid in $3D$, and $2D$ elastic shells was considered in [34, 33] where existence, locally in time, of a unique regular solution was proved. All the above mentioned existence results for strong solutions are local in time. We also mention that the works of Shkoller et al., and Kukavica at al. were obtained in the context of Lagrangian coordinates, which were used for both the structure and fluid problems.

In the context of weak solutions, the following results have been obtained. Continuous dependence of weak solutions on initial data for a fluid structure interaction problem with a free boundary type coupling condition was studied in [84]. Existence of a weak solution for a FSI problem between a $3D$ incompressible, viscous fluid and a $2D$ viscoelastic plate was considered by Chambolle et al. in

[32], while Grandmont improved this result in [78] to hold for a $2D$ elastic plate. These results were extended to a more general geometry in [103], and then to the case of generalized Newtonian fluids in [104], and to a non-Newtonian shear dependent fluid in [92, 94]. In these works existence of a weak solution was proved for as long as the elastic boundary does not touch "the bottom" (rigid) portion of the fluid domain boundary.

Muha and Čanić recently proved existence of weak solutions to a class of FSI problems modeling the flow of an incompressible, viscous, Newtonian fluid flowing through a cylinder whose lateral wall was modeled by either the linearly viscoelastic, or by the linearly elastic Koiter shell equations [119], assuming non-linear coupling at the deformed fluid-structure interface. The fluid flow boundary conditions were not periodic, but rather, the flow was driven by the dynamic pressure drop data. The methodology of proof in [119] was based on a semi-discrete, operator splitting Lie scheme which we discuss later in this chapter, and which was also used in [85] to design a stable, loosely coupled partitioned numerical scheme, called the kinematically coupled scheme (see also [19]). Ideas based on the Lie operator splitting scheme were also used by Temam in [137] to prove the existence of a solution to the nonlinear Carleman equation.

1.4.2   Numerical Simulation Literature

The development of numerical solvers for fluid-structure interaction problems has become particularly active since the 1980's. Among the most popular techniques are the Immersed Boundary Method [127, 128, 60, 70, 111, 117, 79, 80, 81, 82, 83] and the Arbitrary Lagrangian Eulerian (ALE) method [54, 93, 91, 107, 108, 140, 131]. We further mention the Fictitious Domain Method in combination with the mortar element method or ALE approach [7, 106], and the methods recently proposed for the use in the blood flow application such as the Lattice Boltzmann method [59, 62, 98, 99], the Level Set Method [44] and the Coupled Momentum Method [69].

Until recently, only monolithic algorithms seemed applicable to blood flow simulations [49, 69, 76, 125, 142, 15, 16]. These algorithms are based on solving the entire nonlinear coupled problem as one monolithic system. They are, however, generally quite expensive in terms of the computational time, programming time and memory requirements, since they require solving a sequence of strongly coupled problems using, e.g., the fixed point and Newton's methods [31, 125, 49, 64, 91, 115], or the Steklov-Poincaré based domain decomposition methods [50].

The multi-physics features of the blood flow problem strongly suggest to employ partitioned (or staggered) numerical algorithms, where the coupled fluid-structure problem is separated into a pure fluid sub-problem and a pure structure sub-problem. The fluid and structure sub-problems are integrated in time in an alternating way, and the coupling conditions are enforced asynchronously. When the density of the structure is much larger than the density of the fluid, as is the case in

aeroelasticity, it is sufficient to solve, at every time step, just one fluid sub-problem and one structure sub-problem to obtain a solution. The classical *loosely-coupled* partitioned schemes of this kind typically use the structure velocity in the **fluid sub-problem** as <u>Dirichlet</u> data for the fluid velocity (enforcing the no-slip boundary condition at the fluid-structure interface), while in the **structure sub-problem** the structure is loaded by the fluid <u>normal stress</u> calculated in the fluid sub-problem. These <u>Dirichlet-Neumann</u> loosely-coupled schemes work well for problems in which the structure is much heavier than the fluid. Unfortunately, when fluid and structure have comparable densities, which is the case in the blood flow application, the simple strategy of separating the fluid from the structure suffers from severe stability issues [30, 116]. This is because the energy of the discretized problem in Dirichlet-Neumann loosely-coupled schemes does not approximate well the energy of the continuous problem. A partial solution to this problem is to iterate several times between the fluid and structure sub-solvers at every time step until the energy of the continuous problem is well approximated. These *strongly-coupled* partitioned schemes, however, are computationally expensive and may suffer from convergence issues for certain parameter values [30].

To get around these difficulties, and to retain the main advantages of loosely-coupled partitioned schemes such as modularity, simple implementation, and low computational costs, several new loosely-coupled algorithms have been proposed recently. The method proposed in [9] uses a simple membrane model for the structure which can be easily embedded into the fluid problem where it appears as a generalized Robin boundary condition. In this way the original problem reduces to a sequence of fluid problems. A similar approach was proposed in [125] where the fluid and structure were split in the classical way, but the fluid and structure sub-problems were linked via novel transmission (coupling) conditions that improve the convergence rate. A different approach to stabilization of loosely coupled schemes was proposed in [24] where a stabilization based on Nitsche's method [88] was used. We further mention the scheme proposed in [10] where a Robin-Robin type preconditioner was combined with Krylov iterations for a solution of an interface system. For completeness, we also mention several semi-implicit FSI schemes. The schemes proposed in [65, 5, 6] separate the computation of fluid velocity from the coupled pressure-structure velocity system, thereby reducing the computational costs. Similar schemes, derived from algebraic splitting, were proposed in [8, 131]. We also mention [118] where an optimization problem was solved at each time-step to enforce the coupling conditions.

Recently, a novel loosely coupled partitioned scheme, called the "kinematically coupled β-scheme", was introduced by Bukač, Čanić et al. in [19], and applied to FSI problem with thin elastic and viscoelastic structures, modeled by the membrane or shell equations. This scheme successfully deals with stability problems associated with loosely-coupled schemes in a way different from those reported above. Stability is achieved by combining the structure inertia with the fluid sub-problem to mimic the energy balance of the continuous problem. It was shown in [29] that the scheme is unconditionally stable even for the parameters

associated with the blood flow applications. Additionally, Čanić and Muha showed that a version of this scheme with $\beta = 0$ converges to a weak solution of the fully nonlinear FSI problem [119]. This result uses energy estimates combined with compactness arguments to show that the approximate solutions converge to a weak solution of the problem as the time discretization tends to zero. This is a significant result since it proves the existence of a (weak) solution to a nonlinear FSI problem in a constructive way, by using a computational scheme to construct a solution. See [56, 57] for the related results concerning linear FSI problems.

The case $\beta = 0$ considered in [119] corresponds to the classical kinematically-coupled scheme, first introduced in [85]. Parameter β was introduced in [19] to increase the accuracy of the scheme. It was shown in [19] that the accuracy of the kinematically-coupled β-scheme with $\beta = 1$ was comparable to that of monolithic scheme by Badia, Quaini, and Quarteroni in [8] when applied to the nonlinear benchmark FSI problem in hemodynamics, introduced by Formaggia et al. in [71]. A different approach to increasing the accuracy of the classical kinematically-coupled scheme was recently proposed by Fernández et al. [66, 67, 68]. Their modified kinematically-coupled scheme, called "the incremental displacement-correction scheme" threats the structure displacement explicitly in the fluid sub-step and then corrects it in the structure sub-step. Fernández et al. showed that the accuracy of the incremental displacement-correction scheme is first-order in time. The results were obtained for a FSI problem involving a thin elastic structure.

These recent results indicate that the kinematically-coupled scheme and its modifications provide an appealing way to solve FSI problems using partitioned approach. This scheme it is particularly suitable for problems in which the structure consists of several layers, since modeling each additional layer can be accomplished by adding a new module to the partitioned scheme. Indeed, in the sections that follow, we present the kinematically coupled scheme, discuss the numerical results, and show the main steps in the proof of the existence of a weak solution to the class of fluid-multi-layered structure interaction problems discussed in Section 0.3.

1.5   Solution Framework

To study numerical simulation and existence of solutions to the class of problems (58)-(63) we present here a stable, partitioned approach that splits the fluid from the structure problem by using the Lie splitting, also known as the Marchuk-Yanenko scheme. The Lie splitting scheme has been widely used in numerical computations, see [77] and the references therein. Here we discuss an extension of this approach to study fluid-multi-layered structure interaction problems via the Kinematically-Coupled Scheme, which is based on the time-discretization via Lie splitting. The time-dependent coupled problem is discretized in time (semi-discretization) in such a way that at each time step the coupled problem is split into a fluid and a structure subproblem in a particular way so that the energy of

the discretized problem mimics the energy of the continuous problem. As we shall see later, this guarantees stability of the scheme.

1.5.1 The Energy of the Coupled Problem

We present here a general approach to deriving an energy estimate of the coupled FSI benchmark problem, described in Section 0.3, for the class of problems in which the Koiter shell is linear. Thus, we consider a *clamped linearly (visco)elastic Koiter shell* (58), coupled with the equations of linear elasticity (59), and the flow of an incompressible, viscous fluid modeled by the Navier-Stokes equations (60). The inlet and outlet data are given by the *dynamic pressure data*, specified in (64).

We first recall from Section 92 that the linear operators $\mathcal{L}_{el}$ and $\mathcal{L}_{vis}$ are defined as follows:

$$\langle \mathcal{L}_{el}\boldsymbol{\eta}, \boldsymbol{\psi} \rangle := \frac{h}{2} \int_\omega \mathcal{A}\mathbf{G}(\boldsymbol{\eta}) : \mathbf{G}(\boldsymbol{\psi})\sqrt{a} + \frac{h^3}{48} \int_\omega \mathcal{A}\mathbf{R}(\boldsymbol{\eta}) : \mathbf{R}(\boldsymbol{\psi})\sqrt{a}, \ \forall \boldsymbol{\psi} \in C_c^\infty. \tag{1.70}$$

$$\langle \mathcal{L}_{el}\dot{\boldsymbol{\eta}}, \boldsymbol{\psi} \rangle := \frac{h}{2} \int_\omega \mathcal{B}\mathbf{G}(\dot{\boldsymbol{\eta}}) : \mathbf{G}(\boldsymbol{\psi})\sqrt{a} + \frac{h^3}{48} \int_\omega \mathcal{B}\mathbf{R}(\dot{\boldsymbol{\eta}}) : \mathbf{R}(\boldsymbol{\psi})\sqrt{a}, \ \forall \boldsymbol{\psi} \in C_c^\infty, \tag{1.71}$$

where $\mathbf{G}$ and $\mathbf{R}$ are the change of metric, and change of curvature tensors, respectively, and $\mathcal{A}$ and $\mathcal{B}$ are the elasticity tensor and the viscoelasticity tensor, respectively, defined in Example 4 of Section 92. This will be used to obtain the following energy estimate for the coupled problem:

Proposition 1.5.1. *The coupled FSI benchmark problem* (58)-(69) *with multiple structural layers satisfies the following energy estimate:*

$$\frac{d}{dt}\left(E_{kin}(t) + E_{el}(t)\right) + D(t) \le C(P_{in}(t), P_{out}(t)), \tag{1.72}$$

where

$$E_{kin}(t) := \frac{1}{2}\left(\rho_F\|\mathbf{u}\|_{L^2(\Omega_F(t))}^2 + \rho_K h\|\partial_t\boldsymbol{\eta}\|_{L^2(\Gamma)}^2 + \rho_S\|\partial_t\mathbf{d}\|_{L^2(\Omega_S)}^2\right),$$
$$E_{el}(t) := \frac{1}{2}\left(E_{el}(\boldsymbol{\eta}) + 2\mu\|\mathbf{D}(\mathbf{d})\|_{L^2(\Omega_S)}^2 + \lambda\|\nabla\cdot\mathbf{d}\|_{L^2(\Omega_S)}^2\right), \tag{1.73}$$

denote the kinetic and elastic (internal) energy of the coupled problem, respectively, and the term $D(t)$ captures viscous dissipation:

$$D(t) := E_{vis}(\partial_t\boldsymbol{\eta}) + \mu_F\|\mathbf{D}(\mathbf{u})\|_{L^2(\Omega_F(t))}^2. \tag{1.74}$$

The constant $C(P_{in}(t), P_{out}(t)))$ depends only on the inlet and outlet pressure data, which are both functions of time.

The expressions for the energy associated with the Koiter shell are given by:

$$E_{el}(\boldsymbol{\eta}) = \frac{h}{2}\int_\omega \mathcal{A}\mathbf{G}(\boldsymbol{\eta}) : \mathbf{G}(\boldsymbol{\eta})R + \frac{h^3}{48}\int_\omega \mathcal{A}\mathbf{R}(\boldsymbol{\eta}) : \mathbf{R}(\boldsymbol{\eta})R,$$

$$E_{vis}(\partial_t\boldsymbol{\eta}) = \frac{h}{2}\int_\omega \mathcal{B}\mathbf{G}(\partial_t\boldsymbol{\eta}) : \mathbf{G}(\partial_t\boldsymbol{\eta})R + \frac{h^3}{48}\int_\omega \mathcal{B}\mathbf{R}(\partial_t\boldsymbol{\eta}) : \mathbf{R}(\partial_t\boldsymbol{\eta})R.$$

Notice that, due to the presence of an elastic fluid-structure interface with mass, the kinetic energy term $E_{kin}(t)$ contains a contribution from the kinetic energy of the fluid-structure interface $\|\partial_t\boldsymbol{\eta}\|^2_{L^2(\Gamma)}$ incorporating the interface inertia. Furthermore, the elastic energy $E_{el}(t)$ of the FSI problem accounts for the elastic energy $\|\partial_z\boldsymbol{\eta}\|^2_{L^2(\Gamma)}$ of the interface. If a FSI problem between the fluid and a thick structure was considered without the thin FSI interface with mass, these terms would not be present. In fact, the traces of the displacement and velocity at the fluid-structure interface of that FSI problem would not have been even defined for weak solutions.

Proof. A formal calculation of the energy estimate for this class of problems typically entails multiplying the fluid and structure equations in differential form by the fluid and structure velocities, respectively, and performing integration by parts. Integration by parts of the fluid equations takes into account the boundary conditions, which are the conditions at the inlet and outlet boundary of the fluid domain, and the conditions at the lateral boundary of the fluid domain. At the lateral boundary of the fluid domain, the normal fluid stress is coupled with the structure equations, and here is where the dynamic and kinematic coupling conditions come into play. By taking these coupling conditions into account, the energy of the fluid and the energy of the structure are coupled together into the total energy of the coupled FSI problem.

   More precisely, we first multiply equation (60) by $\mathbf{u}$, integrate over $\Omega_F(t)$, and formally integrate by parts to obtain:

$$\int_{\Omega_F(t)}\rho_F\big(\partial_t\mathbf{u}{\cdot}\mathbf{u}+(\mathbf{u}{\cdot}\nabla)\mathbf{u}{\cdot}\mathbf{u}\big)+2\mu_F\int_{\Omega_F(t)}|\mathbf{D}(\mathbf{u})|^2-\int_{\partial\Omega_F(t)}(-p\mathbf{I}+2\mu_F\mathbf{D}(\mathbf{u}))\mathbf{n}(t){\cdot}\mathbf{u} = 0.$$
$$(1.75)$$

To deal with the inertia term we first recall that $\Omega_F(t)$ is moving in time and that the velocity of the lateral boundary is given by $\mathbf{u}|_{\Gamma(t)}$. The transport theorem applied to the first term on the left hand-side of the above equation then gives:

$$\int_{\Omega_F(t)}\partial_t\mathbf{u}\cdot\mathbf{u} = \frac{1}{2}\frac{d}{dt}\int_{\Omega_F(t)}|\mathbf{u}|^2 - \frac{1}{2}\int_{\Gamma(t)}|\mathbf{u}|^2\mathbf{u}\cdot\mathbf{n}(t).$$

The second term on the left hand side can can be rewritten by using integration by parts, and the divergence-free condition, to obtain:

$$\int_{\Omega_F(t)}(\mathbf{u}\cdot\nabla)\mathbf{u}\cdot\mathbf{u} = \frac{1}{2}\int_{\partial\Omega_F(t)}|\mathbf{u}|^2\mathbf{u}\cdot\mathbf{n}(t) = \frac{1}{2}\Big(\int_{\Gamma(t)}|\mathbf{u}|^2\mathbf{u}\cdot\mathbf{n}(t)$$

$$- \int_{\Gamma_{in}} |\mathbf{u}|^2 u_z + \int_{\Gamma_{out}} |\mathbf{u}|^2 u_z.)$$

These two terms added together give

$$\rho_F \int_{\Omega_F(t)} (\partial_t \mathbf{u} \cdot \mathbf{u} + (\mathbf{u} \cdot \nabla)\mathbf{u} \cdot \mathbf{u}) = \frac{\rho_F}{2} \frac{d}{dt} \int_{\Omega_F(t)} |\mathbf{u}|^2 - \frac{\rho_F}{2} \int_{\Gamma_{in}} |\mathbf{u}|^2 u_z + \frac{\rho_F}{2} \int_{\Gamma_{out}} |\mathbf{u}|^2 u_z.$$
$$(1.76)$$

Notice the importance of nonlinear advection in canceling the cubic term $\int_{\Gamma(t)} |\mathbf{u}|^2 \mathbf{u} \cdot \mathbf{n}(t)$!

To deal with the boundary integral over $\partial\Omega_F(t)$, first notice

$$\int_{\partial\Omega_F(t)} (-p\mathbf{I} + 2\mu_F \mathbf{D}(\mathbf{u}))\mathbf{n} \cdot \mathbf{u} = \int_{\Gamma_{in/out} \cup \Gamma(t)} (-p\mathbf{I} + 2\mu_F \mathbf{D}(\mathbf{u}))\mathbf{n} \cdot \mathbf{u}. \qquad (1.77)$$

To calculate the contribution of the integral over $\Gamma_{in/out}$, notice that on $\Gamma_{in/out}$ the outward unit normal is given by $\pm\mathbf{e}_z$. Furthermore, the boundary condition (64) implies $u_r = u_\theta = 0$, or, in Cartesian coordinates $u_x = u_y = 0$. Combined with the divergence-free condition one obtains $\partial_z u_z = 0$. This implies $\mathbf{D}(\mathbf{u}) = 0$ on $\Gamma_{in/out}$. Therefore,

$$\int_{\Gamma_{in/out}} (-p\mathbf{I} + 2\mu_F \mathbf{D}(\mathbf{u}))\mathbf{n} \cdot \mathbf{u} = \int_{\Gamma_{in}} p\, u_z - \int_{\Gamma_{out}} p\, u_z. \qquad (1.78)$$

What is left is to calculate the remaining boundary integral over $\Gamma(t)$, namely

$$- \int_{\Gamma(t)} (-p\mathbf{I} + 2\mu_F \mathbf{D}(\mathbf{u}))\mathbf{n}(t) \cdot \mathbf{u} = - \int_{\Gamma(t)} \boldsymbol{\sigma}\mathbf{n}(t) \cdot \mathbf{u}.$$

By enforcing the dynamic and kinematic coupling conditions (62), (63), we obtain

$$- \int_{\Gamma(t)} \sigma\mathbf{n}(t) \cdot \mathbf{u} = - \int_{\Gamma} J\sigma\mathbf{n} \cdot \mathbf{u} = \int_{\omega} R(\boldsymbol{f} - \mathbf{S}\mathbf{e}_r \cdot \mathbf{e}_r)\partial_t \eta, \qquad (1.79)$$

where $\boldsymbol{f}$ is the function appearing on the right hand-side of the Koiter shell equation (58).

The rest of the proof entails calculating the right hand-side of (79) in terms of the energy of the thin and thick structure problems. We begin with the Koiter shell problem:

$$\rho_K h \partial_{tt}\boldsymbol{\eta} + \mathcal{L}_{el}\boldsymbol{\eta} + \mathcal{L}_{vis}\partial_t\boldsymbol{\eta} = \boldsymbol{f}.$$

Multiply this equation by $\partial_t\boldsymbol{\eta}$ and formally integrate by parts, using, on the way, the definition of operators $\mathcal{L}_{el}$ and $\mathcal{L}_{vis}$, given in (70), and (71), respectively. The resulting equation is given by the following:

$$\frac{1}{2}\frac{d}{dt}\int_{\omega} \rho_K h\, (\boldsymbol{\eta}_t)^2 R + < \mathcal{L}_{el}\boldsymbol{\eta}, \partial_t\boldsymbol{\eta} > + < \mathcal{L}_{vis}\partial_t\boldsymbol{\eta}, \partial_t\boldsymbol{\eta} > = \int_{\omega} \boldsymbol{f}\partial_t\eta R,$$

or, by expanding the operators $\mathcal{L}_{el}$ and $\mathcal{L}_{vis}$, and using $\dot{\boldsymbol{\eta}}$ to denote $\partial_t\boldsymbol{\eta}$:

$$\frac{1}{2}\frac{d}{dt}\int_\omega \rho_K h\left(\boldsymbol{\eta}_t\right)^2 R + \frac{h}{2}\int_\omega \mathcal{A}\mathbf{G}(\boldsymbol{\eta}):\mathbf{G}(\dot{\boldsymbol{\eta}})R + \frac{h^3}{48}\int_\omega \mathcal{A}\mathbf{R}(\dot{\boldsymbol{\eta}}):\mathbf{R}(\dot{\boldsymbol{\eta}})R$$

$$\frac{h}{2}\int_\omega \mathcal{B}\mathbf{G}(\dot{\boldsymbol{\eta}}):\mathbf{G}(\dot{\boldsymbol{\eta}})R + \frac{h^3}{48}\int_\omega \mathcal{B}\mathbf{R}(\dot{\boldsymbol{\eta}}):\mathbf{R}(\dot{\boldsymbol{\eta}})R = \int_\omega \boldsymbol{f}\partial_t\boldsymbol{\eta}R. \quad (1.80)$$

By recalling the definitions of the elastic and viscous energy of the Koiter shell:

$$E_{el}(\boldsymbol{\eta}) = \frac{h}{2}\int_\omega \mathcal{A}\mathbf{G}(\boldsymbol{\eta}):\mathbf{G}(\boldsymbol{\eta})\sqrt{a} + \frac{h^3}{48}\int_\omega \mathcal{A}\mathbf{R}(\boldsymbol{\eta}):\mathbf{R}(\boldsymbol{\eta})\sqrt{a},$$

$$E_{vis}(\boldsymbol{\eta}) = \frac{h}{2}\int_\omega \mathcal{B}\mathbf{G}(\boldsymbol{\eta}):\mathbf{G}(\boldsymbol{\eta})\sqrt{a} + \frac{h^3}{48}\int_\omega \mathcal{B}\mathbf{R}(\boldsymbol{\eta}):\mathbf{R}(\boldsymbol{\eta})\sqrt{a},$$

equation (80) can be written as

$$\frac{\rho_K h}{2}\frac{d}{dt}\|\partial_t\boldsymbol{\eta}\|^2_{L^2(\omega)} + \frac{1}{2}\frac{d}{dt}E_{el}(\boldsymbol{\eta}) + E_{vis}(\partial_t\boldsymbol{\eta}) = \int_\omega R\,\boldsymbol{f}\partial_t\boldsymbol{\eta}. \quad (1.81)$$

Next, consider the elasticity equation (59), multiply it by $\partial_t\mathbf{d}$ and integrate by parts to obtain:

$$\frac{1}{2}\frac{d}{dt}\left(\rho_S\|\partial_t\mathbf{d}\|^2_{L^2(\Omega_S)} + 2\mu\|\mathbf{D}(\mathbf{d})\|^2_{L^2(\Omega_S)} + \lambda\|\nabla\cdot\mathbf{d}\|^2_{L^2(\Omega_S)}\right) = -\int_\Gamma \mathbf{Se}_r\cdot\partial_t\mathbf{d}$$

$$= -\int_\omega R\,\mathbf{Se}_r\cdot\partial_t\mathbf{d}. \quad (1.82)$$

Now, the right hand-side of equation (79) can be calculated by combining (81) and (82) to obtain

$$-\int_{\Gamma(t)} \sigma\mathbf{n}(t)\cdot\mathbf{u} = \frac{\rho_K h}{2}\frac{d}{dt}\|\partial_t\boldsymbol{\eta}\|^2_{L^2(\omega)} + \frac{1}{2}\frac{d}{dt}E_{el}(\boldsymbol{\eta}) + E_{vis}(\partial_t\boldsymbol{\eta})$$

$$\frac{1}{2}\frac{d}{dt}\left(\rho_s\|\partial_t\mathbf{d}\|^2_{L^2(\Omega_S)} + 2\mu\|\mathbf{D}(\mathbf{d})\|^2_{L^2(\Omega_S)} + \lambda\|\nabla\cdot\mathbf{d}\|^2_{L^2(\Omega_S)}\right). \quad (1.83)$$

By combining (75) with (76), (77), (78), and (83), one obtains the following energy equality:

$$\frac{1}{2}\frac{d}{dt}\left\{\rho_F\|\mathbf{u}\|^2_{\Omega_F(t)} + \rho_K h\|\partial_t\boldsymbol{\eta}\|^2_{L^2(\Gamma)} + \rho_S\|\partial_t\mathbf{d}\|^2_{L^2(\Omega_S)} + E_{el}(\boldsymbol{\eta}) + 2\mu\|\mathbf{D}(\mathbf{d})\|^2_{L^2(\Omega_S)}\right.$$

$$\left. + \lambda\|\nabla\cdot\mathbf{d}\|^2_{L^2(\Omega_S)}\right\} + 2\mu_F\|\mathbf{D}(\mathbf{u})\|^2_{\Omega_F(t)} + E_{vis}(\partial_t\boldsymbol{\eta}) = \pm P_{in/out}(t)\int_{\Gamma_{in/out}} u_z$$

Finally, by using the trace inequality and Korn inequality one can estimate:

$$\left|P_{in/out}(t)\int_{\Gamma_{in/out}} u_z\right| \le C|P_{in/out}|\|\mathbf{u}\|_{H^1(\Omega_F(t))} \le \frac{C}{2\epsilon}|P_{in/out}|^2 + \frac{\epsilon C}{2}\|\mathbf{D}(\mathbf{u})\|^2_{L^2(\Omega_F(t))}.$$

By choosing ϵ such that $\frac{\epsilon C}{2} \leq \mu_F$ we get the energy inequality

$$\frac{1}{2}\frac{d}{dt}\left\{\rho_F\|\mathbf{u}\|^2_{\Omega_F(t)} + \rho_K h\|\partial_t\boldsymbol{\eta}\|^2_{L^2(\Gamma)} + \rho_S\|\partial_t\mathbf{d}\|^2_{L^2(\Omega_S)} + E_{el}(\boldsymbol{\eta}) + 2\mu\|\mathbf{D}(\mathbf{d})\|^2_{L^2(\Omega_S)}\right.$$
$$\left. + \lambda\|\nabla\cdot\mathbf{d}\|^2_{L^2(\Omega_S)}\right\} + \mu_F\|\mathbf{D}(\mathbf{u})\|^2_{\Omega_F(t)} + E_{vis}(\partial_t\boldsymbol{\eta}) \leq C(P_{in}(t), P_{out}(t)).$$

$\square$

1.5.2 ALE Formulation

Since the fluid-structure coupling studied in this chapter is preformed along the moving fluid-structure interface, the fluid domain $\Omega(t)$ is not fixed. This is a problem from many points of view. In particular, defining the time discretization of the time derivative $\partial\mathbf{u}/\partial t$, for example $\partial\mathbf{u}/\partial t \approx (\mathbf{u}(t^{n+1},.) - \mathbf{u}(t^n,.))/(t^{n+1} - t^n)$, is not well-defined since $\mathbf{u}(t^{n+1},.)$ and $\mathbf{u}(t^n,.)$ are not defined on the same domain at two different time-steps. To resolve this difficulty, often times the fluid domain is mapped onto a fixed, reference domain via a smooth, invertible ALE mapping [54]:

$$\mathcal{A} : \Omega_F \to \Omega_F(t).$$

An example of such a mapping is the harmonic extension of the boundary $\partial\Omega_F(t)$ onto the fluid domain. See Section 0.7. Another example is a mapping particularly convenient for the existence proof, presented in Section 0.6. This introduces additional nonlinearities into the equations, reflecting the geometric nonlinearities of the moving interface. The transformed gradient, which we denote by $\nabla^{\boldsymbol{\eta}}$, will depend on the fluid-structure interface $\boldsymbol{\eta}$. Furthermore, by using the chain rule, one can see that the the time derivative of the transformed fluid velocity will have an additional advection term with the coefficient given by the domain velocity $\mathbf{w} := \mathcal{A}_t \circ \mathcal{A}^{-1}$, where $\mathcal{A}_t$ denotes the time derivative of $\mathcal{A}$. Finally, the mapped fluid equations in Ω_F read:

$$\left.\begin{array}{rcl}\rho_F\left(\partial_t\mathbf{u} + ((\mathbf{u}-\mathbf{w})\cdot\nabla^{\eta})\mathbf{u}\right) & = & \nabla^{\eta}\cdot\boldsymbol{\sigma}^{\eta} \\ \nabla^{\eta}\cdot\mathbf{u} & = & 0\end{array}\right\} \text{ in } \Omega_F \times (0,T). \qquad (1.84)$$

Here, the notation $\boldsymbol{\sigma}^{\eta}$ reflects the dependence of $\mathbf{D}^{\eta}(\mathbf{u}) = \frac{1}{2}(\nabla^{\eta}\mathbf{u} + \nabla^{\eta T}\mathbf{u})$ on η. Therefore, our problem in ALE formulation reads as follows:

THE COUPLED PROBLEM IN ALE FORM DEFINED ON Ω_F

Find $\mathbf{u}$, p, η and $\mathbf{d}$ such that:

$$\left.\begin{aligned}
\rho_F \left(\partial_t \mathbf{u} + ((\mathbf{u} - \mathbf{w}) \cdot \nabla^\eta)\mathbf{u}\right) &= \nabla^\eta \cdot \boldsymbol{\sigma}^\eta \\
\nabla^\eta \cdot \mathbf{u} &= 0
\end{aligned}\right\} \text{ in } \Omega_F \times (0, T),$$

$$\rho_S \partial_{tt} \mathbf{d} = \nabla \cdot \mathbf{S} \quad \text{in } \Omega_S \times (0, T),$$

$$\left.\begin{aligned}
\partial_t \eta \mathbf{e}_r &= \boldsymbol{u}|_{R+\eta}, \\
\eta \mathbf{e}_r &= \mathbf{d}, \\
\rho_K h \partial_{tt} \eta + \mathcal{L}_{el}(\eta) + \mathcal{L}_{vis} \partial_t \eta &= -J(\sigma \mathbf{n})|_{R+\eta} \cdot \mathbf{e}_r + R\, \mathbf{S} \mathbf{e}_r \cdot \mathbf{e}_r
\end{aligned}\right\} \text{on } \Gamma \times (0, T).$$

As we shall see in Section 0.7, the actual numerical simulations at each time step are typically performed on the current (fixed) domain $\Omega_F^n(t)$, with only the time-derivative calculated on Ω_F, thereby avoiding the need to calculate the transformed gradients ∇^η. The corresponding continuous problem in ALE form can be written as follows:

THE COUPLED PROBLEM IN ALE FORM DEFINED ON $\Omega_F(t)$

Find $\mathbf{u}$, p, η and $\mathbf{d}$ such that:

$$\left.\begin{aligned}
\rho_F \left(\partial_t \mathbf{u}|_{\Omega_F} + ((\mathbf{u} - \mathbf{w}) \cdot \nabla)\mathbf{u}\right) &= \nabla \cdot \boldsymbol{\sigma} \\
\nabla \cdot \mathbf{u} &= 0
\end{aligned}\right\} \text{ in } \Omega_F(t) \times (0, T),$$

$$\rho_S \partial_{tt} \mathbf{d} = \nabla \cdot \mathbf{S} \quad \text{in } \Omega_S \times (0, T),$$

$$\left.\begin{aligned}
\partial_t \eta \mathbf{e}_r &= \boldsymbol{u}|_{R+\eta}, \\
\eta \mathbf{e}_r &= \mathbf{d}, \\
\rho_K h \partial_{tt} \eta + \mathcal{L}_{el}(\eta) + \mathcal{L}_{vis} \partial_t \eta &= -J(\sigma \mathbf{n})|_{R+\eta} \cdot \mathbf{e}_r + R\, \mathbf{S} \mathbf{e}_r \cdot \mathbf{e}_r
\end{aligned}\right\} \text{on } \Gamma \times (0, T).$$

Here, $\partial_t \mathbf{u}|_{\Omega_F}$ denotes the time derivative calculated on Ω_F. This approach is standard in ALE methods applied to partitioned schemes. In our existence proof, and in our definition of the splitting scheme, however, it will be convenient to use the fully mapped problem onto the fixed reference domain Ω_F.

1.5.3   The Splitting Scheme – General Framework

To apply the Lie splitting scheme the problem must first be written as a first-order system in time:

$$\frac{\partial \phi}{\partial t} + A(\phi) = 0, \quad \text{in } (0, T), \tag{1.85}$$

$$\phi(0) = \phi_0, \tag{1.86}$$

where A is an operator from a Hilbert space into itself. Operator A is then split, in a non-trivial decomposition, as

$$A = \sum_{i=1}^{I} A_i. \tag{1.87}$$

The Lie scheme consists of the following. Let $\triangle t > 0$ be a time discretization step. Denote $t^n = n\triangle t$ and let ϕ^n be an approximation of $\phi(t^n)$. Set $\phi^0 = \phi_0$. Then, for $n \geq 0$ compute ϕ^{n+1} by solving

$$\frac{\partial \phi_i}{\partial t} + A_i(\phi_i) = 0 \quad \text{in } (t^n, t^{n+1}), \tag{1.88}$$

$$\phi_i(t^n) = \phi^{n+(i-1)/I}, \tag{1.89}$$

and then set $\phi^{n+i/I} = \phi_i(t^{n+1})$, for $i = 1, \ldots . I$. Thus, the value at $t = t^{n+1}$ of the solution of the i-th problem is taken as the initial data for the $(i + 1)$-st problem on (t^n, t^{n+1}).

This method is first-order accurate in time. More precisely, if (85) is defined on a finite-dimensional space, and if operators A_i are smooth enough, then $\|\phi(t^n) - \phi^n\| = O(\Delta t)$ [77].

To solve the class of problems (58)-(63), we split the fluid from the structure subproblem to separate the different physics in the coupled problem. Thus, the coupled problem, which defines operator A, is split into a sum of two operators:

1. An elastodynamics problem for the thick structure, and

2. A fluid problem with suitable boundary conditions involving structure velocity and fluid stress at the boundary.

The thin-structure problem will enter through the boundary conditions, enforcing the dynamic coupling condition between the fluid and thick structure.

Thus, this scheme works as follows: first the structure problem is solved on the time-interval (t^n, t^{n+1}) with the initial data obtained from the previous time-step. Then, the fluid problem is solved on the same-time interval (t^n, t^{n+1}), but with the initial data obtained from the just calculated solution in the first step.

Not every splitting of this kind would lead to a stable, convergent scheme. Our strategy is to split the fluid from the structure subproblem in such a way that the energy of the discretized problem approximates well the energy of the continuous problem. To achieve this goal, a key role is played by the kinematic coupling condition, which will be enforced implicitly in both steps of the splitting scheme, keeping the two sub-problems tightly coupled at all times.

Before we apply the Lie splitting, we rewrite our coupled problem in first-order form with respect to time. For this purpose we introduce the following notation:

- the trace of the fluid velocity at the moving interface $\Gamma(t)$ will be denoted by v, i.e.,

$$v\mathbf{e_r} := \mathbf{u}|_{\Gamma(t)}.$$

  Namely, v, which is defined on Γ, is equal to the trace of $\mathbf{u}$ evaluated at $R+\eta$. The kinematic coupling condition (no-slip) then reads $\partial_t\eta = v$.

- the thick structure velocity will be denoted by:

$$\mathbf{V} := \frac{\partial \mathbf{d}}{\partial t}.$$

The system in ALE form is now rewritten by using the above-mentioned notation, and by employing the *kinematic coupling condition* in the thin structure model. This way the kinematic coupling condition will be enforced everywhere, in all the steps of the splitting scheme. The resulting coupled problem in first-order ALE form is given by the following:

The Coupled Problem in First-Order ALE Form

Find $\mathbf{u}$, p, η, $\mathbf{d}$, v, and $\mathbf{V}$ such that:

$$\left.\begin{aligned}
\rho_F\left(\partial_t\mathbf{u} + ((\mathbf{u}-\mathbf{w})\cdot\nabla^\eta)\mathbf{u}\right) &= \nabla^\eta\cdot\boldsymbol{\sigma}^\eta \\
\nabla^\eta\cdot\mathbf{u} &= 0
\end{aligned}\right\} \text{ in } \Omega_F \times (0,T),$$

$$\left.\begin{aligned}
\rho_S\partial_t\mathbf{V} &= \nabla\cdot\mathbf{S} \\
\mathbf{d}_t &= \mathbf{V},
\end{aligned}\right\} \text{ in } \Omega_S \times (0,T),$$

$$\left.\begin{aligned}
&\partial_t\eta = v, \\
&v\mathbf{e}_r = \mathbf{u}, \\
&\eta\mathbf{e}_r = \mathbf{d}, \\
&\rho_K h\partial_t v + \mathcal{L}_{el}(\eta) + \mathcal{L}_{vis}v = -J\ \sigma^\eta\mathbf{n}\cdot\mathbf{e}_r + R\ \mathbf{S}\mathbf{e}_r\cdot\mathbf{e}_r
\end{aligned}\right\} \text{ on } \Gamma \times (0,T).$$

Notice that we have enforced the kinematic coupling condition both in the thin structure acceleration term, and in the viscous part of the thin structure equation.

We are now ready to split the problem. For this purpose, observe that the portion $\rho_K h\ \partial_t v + \mathcal{L}_{vis}v = -J\boldsymbol{\sigma}\mathbf{n}\cdot\mathbf{e}_r$ of the dynamic coupling condition is all given in terms of the trace v of the fluid velocity on Γ (recall, $\boldsymbol{\sigma}$ depends on v.) We can, therefore, use this as a lateral boundary condition on Γ for the fluid sub-problem. This observation is crucial because keeping the structure inertia term $\rho_K h\partial_t v$ together with the inertia of the fluid in the fluid sub-problem is of paramount importance for designing a stable and convergence scheme.

This is different from the classical loosely coupled schemes. In classical Dirichlet-Neumann loosely coupled scheme, the boundary condition for the fluid subproblem is the Dirichlet condition for the fluid velocity v on Γ given in terms of the structure velocity $\partial\eta/\partial t$, namely $v = \partial\eta/\partial t$, where $\partial\eta/\partial t$ is *calculated at the previous*

time step! This inclusion of the structure inertia from the previous time step (explicitly) makes the fluid subproblem unstable for certain parameters values [30]. The main reason for this is that the kinetic energy at this time step, includes only the fluid kinetic energy from the current time step, and not the thin structure kinetic energy, since the thin structure velocity enters from the previously calculated time step. For strong geometric nonlinearities, which often happen when the fluid and structure densities are comparable, this miss-match between the kinetic energy of the discretized problem (where only the fluid kinetic energy appears in the current time-step), and the kinetic energy of the continuous problem (where both the fluid and structure kinetic energy are tied together in a strongly coupled FSI problem) gives rise to an unstable numerical scheme [30].

Therefore, the strategy of our splitting, mentioned above, to keep the thin structure inertia together with the fluid inertia in the fluid sub-step, will give rise to the kinetic energy of the discretized problem that approximates well the kinetic energy of the continuous problem, giving rise to a scheme that is unconditionally stable for all the parameters in the problem [29]. In Section 0.6 we prove that the scheme converges to a weak solution to the underlying FSI problem.

We therefore define the operators A_1 and A_2 as follows:

$$
\boxed{
\begin{array}{l}
\textbf{Problem A1} : \textbf{STRUCTURE} \\
\begin{array}{rcll}
\rho_S \partial_t \mathbf{V} & = & \nabla \cdot \mathbf{S}, & \text{in } \Omega_S \\
\partial_t \mathbf{d} & = & \mathbf{V}, & \text{in } \Omega_S \\
\mathbf{d} & = & \eta \mathbf{e}_r, & \text{on } \Gamma \\
\partial_t \eta & = & v, & \text{on } \Gamma \\
\rho_K h \partial_t v & = & \mathcal{L}_{el}(\eta) + R\,\mathbf{S}\mathbf{e}_r \cdot \mathbf{e}_r & \text{on } \Gamma
\end{array}
\end{array}
}
$$

Here, of course, the PDE system in Ω_S can be solved just as a single second-order PDE for $\mathbf{d}$: $\rho_S \mathbf{d}_{tt} = \nabla \cdot \mathbf{S}$. Problem A1 is solved with the initial data $(\mathbf{d}, \mathbf{V}, \eta, v)$ given by the solution from the previous time-step. This means, in particular, that the thin structure velocity v is set to be equal to the trace of the fluid velocity on Γ, calculated in the previous time-step. Thus, we are solving the elastodynamics problem for the linearly elastic thick structure in Ω_S, with the boundary condition at the lateral boundary Γ given by a PDE that determines the motion of the lateral boundary. The motion of the lateral boundary in this sub-problem is driven by the normal component of the first Piola-Kirchhoff stress tensor $\mathbf{S}$, and by the initial data for the velocity of the thin structure, which is given by the trace of the fluid velocity, just calculated in the previous time-step. In this step we also calculate the domain velocity $\mathbf{w}$, which is given by the time-derivative of the ALE mapping, associated with Problem A1.

$$
\boxed{
\begin{array}{rcl l}
\multicolumn{4}{l}{\textbf{Problem A2} : \textbf{FLUID}} \\
\partial_t \mathbf{u} + ((\hat{\mathbf{u}} - \mathbf{w}) \cdot \nabla^\eta)\mathbf{u} & = & \nabla^\eta \cdot \boldsymbol{\sigma}^\eta, & \text{in } \Omega_F \\
\nabla^\eta \cdot \mathbf{u} & = & 0, & \text{in } \Omega_F \\
\mathbf{u} & = & v\mathbf{e}_r, & \text{on } \Gamma \\
\rho_K h \partial_t v + \mathcal{L}_{vis} v & = & -J\boldsymbol{\sigma}^\eta \mathbf{n} \cdot \mathbf{e}_r & \text{on } \Gamma
\end{array}
}
$$

Here $\hat{\mathbf{u}}$ is the value of $\mathbf{u}$ from the previous time step, and $\mathbf{w}$, which is the domain velocity (the time derivative of the ALE mapping), is obtained from the just calculated Problem A1. Furthermore, $\nabla^{\boldsymbol{\eta}}$ is the transformed gradient, which is based on the value of $\boldsymbol{\eta}$ from the previous time-step. The initial data for $\mathbf{u}$ is given from the previous time step, while the initial data for the trace of the fluid velocity v is given by the just calculated velocity of the thin structure $\partial_t \eta$.

This concludes our description of the general framework based on the Lie splitting scheme for solving the class of fluid-structure interaction problems (58)-(63) with multiple structural layers.

Before we continue, several remarks are in order:

- The splitting works as well when the thin structure is purely elastic, i.e., when $\mathcal{L}_{vis} = 0$.

- Switching the order of solution (fluid step first, structure second) works as well. The corresponding algorithm is explicitly shown below in the corresponding block-diagram.

- The symmetrized Lie splitting obtained by solving the structure problem, followed by the fluid problem, and then the structure problem, increases the accuracy of the scheme to second-order in time.

- A version of Strang splitting for this problem was performed by Lukačova et al. in [95, 94] achieving second-order accuracy in time.

- Adding additional modules to capture different physics in a given multiphysics problem can be accomplished in a similar way. See [23] for an application of this scheme to a FSI problem with multiple *poroelastic* structural layers. Also, see [123] for an application of this scheme to a FSI between a vascular device called *stent*, elastic arterial wall, and the flow of an incompressible, viscous fluid.

- A modification of this scheme to achieve higher accuracy within the class of first-order schemes, was introduced in [19, 20]. Details of this modified scheme, called the Kinematically-Coupled β-scheme, are presented next.

1.5.4   A Modified Splitting Scheme achieving Higher Accuracy

To increase the accuracy, the kinematically-coupled β-scheme is based on additionally splitting the normal fluid stress as follows:

$$\boldsymbol{\sigma}\mathbf{n} = \underbrace{\boldsymbol{\sigma}\mathbf{n} + \beta p\mathbf{n}}_{(I)} \underbrace{-\beta p\mathbf{n}}_{(II)},$$

where $\beta \in [0,1]$. Part I of the fluid stress is treated with the fluid sub-problem, while Part II with the structure sub-problem. The new boundary condition for the fluid sub-problem, written in the framework in which the entire fluid sub-problem is considered on the fixed, reference domain Ω_F, becomes

$$\rho_S h \partial_t v + \mathcal{L}_{vis} v = -J \left(\boldsymbol{\sigma}^\eta \mathbf{n} + \beta \hat{p} \mathbf{n} \right) \cdot \mathbf{e}_r \quad \text{on } \Gamma,$$

where $\hat{p}$ denotes the explicit use of the pressure calculated from the previous step. Part II of the fluid stress is then used to load the structure so that the new boundary condition for the structure sub-problem becomes

$$\rho_K h \partial_t v = \mathcal{L}_{el}(\eta) + \left(R \, \mathbf{S} \mathbf{e}_r - \beta J p \mathbf{n} \right) \cdot \mathbf{e}_r \quad \text{on } \Gamma. \tag{1.90}$$

A block diagram shown in Figure 8 below summarizes the splitting in each iteration.

The main reason for the increase in accuracy of the β-scheme is the inclusion of the pressure loading $\beta J p \mathbf{n}$ by the fluid onto the structure in the structure sub-problem. This way the structure "feels" the fluid not only through the kinematic coupling condition enforced via the initial condition for the structure sub-problem ($\partial_t \eta = v$), but also through the leading contribution of the normal stress, i.e. the pressure, exerted by the fluid onto the structure. Typically, the highest accuracy is achieved for $\beta = 1$. The accuracy of this modified scheme is still first-order, but the error is closer to the error of a monolithic scheme, as we shall see in Section 0.7.

Numerical Implementation. Typically, numerical implementation of the fluid sub-problem entails solving the fluid equations on the "current domain". Namely, numerical implementation is performed for the ALE problem written on $\Omega_F(t)$, and not Ω_F, as was discussed at the end of Section 0.5.2. In this case, the fluid sub-problem written above takes the following form:

Problem A2 (FLUID)

$$
\begin{aligned}
\partial_t \mathbf{u}|_{\Omega_F} + ((\mathbf{u}^n - \mathbf{w}^{n+1}) \cdot \nabla)\mathbf{u} &= \nabla \cdot \boldsymbol{\sigma}, & \text{in } \Omega_F^n \\
\nabla \cdot \mathbf{u} &= 0, & \text{in } \Omega_F^n \\
(\rho_K h \partial_t \mathbf{u}|_{R+\eta} + \mathcal{L}_{vis}\mathbf{u}|_{R+\eta}) \cdot \mathbf{e}_r &= -J \left(\boldsymbol{\sigma}\mathbf{n} + \beta p^n \mathbf{n} \right)|_{R+\eta} \cdot \mathbf{e}_r & \text{on } \Gamma_F^n
\end{aligned}
$$
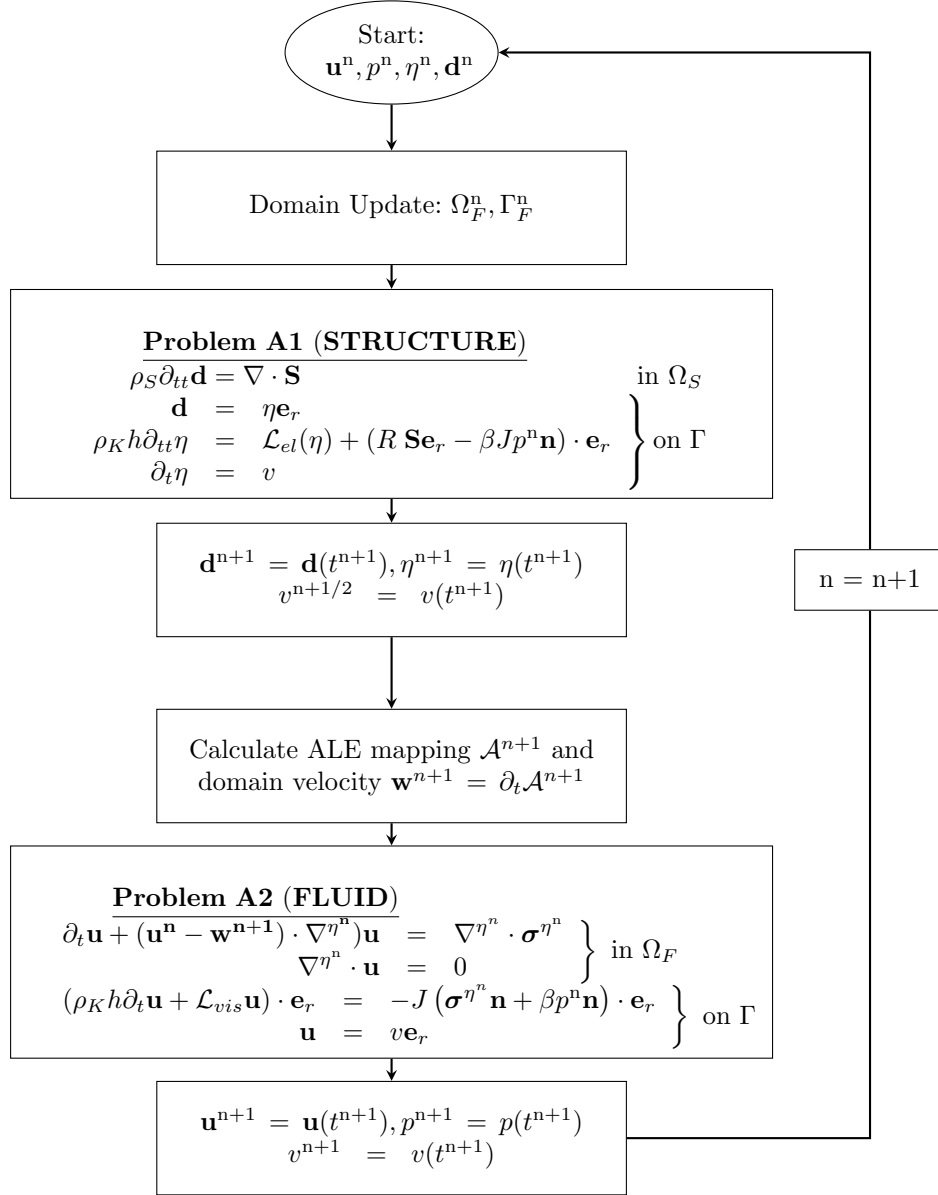
Figure 1.8: A block diagram showing the main steps of the Kinematically Coupled β-Scheme.

1.6 Existence of a Weak Solution

In this section we present details of the analysis of the existence of a weak solution to a previously discussed FSI problem with a multi-layered structure in two space dimensions. For related results in 3D, please see [121]. The most difficult case from the analysis point of view, is the case when the viscoelastic effects in the thin structure model are ignored, and the highest order spatial derivatives (the 4-th order spatial derivatives) in the Koiter shell have the coefficients equal to zero. The resulting thin-structure model is the linear wave equation. Thus, in this section we study fluid-structure interaction between an incompressible, viscous fluid flowing through a 2D cylinder with compliant walls, consisting of a thin and a thick layer, modeled by the linear wave equation, and the equations of linear elasticity, respectively. As before, we will also be assuming that only the radial displacement in the thin structure is different from zero.

The existence result for the FSI problem in which the thin structure is modeled by the full linearly elastic/viscoelastic Koiter shell equations, and the thick structure is modeled by the equations of linear elasticity, can be obtained by combining the results of [119] and the results of [122].

1.6.1 Problem definition

We consider the flow of an incompressible, viscous fluid modeled by the Navier-Stokes equations in a 2D, time-dependent cylindrical fluid domain $\Omega_F(t)$, which is not known *a priori*:

$$\textbf{FLUID}: \quad \left.\begin{array}{rcl} \rho_F(\partial_t \mathbf{u} + \mathbf{u} \cdot \nabla \mathbf{u}) & = & \nabla \cdot \boldsymbol{\sigma}, \\ \nabla \cdot \mathbf{u} & = & 0, \end{array}\right\} \text{ in } \Omega_F(t),\ t \in (0, T), \quad (1.91)$$

where ρ_F denotes the fluid density; $\mathbf{u}$ the fluid velocity; $\boldsymbol{\sigma} = -p\mathbf{I} + 2\mu_F \mathbf{D}(\mathbf{u})$ is the fluid Cauchy stress tensor; p is the fluid pressure; μ is the kinematic viscosity coefficient; and $\mathbf{D}(\mathbf{u}) = \frac{1}{2}(\nabla \mathbf{u} + \nabla^\tau \mathbf{u})$ is the symmetrized gradient of $\mathbf{u}$.

The cylindrical fluid domain is of length L, with reference radius $r = R$. The radial (vertical) displacement of the cylinder radius at time t and position $z \in (0, L)$ will be denoted by $\eta(t, z)$, giving rise to a deformed domain with radius $R + \eta(t, z)$. Thus, the fluid domain, sketched in Figure 9, is given by

$$\Omega_F(t) = \{(z, r) \in \mathbb{R}^2 : z \in (0, L),\ r \in (0, R + \eta(t, z))\},$$

where the lateral boundary of the cylinder corresponds to the fluid-structure interface, denoted by

$$\Gamma(t) = \{(z, r) \in \mathbb{R}^2 : z \in (0, L),\ r = R + \eta(t, z)\}.$$

Without loss of generality we only consider the upper half of the fluid cylinder, with a symmetry boundary condition prescribed at the axis of symmetry, denoted by Γ_b in Figure 9.
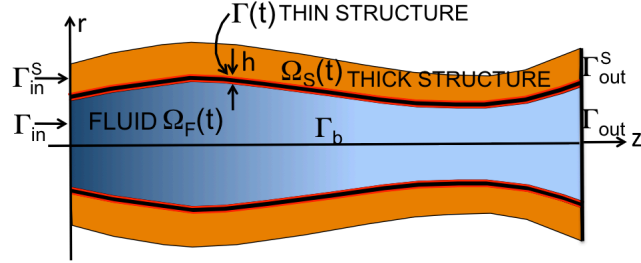
Figure 1.9: 2D Domain sketch.

The fluid is in contact with a thin elastic structure, which is located between the fluid and the thick structural layer. The thin structure thereby serves as a fluid-structure interface with mass. We will be assuming that the elastodynamics of the thin elastic structure is governed by the 1D wave equation

THIN STRUCTURE : $\rho_K h\ \partial_{tt}\eta = c^2\partial_{zz}\eta + f, \quad z \in (0,L),\ t \in (0,T),$
$$\tag{1.92}$$

where η denotes radial (vertical) displacement. Here, ρ_K is the structure density, h denotes structure thickness, and f denotes force density in the radial (vertical) direction acting on the structure. The wave equation can be viewed as a special case of the linearly (visco)elastic cylindrical Koiter shell model

$$\rho_K h\partial_t^2\eta + C_0\eta - C_1\partial_z^2\eta + C_2\partial_z^4\eta + D_0\partial_t\eta - D_1\partial_t\partial_z^2\eta + D_2\partial_t\partial_z^4\eta = f, \quad (1.93)$$

with $C_0 = C_2 = D_0 = D_1 = D_2 = 0$. See Section 92.

The thick structural layer will be modeled by the equations of linear elasticity

THICK STRUCTURE : $\rho_S\ \partial_{tt}\mathbf{d} = \nabla \cdot \mathbf{S}$ in $\Omega_S,\ t \in (0,T),$ (1.94)

where $\mathbf{d}(t,z,r) = (d_z(t,z,r), d_r(t,z,r))$ denotes structural displacement of the thick elastic wall at point $(z,r) \in \Omega_S$ and time t, $\boldsymbol{S}$ is the first Piola-Kirchhoff stress tensor given by $\mathbf{S} = \mu\ (\nabla\mathbf{d} + (\nabla\mathbf{d})^T) + \lambda(\nabla \cdot \mathbf{d})\mathbf{I}$, where λ and μ are the Lamé constants, and ρ_S is density of the thick structure. Domain Ω_S corresponds to a fixed, reference domain which is independent of time, and is given by

$$\Omega_S = (0,L) \times (R, R + H).$$

A deformation of Ω_S at time t is denoted by $\Omega_S(t)$ in Figure 9.

THE COUPLING between the fluid, the thin structural layer, and the thick structural layer is achieved via

- the kinematic coupling condition:

$$(\partial_t \eta(t,z), 0) = \boldsymbol{u}(t, z, R + \eta(t,z)), \quad \text{(continuity of velocity)}$$
$$(\eta(t,z), 0) = \mathbf{d}(t, z, R), \quad \text{(continuity of displacement)} \tag{1.95}$$

- the dynamic coupling condition:

$$\rho_{s_1} h \partial_{tt} \eta = c^2 \partial_{zz} \eta - J(t,z)(\sigma\mathbf{n})|_{(t,z,R+\eta(t,z))} \cdot \mathbf{e}_r + \mathbf{S}(t, z, R)\mathbf{e}_r \cdot \mathbf{e}_r. \tag{1.96}$$

Here $J(t,z) = \sqrt{1 + (\partial_z \eta(t,z))^2}$ denotes the Jacobian of the transformation from Eulerian to Lagrangian coordinates, and $\mathbf{e}_r$ is the unit vector associated with the vertical, r-direction.

Notice that in this 2D problem both the structure and fluid equations are written in Cartesian coordinates, and so the Jacobian of the transformation between the cylindrical and Cartesian coordinates does not appear in these equations. This means, in particular, that the factor R that appears in equation (63) does not appear in (96).

THE BOUNDARY AND INITIAL CONDITIONS:

At the **inlet and outlet boundaries** to the fluid domain we prescribe zero tangential velocity and a given dynamic pressure $p + \frac{\rho_f}{2}|u|^2$:

$$\left. \begin{array}{rcl} p + \frac{\rho_f}{2}|u|^2 & = & P_{in/out}(t), \\ u_r & = & 0, \end{array} \right\} \quad \text{on } \Gamma_{in/out}, \tag{1.97}$$

where $P_{in/out} \in L^2_{loc}(0, \infty)$ are given. Therefore, the fluid flow is driven by a prescribed dynamic pressure drop, and the flow enters and leaves the fluid domain orthogonally to the inlet and outlet boundary.

At the **bottom boundary** we prescribe the symmetry boundary condition:

$$u_r = \partial_r u_z = 0, \quad \text{on } \Gamma_b. \tag{1.98}$$

At the **end points of the thin structure** we prescribe zero displacement:

$$\eta(t,0) = \eta(t,L) = 0. \tag{1.99}$$

For the **thick structure**, we assume that the **external (top) boundary** $r = H$ is exposed to an external ambient pressure P_e:

$$\mathbf{S}\mathbf{e}_r = -P_e\mathbf{e}_r, \quad \text{on } \Gamma_{ext}, \tag{1.100}$$

while at the **end points** of the annular sections of the thick structure, $\Gamma^s_{in/out}$, we assume that the displacement is zero

$$\mathbf{d}(t,0,r) = \mathbf{d}(t,L,r) = 0, \quad \text{for } r \in (R, H).$$

The **initial** fluid and structural velocities, and the initial displacements are given by

$$\mathbf{u}(0,.) = \mathbf{u}_0, \ \eta(0,.) = \eta_0, \ \partial_t \eta(0,.) = v_0, \ \mathbf{d}(0,.) = \mathbf{d}_0, \ \partial_t \mathbf{d}(0,.) = \mathbf{V}_0, \quad (1.101)$$

and are assumed to belong to the following spaces: $\mathbf{u}_0 \in L^2(\Omega_F(0))$, $\eta_0 \in H_0^1(0,1)$, $v_0 \in L^2(0,1)$, $\mathbf{V}_0 \in L^2(\Omega_S)$, $\mathbf{d}_0 \in H^1(\Omega_S)$, satisfying the following compatibility conditions:

$$(\eta_0(z), 0) = \mathbf{d}_0(z, R),$$
$$\eta_0(0) = \eta_0(L) = v_0(0) = v_0(L) = 0 = \mathbf{d}_0(0,.) = \mathbf{d}_0(L,.) = \mathbf{V}_0(0,.) = \mathbf{V}_0(L,.),$$
$$R + \eta_0(z) > 0, \quad z \in [0, L].$$
$$(1.102)$$

We study the existence of a weak solution to the nonlinear FSI problem (91)-(102), in which the flow is driven by the time-dependent inlet and outlet dynamic pressure data.

For simplicity, in the rest of this section, we will be setting all the parameters in the problem to be equal to 1. This includes the domain parameters R and L, the Lamé constants λ and μ, and the structure parameters ρ_K, ρ_S and h. Furthermore, we will be assuming that the external pressure, given in (100), is equal to zero. Alternatively, we subtract the constant external pressure data from the inlet and outlet dynamic pressure data to obtain an equivalent problem.

1.6.2   The energy of the coupled problem

By using the same approach as described in Section 0.5.1, one can now show that the following energy estimate holds:

$$\frac{d}{dt}\left(E_{kin}(t) + E_{el}(t)\right) + D(t) \leq C(P_{in}(t), P_{out}(t)), \qquad (1.103)$$

where

$$E_{kin}(t) \ := \ \tfrac{1}{2}\left(\|\mathbf{u}\|_{L^2(\Omega_F(t))}^2 + \|\partial_t \eta\|_{L^2(\Gamma)}^2 + \|\partial_t \mathbf{d}\|_{L^2(\Omega_S)}^2\right),$$
$$(1.104)$$
$$E_{el}(t) \ := \ \tfrac{1}{2}\left(\|\partial_z \eta\|_{L^2(\Gamma)}^2 + 2\|\mathbf{D}(\mathbf{d})\|_{L^2(\Omega_S)}^2 + \|\nabla \cdot \mathbf{d}\|_{L^2(\Omega_S)}^2\right),$$

denote the kinetic and elastic energy of the coupled problem, respectively, and the term $D(t)$ captures viscous dissipation in the fluid:

$$D(t) := \|\mathbf{D}(\mathbf{u})\|_{L^2(\Omega_F(t))}^2. \qquad (1.105)$$

The constant $C(P_{in}(t), P_{out}(t)))$ depends only on the inlet and outlet pressure data, which are both functions of time.

1.6.3 The ALE formulation and Lie splitting

First order ALE formulation

As mentioned earlier, since we consider nonlinear coupling between the fluid and structure, the fluid domain changes in time. To prove the existence of a weak solution to (91)-(102) it is convenient to map the fluid domain onto a fixed domain Ω_F. The structural problems are already defined on fixed domains since they are formulated in the Lagrangian framework. We map our fluid domain $\Omega_F(t)$ onto Ω_F by using an Arbitrary Lagrangian-Eulerian (ALE) mapping [19, 85, 54, 131, 140]. We remark here that in our problem it is not convenient to use Lagrangian formulation for the fluid sub-problem, as is done in e.g., [46, 34, 101], since, in our problem, the fluid domain consists of a fixed, control volume of a cylinder, with prescribed inlet and outlet pressure data, which does not follow Largangian flow.

We begin by defining a family of ALE mappings A_η parameterized by η:

$$A_\eta(t) : \Omega_F \to \Omega_F(t), \quad A_\eta(t)(\tilde{z}, \tilde{r}) := \begin{pmatrix} \tilde{z} \\ (1 + \eta(t, \tilde{z}))\tilde{r} \end{pmatrix}, \quad (\tilde{z}, \tilde{r}) \in \Omega_F, \quad (1.106)$$

where $(\tilde{z}, \tilde{r})$ denote the coordinates in the reference domain $\Omega_F = (0, 1) \times (0, 1)$. The mapping $A_\eta(t)$ is a bijection, and its Jacobian is given by

$$|\det \nabla A_\eta(t)| = |1 + \eta(t, \tilde{z})|. \quad (1.107)$$

Composite functions with the ALE mapping will be denoted by

$$\mathbf{u}^\eta(t, .) = \mathbf{u}(t, .) \circ A_\eta(t) \quad \text{and} \quad p^\eta(t, .) = p(t, .) \circ A_\eta(t). \quad (1.108)$$

The derivatives of composite functions satisfy:

$$\partial_t \mathbf{u} = \partial_t \mathbf{u}^\eta - (\mathbf{w}^\eta \cdot \nabla^\eta)\mathbf{u}^\eta, \quad \nabla \mathbf{u} = \nabla^\eta \mathbf{u}^\eta, \quad (1.109)$$

where the ALE domain velocity, $\mathbf{w}^\eta$, and the transformed gradient, ∇^η, are given by:

$$\mathbf{w}^\eta = \partial_t \eta \tilde{r} \mathbf{e}_r, \quad \nabla^\eta = \begin{pmatrix} \partial_{\tilde{z}} - \tilde{r} \dfrac{\partial_z \eta}{1 + \eta} \partial_{\tilde{r}} \\ \dfrac{1}{1 + \eta} \partial_{\tilde{r}} \end{pmatrix}. \quad (1.110)$$

One can see that $\nabla^\eta \mathbf{v} = \nabla \mathbf{v}(\nabla A_\eta)^{-1}$. For the purposes of the existence proof we also introduce the following notation:

$$\sigma^\eta = -p^\eta \mathbf{I} + 2\mathbf{D}^\eta(\mathbf{u}^\eta), \quad \mathbf{D}^\eta(\mathbf{u}^\eta) = \frac{1}{2}(\nabla^\eta \mathbf{u}^\eta + (\nabla^\eta)^\tau \mathbf{u}^\eta).$$

We are now ready to rewrite problem (91)-(102) in ALE formulation. However, before we do that, we will make one more important step in our strategy to prove the existence of a weak solution to (91)-(102). Namely, as mentioned earlier, we

would like to "solve" the coupled FSI problem by approximating the problem using the time-discretization via Lie operator splitting. Since Lie operator splitting is defined for systems that are first-order in time, see Section 0.5.3, we have to replace the second-order time-derivatives of η and $\mathbf{d}$, with the first-order time-derivatives of the thin and thick structure velocities, respectively. In Section 0.5.3 we use the kinematic coupling condition (62) to achieve this goal. The kinematic coupling condition states that the fluid-structure interface velocity is equal to the normal trace of the fluid velocity on $\Gamma_\eta(t)$, and so we will introduce a new variable, v, to denote this trace, and replace $\partial_t \eta$ by v **everywhere** in the structure equation. We also introduce another new variable $\mathbf{V} = \partial_t \mathbf{d}$ which denotes the thick structure velocity. This enables us to rewrite problem (91)-(102) as a first-order system in time.

Thus, the ALE formulation of problem (91)-(102), defined on the reference domain Ω_F, and written as a first-order system in time, is given by the following (we drop the superscript η in $\mathbf{u}^\eta$ to simplify notation):

Find $\mathbf{u}(t, \tilde{z}, \tilde{r}), p(t, \tilde{z}, \tilde{r}), \eta(t, \tilde{z}), \, v(t, \tilde{z}), \, \mathbf{d}(t, \tilde{z})$ *and* $\mathbf{V}(t, \tilde{z})$ *such that*

$$\left. \begin{aligned} \partial_t \mathbf{u} + ((\mathbf{u} - \mathbf{w}^\eta) \cdot \nabla^\eta)\mathbf{u} &= \nabla^\eta \cdot \sigma^\eta, \\ \nabla^\eta \cdot \mathbf{u} &= 0, \end{aligned} \right\} \text{in } (0,T) \times \Omega_F, \qquad (1.111)$$

$$\left. \begin{aligned} u_r &= 0, \\ \partial_r u_z &= 0 \end{aligned} \right\} \text{on } (0,T) \times \Gamma_b, \qquad (1.112)$$

$$\left. \begin{aligned} p + \tfrac{1}{2}|u|^2 &= P_{in/out}(t), \\ u_r &= 0, \end{aligned} \right\} \text{on } (0,T) \times \Gamma_{in/out}, \qquad (1.113)$$

$$\left. \begin{aligned} \mathbf{u} &= v\mathbf{e}_r, \\ \mathbf{d} &= \eta\mathbf{e}_r, \\ \partial_t \eta &= v, \\ \partial_t v - \partial_z^2 \eta &= -J\sigma\mathbf{n} \cdot \mathbf{e}_r + \mathbf{S}\mathbf{e}_r \cdot \mathbf{e}_r \end{aligned} \right\} \text{on } (0,T) \times (0,1), \qquad (1.114)$$

$$\left. \begin{aligned} \partial_t \mathbf{d} &= \mathbf{V}, \\ \partial_t \mathbf{V} &= \nabla \cdot \mathbf{S}, \end{aligned} \right\} \text{ on } \Omega_S, \qquad (1.115)$$

$$\begin{aligned} \eta &= 0 \text{ on } (0,T) \times \partial\Gamma, \\ \mathbf{d} &= 0 \text{ on } (0,T) \times \Gamma_{in/out}^s \end{aligned} \qquad (1.116)$$

$$\mathbf{S}\mathbf{e}_r = 0 \text{ on } (0,T) \times \Gamma_{ext}. \qquad (1.117)$$

$$\mathbf{u}(0,.) = \mathbf{u}_0, \eta(0,.) = \eta_0, v(0,.) = v_0, \mathbf{d}(0,.) = \mathbf{d}_0, \mathbf{V}(0,.) = \mathbf{V}_0 \quad \text{at} \quad t = 0. \qquad (1.118)$$

This defines a parabolic-hyperbolic-hyperbolic nonlinear moving boundary problem. The nonlinearity appears in the equations (111), and in the coupling conditions (114) where the fluid quantities are evaluated at the deformed fluid-structure

interface $\eta(t, z)$. Parabolic features are associated with the fluid problem (111)-(113), while hyperbolic features come from the 2D equations of elasticity, and from the 1D wave equation modeling the fluid-structure interface, described by the last equation in (114).

The operator splitting scheme

To prove the existence of a weak solution to (111)-(118) we use the time-discretization via operator splitting, see Section 0.5.3. We apply the splitting strategy, described in Section 0.5.3, to separate the fluid sub-problem from the structure sub-problem.

Problem A1: The structure elastodynamics problem. In this step we solve an elastodynamics problem for the location of the multi-layered cylindrical wall. The problem is driven only by the initial data, i.e., the initial boundary velocity, taken from the previous time step as the trace of the fluid velocity at the fluid-structure interface. The fluid velocity $\mathbf{u}$ remains unchanged in this step. More precisely, the problem reads:

Given $(\mathbf{u}^n, \eta^n, v^n, \boldsymbol{d}^n, \boldsymbol{V}^n)$ *from the previous time step, find* $(\mathbf{u}, v, \eta, \boldsymbol{V}, \boldsymbol{d})$ *such that:*

$$\partial_t \mathbf{u} = 0, \qquad \qquad in\ (t_n, t_{n+1}) \times \Omega_F,$$

$$\left.\begin{array}{rcl} \partial_t \mathbf{V} & = & \nabla \cdot \mathbf{S}, \\ \partial_t \boldsymbol{d} & = & \mathbf{V} \end{array}\right\} \qquad in\ (t_n, t_{n+1}) \times \Omega_S, \qquad (1.119)$$

$$\begin{array}{rl} \boldsymbol{d} = 0 & on\ \Gamma^s_{in/out}, \\ \mathbf{S}\mathbf{e}_r = 0 & on\ (t_n, t_{n+1}) \times \Gamma_{ext}, \end{array}$$

$$\left.\begin{array}{rcl} \boldsymbol{d} & = & \eta \mathbf{e}_r \\ \partial_t v - \partial_z^2 \eta & = & \mathbf{S}\mathbf{e}_r \cdot \mathbf{e}_r, \\ \partial_t \eta & = & v \\ \eta(0) = \eta(1) = 0, \end{array}\right\}$$

$$\begin{array}{l} on\ (t_n, t_{n+1}) \times (0, 1), \\ on\ (t_n, t_{n+1}) \times (0, 1), \qquad (1.120) \end{array}$$

with $\mathbf{u}(t_n) = \mathbf{u}^n$, $\eta(t_n) = \eta^n$, $v(t_n) = v^n$, $\mathbf{d}(t_n) = \mathbf{d}^n$, $\mathbf{V}(t_n) = \mathbf{V}^n$.
Then set $\mathbf{u}^{n+\frac{1}{2}} = \mathbf{u}(t_{n+1})$, $\eta^{n+\frac{1}{2}} = \eta(t_{n+1})$, $v^{n+\frac{1}{2}} = v(t_{n+1})$, $\mathbf{d}^{n+\frac{1}{2}} = \mathbf{d}(t_{n+1})$, $\mathbf{V}^{n+\frac{1}{2}} = \mathbf{V}(t_{n+1})$.

Problem A2: The fluid problem. In this step we solve the Navier-Stokes equations coupled with structure inertia through a "Robin-type" boundary condition on Γ (lines 5 and 6 in (121) below). The kinematic coupling condition is implicitly satisfied. The structure displacement remains unchanged. With a slight abuse of notation, the problem can be written as follows:

Find $(\mathbf{u}, v, \eta, \boldsymbol{V}, \boldsymbol{d})$ *such that:*

$$\partial_t \eta = 0 \qquad\qquad on\ (t_n, t_{n+1}) \times (0,1),$$

$$\partial_t \mathbf{d} = 0 \qquad\qquad on\ (t_n, t_{n+1}) \times \Omega_S,$$

$$\left.\begin{array}{rcl} \partial_t \mathbf{u} + ((\mathbf{u}^n - \mathbf{w}^{\eta^{n+\frac{1}{2}}}) \cdot \nabla^{\eta^n})\mathbf{u} &=& \nabla^{\eta^n} \cdot \sigma^{\eta^n} \\ \nabla^{\eta^n} \cdot \mathbf{u} &=& 0 \end{array}\right\} \quad in\ (t_n, t_{n+1}) \times \Omega_F,$$

$$\left.\begin{array}{rcl} \partial_t v &=& -J\sigma \mathbf{n} \cdot \mathbf{e}_r \\ \mathbf{u} &=& v\mathbf{e}_r \end{array}\right\} \quad on\ (t_n, t_{n+1}) \times (0,1) \qquad (1.121)$$

$$\left.\begin{array}{rcl} u_r &=& 0 \\ \partial_r u_z &=& 0 \end{array}\right\} \quad on\ (t_n, t_{n+1}) \times \Gamma_b,$$

$$\left.\begin{array}{rcl} p + \frac{\rho_f}{2}|u|^2 &=& P_{in/out}(t) \\ u_r &=& 0 \end{array}\right\} \quad on\ (t_n, t_{n+1}) \times \Gamma_{in/out},$$

with $\mathbf{u}(t_n, .) = \mathbf{u}^{n+\frac{1}{2}}$, $\eta(t_n, .) = \eta^{n+\frac{1}{2}}$, $v(t_n, .) = v^{n+\frac{1}{2}}$, $\mathbf{d}(t_n, .) = \mathbf{d}^{n+\frac{1}{2}}$, $\mathbf{V}(t_n, .) = \mathbf{V}^{n+\frac{1}{2}}$.
Then set $\mathbf{u}^{n+1} = \mathbf{u}(t_{n+1})$, $\eta^{n+1} = \eta(t_{n+1})$, $v^{n+1} = v(t_{n+1})$, $\mathbf{d}^{n+1} = \eta(t_{n+1})$, $\mathbf{V}^{n+1} = \mathbf{V}(t_{n+1})$.

Notice that, since in this step η does not change, this problem is linear.

In numerical simulations, one can use the ALE mapping A_{η^n} to "transform" only the time derivative term $\partial_t \mathbf{u}$ onto the fixed domain Ω_F while the rest of the PDE is discretized on the current domain $\Omega_F(t^n)$. This gives rise to the domain velocity term $\mathbf{w}$ in the equations, but avoids the un-necessary calculation of the transformed gradient ∇^{η^n}. See equation (195a) in Section 0.7.3, and **Problem A2(b)** in Section 0.7.5. For the purposes of our proof, we will, however, remain working on the fixed, reference domain Ω_F.

It is important to notice that in Problem A2, the problem is "linearized" around the previous location of the boundary, i.e., we work with the domain determined by η^n, and not by $\eta^{n+1/2}$. This is in direct relation with the implementation of the numerical scheme studied in [19, 29]. However, we also notice that ALE velocity, $w^{n+\frac{1}{2}}$, is taken from the just calculated Problem A1! This choice is *crucial* for obtaining a semi-discrete version of an energy inequality, which will be discussed in Section 0.6.5.

Next we use the splitting scheme described above to define approximate solutions of (111)-(118) (or equivalently of problem (91)-(102)) and show that the approximate solutions converge to a weak solution, as $\Delta t \to 0$.

1.6.4 Weak solutions

Notation and function spaces

Notation. To define weak solutions of the moving-bounday problem (91)-(102) and of the moving-boundary problem (111)-(118) defined on a fixed domain, the following notation will be useful:

- a_S will denote the bilinear form associated with the elastic energy of the thick structure:

$$a_S(\mathbf{d}, \boldsymbol{\psi}) = \int_{\Omega_S} \left(2\mathbf{D}(\mathbf{d}) : \mathbf{D}(\boldsymbol{\psi}) + (\nabla \cdot \mathbf{d}) \cdot (\nabla \cdot \boldsymbol{\psi}) \right). \tag{1.122}$$

Here ":" denotes the scalar product defined in (7).

- b will denote the following trilinear form corresponding to the (symmetrized) nonlinear advection term in the Navier-Stokes equations:

$$b(t, \mathbf{u}, \mathbf{v}, \mathbf{w}) = \frac{1}{2} \int_{\Omega_F(t)} (\mathbf{u} \cdot \nabla)\mathbf{v} \cdot \mathbf{w} - \frac{1}{2} \int_{\Omega_F(t)} (\mathbf{u} \cdot \nabla)\mathbf{w} \cdot \mathbf{v}. \tag{1.123}$$

- The linear functional which associates the inlet and outlet dynamic pressure boundary data to a test function $\mathbf{v}$ will be denoted by:

$$\langle F(t), \mathbf{v} \rangle_{\Gamma_{in/out}} = P_{in}(t) \int_{\Gamma_{in}} v_z - P_{out}(t) \int_{\Gamma_{out}} v_z.$$

Function spaces. For the fluid velocity we would like to work with the classical function space associated with weak solutions of the Navier-Stokes equations. This, however, requires some additional consideration. Namely, since our thin structure is governed by the linear wave equation, lacking the bending rigidity terms, weak solutions cannot be expected to be Lipschitz-continuous. Indeed, from the energy inequality (103) we only have $\eta \in H^1(0, 1)$, and from Sobolev embedding we get that $\eta \in C^{0,1/2}(0, 1)$, which means that $\Omega_F(t)$ is not necessarily a Lipshitz domain. However, $\Omega_F(t)$ is locally a sub-graph of a Hölder continuous function. In that case one can define "Lagrangian" trace

$$\begin{aligned} &\gamma_{\Gamma(t)} : C^1(\overline{\Omega_F(t)}) \to C(\Gamma), \\ &\gamma_{\Gamma(t)} : v \mapsto v(t, z, r + \eta(t, z)). \end{aligned} \tag{1.124}$$

Furthermore, it was shown in [32, 78, 120] that the trace operator $\gamma_{\Gamma(t)}$ can be extended by continuity to a linear operator from $H^1(\Omega_F(t))$ to $H^s(\Gamma)$, $0 \le s < \frac{1}{4}$. For a precise statement of the results about "Lagrangian" trace, see Theorem 0.6.2. Now, the velocity solution space can be defined in the following way:

$$\begin{aligned} V_F(t) &= \{\mathbf{u} = (u_z, u_r) \in C^1(\overline{\Omega_F(t)})^2 : \nabla \cdot \mathbf{u} = 0, \\ &\quad u_z = 0 \text{ on } \Gamma(t), \; u_r = 0 \text{ on } \partial\Omega_F(t) \setminus \Gamma(t)\}, \\ \mathcal{V}_F(t) &= \overline{V_F(t)}^{H^1(\Omega_F(t))}. \end{aligned} \tag{1.125}$$

Using the fact that $\Omega_F(t)$ is locally a sub-graph of a Hölder continuous function we can get the following characterization of the velocity solution space $\mathcal{V}_F(t)$ (see [32, 78]):

$$\begin{aligned} \mathcal{V}_F(t) &= \{\mathbf{u} = (u_z, u_r) \in H^1(\Omega_\eta(t))^2 : \nabla \cdot \mathbf{u} = 0, \\ &\quad u_z = 0 \text{ on } \Gamma(t), \; u_r = 0 \text{ on } \partial\Omega_\eta(t) \setminus \Gamma(t)\}. \end{aligned} \tag{1.126}$$

The function space associated with weak solutions of the 1D linear wave equation and the thick wall are given, respectively, by

$$\mathcal{V}_W = H_0^1(0,1), \tag{1.127}$$

$$\mathcal{V}_S = \{\boldsymbol{\psi} = (\psi_z, \psi_r) \in H^1(\Omega_S)^2 : \psi_z = 0 \text{ on } \Gamma, \ \boldsymbol{\psi} = 0 \text{ on } \Gamma_{in/out}^s\}. \tag{1.128}$$

Motivated by the energy inequality we also define the corresponding evolution spaces for the fluid and structure sub-problems, respectively:

$$\mathcal{W}_F(0,T) = L^\infty(0,T; L^2(\Omega_F(t))) \cap L^2(0,T; \mathcal{V}_F(t)), \tag{1.129}$$

$$\mathcal{W}_W(0,T) = W^{1,\infty}(0,T; L^2(0,1)) \cap L^2(0,T; \mathcal{V}_W), \tag{1.130}$$

$$\mathcal{W}_S(0,T) = W^{1,\infty}(0,T; L^2(\Omega_S)) \cap L^2(0,T; \mathcal{V}_S). \tag{1.131}$$

Finally, we are in a position to define the solution space for the coupled fluid-multi-layered-structure interaction problem. This space involves the kinematic coupling condition, which is enforced in strong sense. The dynamic coupling condition will be enforced in weak sense, through integration by parts in the weak formulation of the problem. Thus, we define

$$\mathcal{W}(0,T) = \{(\mathbf{u}, \eta, \boldsymbol{d}) \in \mathcal{W}_F(0,T) \times \mathcal{W}_W(0,T) \times \mathcal{W}_S(0,T) : \\ \mathbf{u}(t,z,1+\eta(t,z)) = \partial_t \eta(t,z)\mathbf{e}_r, \ \boldsymbol{d}(t,z,1) = \eta(t,z)\mathbf{e}_r\}. \tag{1.132}$$

Equality $\mathbf{u}(t,z,1+\eta(t,z)) = \partial_t\eta(t,z)\mathbf{e}_r$ is taken in the sense defined in [32, 120]. The corresponding test space will be denoted by

$$\mathcal{Q}(0,T) = \{(\mathbf{q}, \psi, \boldsymbol{\psi}) \in C_c^1([0,T]; \mathcal{V}_F \times \mathcal{V}_W \times \mathcal{V}_S) : \\ \mathbf{q}(t,z,1+\eta(t,z)) = \psi(t,z)\mathbf{e}_r, \boldsymbol{\psi}(t,z,1) = \psi(t,z)\mathbf{e}_r\}. \tag{1.133}$$

Notice the coupling conditions in the test space that are enforced at the fluid-structure interface.

Weak solutions for the problem defined on the moving domain

We are now in a position to define weak solutions of fluid-multi-layered structure interaction problem, defined on the moving domain $\Omega_F(t)$.

Definition 1.6.1. *We say that* $(\mathbf{u}, \eta, \boldsymbol{d}) \in \mathcal{W}(0,T)$ *is a weak solution of problem* (91)-(102) *if for every* $(\mathbf{q}, \psi, \boldsymbol{\psi}) \in \mathcal{Q}(0,T)$ *the following equality holds:*

$$-\int_0^T \int_{\Omega_F(t)} \mathbf{u} \cdot \partial_t \mathbf{q} + \int_0^T b(t, \mathbf{u}, \mathbf{u}, \mathbf{q}) + 2\int_0^T \int_{\Omega_F(t)} \mathbf{D}(\mathbf{u}) : \mathbf{D}(\mathbf{q}) - \frac{1}{2}\int_0^T \int_0^1 (\partial_t \eta)^2 \psi$$

$$-\int_0^T \int_0^1 \partial_t \eta \partial_t \psi + \int_0^T \int_0^1 \partial_z \eta \partial_z \psi - \int_0^T \int_{\Omega_S} \partial_t \boldsymbol{d} \cdot \partial_t \boldsymbol{\psi} + \int_0^T a_S(\boldsymbol{d}, \boldsymbol{\psi})$$

$$= \int_0^T \langle F(t), \mathbf{q}\rangle_{\Gamma_{in/out}} + \int_{\Omega_{\eta_0}} \mathbf{u}_0 \cdot \mathbf{q}(0) + \int_0^1 v_0 \psi(0) + \int_{\Omega_S} \mathbf{V}_0 \cdot \boldsymbol{\psi}(0). \tag{1.134}$$

In deriving the weak formulation we used integration by parts, and the following equalities which hold for smooth functions:

$$\int_{\Omega_F(t)} (\mathbf{u} \cdot \nabla)\mathbf{u} \cdot \mathbf{q} = \frac{1}{2}\int_{\Omega_F(t)} (\mathbf{u} \cdot \nabla)\mathbf{u} \cdot \mathbf{q} - \frac{1}{2}\int_{\Omega_F(t)} (\mathbf{u} \cdot \nabla)\mathbf{q} \cdot \mathbf{u}$$

$$+ \frac{1}{2}\int_0^1 (\partial_t \eta)^2 \psi \pm \frac{1}{2}\int_{\Gamma_{out/in}} |u_r|^2 v_r,$$

$$\int_0^T \int_{\Omega_F(t)} \partial_t \mathbf{u} \cdot \mathbf{q} = -\int_0^T \int_{\Omega_F(t)} \mathbf{u} \cdot \partial_t \mathbf{q} - \int_{\Omega_{\eta_0}} \mathbf{u}_0 \cdot \mathbf{q}(0) - \int_0^T \int_0^1 (\partial_t \eta)^2 \psi.$$

Weak solutions for the problem defined on a fixed, reference domain

Since most of the analysis will be performed on the problem mapped to Ω_F, we rewrite the above definition in terms of Ω_F using the ALE mapping $A_\eta(t)$ defined in (106). For this purpose, the following notation will be useful. We define the transformed trilinear functional b^η:

$$b^\eta(\mathbf{u}, \mathbf{u}, \mathbf{q}) := \frac{1}{2}\int_{\Omega_F} (1+\eta)((\mathbf{u}-\mathbf{w}^\eta) \cdot \nabla^\eta)\mathbf{u} \cdot \mathbf{q} - \frac{1}{2}\int_{\Omega_F} (1+\eta)((\mathbf{u}-\mathbf{w}^\eta) \cdot \nabla^\eta)\mathbf{q} \cdot \mathbf{u}, \tag{1.135}$$

where $1 + \eta$ is the Jacobian of the ALE mapping, calculated in (107). Notice that we have included the ALE domain velocity $\mathbf{w}^\eta$ into b^η.

It is important to point out that the transformed fluid velocity $\mathbf{u}^\eta$ is not divergence-free anymore. Rather, it satisfies the transformed divergence-free condition $\nabla^\eta \cdot \mathbf{u}^\eta = 0$. Furthermore, since η is not a Lipschitz function, the ALE mapping is not necessarily a Lipschitz function either, and, as a result, $\mathbf{u}^\eta$ is not necessarily an H^1 function on Ω_F. Therefore we need to redefine the function spaces for the fluid velocity by introducing

$$\mathcal{V}_F^\eta = \{\mathbf{u}^\eta : \mathbf{u} \in \mathcal{V}_F(t)\},$$

where $\mathbf{u}^\eta$ is defined in (108). Under the assumption $1 + \eta(z) > 0$, $z \in [0,1]$, the following defines a scalar product on $\mathcal{V}_F^\eta$:

$$(\mathbf{u}^\eta, \mathbf{v}^\eta)_{\mathcal{V}_F^\eta} = \int_{\Omega_F} (1+\eta)\big(\mathbf{u}^\eta \cdot \mathbf{v}^\eta + \nabla^\eta \mathbf{u}^\eta : \nabla^\eta \mathbf{v}^\eta\big) = (\mathbf{u}, \mathbf{v})_{H^1(\Omega_F(t))}.$$

Therefore, $\mathbf{u} \mapsto \mathbf{u}^\eta$ is an isometric isomorphism between $\mathcal{V}_F(t)$ and $\mathcal{V}_F^\eta$, so $\mathcal{V}_F^\eta$ is also a Hilbert space. The function spaces $\mathcal{W}_F^\eta(0,T)$ and $\mathcal{W}^\eta(0,T)$ are defined as before, but with $\mathcal{V}_F^\eta$ instead $\mathcal{V}_F(t)$. More precisely:

$$\mathcal{W}_F^\eta(0,T) = L^\infty(0,T; L^2(\Omega_F)) \cap L^2(0,T; \mathcal{V}_F^\eta(t)), \tag{1.136}$$

$$\mathcal{W}^\eta(0,T) = \{(\mathbf{u}, \eta, \boldsymbol{d}) \in \mathcal{W}_F^\eta(0,T) \times \mathcal{W}_W(0,T) \times \mathcal{W}_S(0,T) : \\ \mathbf{u}(t,z,1) = \partial_t \eta(t,z)\mathbf{e}_r, \ \eta(t,z) = \boldsymbol{d}(t,z,1)\}. \tag{1.137}$$

The corresponding test space is defined by

$$\mathcal{Q}^\eta(0,T) = \{(\mathbf{q}, \psi, \boldsymbol{\psi}) \in C^1_c([0,T); \mathcal{V}^\eta_F \times \mathcal{V}_W \times \mathcal{V}_S) :$$
$$\mathbf{q}(t,z,1) = \psi(t,z)\mathbf{e}_r, \boldsymbol{\psi}(t,z,1) = \psi(t,z)\mathbf{e}_r\}. \qquad (1.138)$$

Definition 1.6.2. *We say that* $(\mathbf{u}, \eta, \boldsymbol{d}) \in \mathcal{W}^\eta(0,T)$ *is a weak solution of problem* (111)-(118) *defined on the reference domain* Ω_F, *if for every* $(\mathbf{q}, \psi, \boldsymbol{\psi}) \in \mathcal{Q}^\eta(0,T)$ *the following equality holds:*

$$-\int_0^T \int_{\Omega_F} (1+\eta)\mathbf{u} \cdot \partial_t \mathbf{q} + \int_0^T b^\eta(\mathbf{u}, \mathbf{u}, \mathbf{q}) + 2\int_0^T \int_{\Omega_F} (1+\eta)\mathbf{D}^\eta(\mathbf{u}) : \mathbf{D}^\eta(\mathbf{q})$$

$$-\frac{1}{2}\int_0^T \int_{\Omega_F} (\partial_t \eta)\mathbf{u} \cdot \mathbf{q} - \int_0^T \int_0^1 \partial_t \eta \partial_t \psi + \int_0^T \int_0^1 \partial_z \eta \partial_z \psi$$

$$-\int_0^T \int_{\Omega_S} \partial_t \boldsymbol{d} \cdot \partial_t \boldsymbol{\psi} + \int_0^T a_S(\boldsymbol{d}, \boldsymbol{\psi})$$

$$= \int_0^T \langle F(t), \mathbf{q} \rangle_{\Gamma_{in/out}} + \int_{\Omega_{\eta_0}} \mathbf{u}_0 \cdot \mathbf{q}(0) + \int_0^1 v_0 \psi(0) + \int_{\Omega_S} \mathbf{V}_0 \cdot \boldsymbol{\psi}(0).$$
$$(1.139)$$

To see that this is consistent with the weak solution defined in Definition 0.6.1, we present the main steps in the transformation of the first integral on the left hand-side in (134), responsible for the fluid kinetic energy. Namely, we formally calculate:

$$-\int_{\Omega_F(t)} \mathbf{u} \cdot \partial_t \mathbf{q} = -\int_{\Omega_F} (1+\eta)\mathbf{u}^\eta \cdot (\partial_t \mathbf{q} - (\mathbf{w}^\eta \cdot \nabla^\eta)\mathbf{q}) = -\int_{\Omega_F} (1+\eta)\mathbf{u}^\eta \cdot \partial_t \mathbf{q}$$

$$+\frac{1}{2}\int_{\Omega_F} (1+\eta)(\mathbf{w}^\eta \cdot \nabla^\eta)\mathbf{q} \cdot \mathbf{u}^\eta + \frac{1}{2}\int_{\Omega_F} (1+\eta)(\mathbf{w}^\eta \cdot \nabla^\eta)\mathbf{q} \cdot \mathbf{u}^\eta.$$

In the last integral on the right hand-side we use the definition of $\mathbf{w}^\eta$ and of ∇^η, given in (110), to obtain

$$\int_{\Omega_F} (1+\eta)(\mathbf{w}^\eta \cdot \nabla^\eta)\mathbf{q} \cdot \mathbf{u}^\eta = \int_{\Omega_F} \partial_t \eta \; \tilde{r} \; \partial_{\tilde{r}}\mathbf{q} \cdot \mathbf{u}^\eta.$$

Using integration by parts with respect to r, keeping in mind that η does not depend on r, we obtain

$$-\int_{\Omega_F(t)} \mathbf{u} \cdot \partial_t \mathbf{q} = -\int_{\Omega_F} (1+\eta)\mathbf{u}^\eta \cdot (\partial_t \mathbf{q} - (\mathbf{w}^\eta \cdot \nabla^\eta)\mathbf{q}) = -\int_{\Omega_F} (1+\eta)\mathbf{u}^\eta \cdot \partial_t \mathbf{q}$$

$$+\frac{1}{2}\int_{\Omega_F} (1+\eta)(\mathbf{w}^\eta \cdot \nabla^\eta)\mathbf{q} \cdot \mathbf{u}^\eta - \frac{1}{2}\int_{\Omega_F} (1+\eta)(\mathbf{w}^\eta \cdot \nabla^\eta)\mathbf{u}^\eta \cdot \mathbf{q} - \frac{1}{2}\int_{\Omega_F} \partial_t \eta \mathbf{u}^\eta \cdot \mathbf{q} + \frac{1}{2}\int_0^1 (\partial_t \eta)^2 \psi,$$

By using this identity in (134), and by recalling the definitions for b and b^η, we obtain exactly the weak form (139).

In the remainder of this Section we will be working on the fluid-multi-layered structure interaction problem defined on the fixed domain Ω_F, satisfying the weak formulation presented in Definition 0.6.2. For brevity of notation, since no confusion is possible, we omit the superscript "tilde" which is used to denote the coordinates of points in Ω_F.

1.6.5 Approximate solutions

In this section we use the Lie operator splitting scheme and semi-discretization to define a sequence of approximate solutions of the FSI problem (111)-(118). Each of the sub-problems defined by the Lie splitting in Section 0.6.3 as Problem A1 and Problem A2, will be discretized in time using the Backward Euler scheme. This approach defines a time step, which will be denoted by Δt, and a number of time sub-intervals $N \in \mathbb{N}$, so that

$$(0,T) = \cup_{n=0}^{N-1}(t^n, t^{n+1}), \quad t^n = n\Delta t, \ n = 0, ..., N-1.$$

For every subdivision containing $N \in \mathbb{N}$ sub-intervals, the vector of unknown approximate solutions will be denoted by

$$\mathbf{X}_N^{n+\frac{i}{2}} = \left(\mathbf{u}_N^{n+\frac{i}{2}}, v_N^{n+\frac{i}{2}}, \eta_N^{n+\frac{i}{2}}, \mathbf{V}_N^{n+\frac{i}{2}}, \mathbf{d}_N^{n+\frac{i}{2}}\right)^T, n = 0, 1, \ldots, N-1, \ i = 1, 2,$$
(1.140)

where $i = 1, 2$ denotes the solution of Problem A1 or A2, respectively. The initial condition will be denoted by $\mathbf{X}^0 = (\mathbf{u}_0, v_0, \eta_0, \mathbf{V}_0, \mathbf{d}_0)^T$.

The semi-discretization and the splitting of the problem will be performed in such a way that the semi-discrete version of the energy inequality (103) is preserved at every time step. This is a crucial ingredient for the existence proof.

The semi-discrete versions of the kinetic and elastic energy (104), and of dissipation (105) are defined by the following:

$$E_{kin,N}^{n+\frac{i}{2}} = \frac{1}{2}\left(\int_{\Omega_F}(1+\eta^{n-1+i})|\mathbf{u}_N^{n+\frac{i}{2}}|^2 + \|v_N^{n+\frac{i}{2}}\|_{L^2(0,1)}^2 + \|\mathbf{V}_N^{n+\frac{i}{2}}\|_{L^2(\Omega_S)}^2\right),$$
$$E_{el,N}^{n+1} = \frac{1}{2}\left(\|\partial_z\eta_N^{n+\frac{1}{2}}\|_{L^2(0,1)}^2 + 2\|\mathbf{D}(\mathbf{d}_N^{n+\frac{1}{2}})\|_{L^2(\Omega_S)}^2 + \|\nabla\cdot\mathbf{d}_N^{n+\frac{1}{2}}\|_{L^2(\Omega_S)}^2\right),$$
$$E_N^{n+\frac{i}{2}} = E_{kin,N}^{n+\frac{i}{2}} + E_{el,N}^{n+1},$$
(1.141)

$$D_N^{n+1} = \Delta t\int_{\Omega_F}(1+\eta^n)|D^{\eta^n}(\mathbf{u}_N^{n+1})|^2, \ n = 0, \ldots, N-1, \ i = 0, 1. \quad (1.142)$$

Throughout the rest of this section we fix the time step Δt, i.e., we keep $N \in \mathbb{N}$ fixed, and study the semi-discretized sub-problems defined by the Lie splitting. To simplify notation, we omit the subscript N and write $(\mathbf{u}^{n+\frac{i}{2}}, v^{n+\frac{i}{2}}, \eta^{n+\frac{i}{2}}, \mathbf{V}^{n+\frac{i}{2}}, \mathbf{d}^{n+\frac{i}{2}})$ instead of $(\mathbf{u}_N^{n+\frac{i}{2}}, v_N^{n+\frac{i}{2}}, \eta_N^{n+\frac{i}{2}}, \mathbf{V}_N^{n+\frac{i}{2}}, \mathbf{d}_N^{n+\frac{i}{2}})$.

Semi-discretization of Problem A1

In this step $\mathbf{u}$ does not change, and so

$$\mathbf{u}^{n+\frac{1}{2}} = \mathbf{u}^n.$$

Functions $(v^{n+\frac{1}{2}}, \eta^{n+\frac{1}{2}}, \mathbf{V}^{n+\frac{1}{2}}, \mathbf{U}^{n+\frac{1}{2}}) \in \mathcal{V}_W^2 \times \mathcal{V}_S^2$ define a weak solution of the semi-discretized Problem A1 if the following holds:

$$\boldsymbol{d}^{n+\frac{1}{2}}(z,1) = \eta^{n+\frac{1}{2}}(z,1)\mathbf{e}_r, \ z \in (0,1),$$

$$\frac{\boldsymbol{d}^{n+\frac{1}{2}} - \boldsymbol{d}^n}{\Delta t} = \mathbf{V}^{n+\frac{1}{2}}, \ \frac{\eta^{n+\frac{1}{2}} - \eta^n}{\Delta t} = v^{n+\frac{1}{2}},$$

$$\int_{\Omega_S} \frac{\mathbf{V}^{n+\frac{1}{2}} - \mathbf{V}^n}{\Delta t} \cdot \boldsymbol{\Psi} + \int_0^1 \frac{v^{n+\frac{1}{2}} - v^n}{\Delta t}\psi + a_S(\boldsymbol{d}^{n+\frac{1}{2}}, \boldsymbol{\Psi}) + \int_0^1 \partial_z \eta^{n+\frac{1}{2}}\partial_z \psi = 0,$$

$$(1.143)$$

for all $(\psi, \boldsymbol{\Psi}) \in \mathcal{V}_W \times \mathcal{V}_S$ such that $\boldsymbol{\Psi}(t,z,1) = \psi(t,z)$. The first equation enforces the kinematic coupling condition, the second row in (143) introduces the structure velocities, while the third equation corresponds to a weak form of the semi-discretized elastodynamics problem. Notice that we solve the thin and thick structure problems as one problem. The thin structure enters as a boundary condition for the thick structure problem.

Proposition 1.6.2. *For each fixed $\Delta t > 0$, problem (143) has a unique solution $(v^{n+\frac{1}{2}}, \eta^{n+\frac{1}{2}}, \mathbf{V}^{n+\frac{1}{2}}, \boldsymbol{d}^{n+\frac{1}{2}}) \in \mathcal{V}_W^2 \times \mathcal{V}_S^2$.*

Proof. First notice that Korn's inequality implies that the bilinear form a_S is coercive on $\mathcal{V}_S$. From here, the proof is a direct consequence of the Lax-Milgram Lemma applied to the weak form

$$\int_0^1 \eta^{n+\frac{1}{2}}\psi + \int_{\Omega_S} \boldsymbol{d}^{n+1} \cdot \boldsymbol{\Psi} + (\Delta t)^2 \Big(\int_0^1 \partial_z \eta \partial_z \psi + a_S(\boldsymbol{d}^{n+\frac{1}{2}}, \boldsymbol{\Psi}) \Big)$$

$$= \int_0^L (\Delta t v^n + \eta^n)\psi + \int_{\Omega_S} (\Delta t \mathbf{V}^n + \boldsymbol{d}^n) \cdot \boldsymbol{\Psi}, \ \forall (\psi, \boldsymbol{\Psi}) \in \{\mathcal{V}_W \times \mathcal{V}_S | \boldsymbol{\Psi}(t,z,1) = \psi(z,1)\},$$

which is obtained after a substitution of $v^{n+\frac{1}{2}}$ and $\mathbf{V}^{n+\frac{1}{2}}$ in the third equation in (143), by using the equations $(143)_2$.   □

Proposition 1.6.3. *For each fixed $\Delta t > 0$, solution of problem (143) satisfies the following discrete energy equality:*

$$E_{kin,N}^{n+\frac{1}{2}} + E_{el,N}^{n+1} + \frac{1}{2}\big(\|v^{n+\frac{1}{2}} - v^n\|_{L^2(0,1)}^2 + \|\mathbf{V}^{n+\frac{1}{2}} - \mathbf{V}^n\|_{L^2(\Omega_S)}^2$$

$$+\|\partial_z(\eta^{n+\frac{1}{2}} - \eta^n)\|_{L^2(0,1)}^2 + a_S(\boldsymbol{d}^{n+\frac{1}{2}} - \boldsymbol{d}^n, \boldsymbol{d}^{n+\frac{1}{2}} - \boldsymbol{d}^n)\big) = E_{kin,N}^n + E_{el,N}^n,$$

$$(1.144)$$

where the kinetic and elastic energy, $E_{kin,N}^n$, $E_{el,N}^n$, are defined in (141).

Proof. From the second row in (143) we immediately get

$$v^{n+\frac{1}{2}} = \frac{\eta^{n+\frac{1}{2}} - \eta^n}{\Delta t} \in \mathcal{V}_W, \quad \boldsymbol{V}^{n+\frac{1}{2}} = \frac{\boldsymbol{d}^{n+\frac{1}{2}} - \boldsymbol{d}^n}{\Delta t} \in \mathcal{V}_S.$$

Therefore, we can proceed as usual, by substituting the test functions in (143) with structure velocities. More precisely, we replace the test function $(\psi, \boldsymbol{\psi})$ by $(v^{n+\frac{1}{2}}, \boldsymbol{V}^{n+\frac{1}{2}})$ in the first term on the left hand-side, and then replace $(\psi, \boldsymbol{\psi})$ by $((\eta^{n+\frac{1}{2}} - \eta^n)/\Delta t, (\boldsymbol{d}^{n+\frac{1}{2}} - \boldsymbol{d}^n)/\Delta t)$ in the bilinear forms that correspond to the elastic energy. To deal with the terms $(v^{n+1/2} - v^n)v^{n+1/2}$, $(\eta^{n+1/2} - \eta^n)\eta^{n+1/2}$, $(\boldsymbol{V}^{n+1/2} - \boldsymbol{V}^n) \cdot \boldsymbol{V}^{n+1/2}$, and $(\boldsymbol{d}^{n+1/2} - \boldsymbol{d}^n) \cdot \boldsymbol{d}^{n+1/2}$, we use the algebraic identity $(a - b) \cdot a = \frac{1}{2}(|a|^2 + |a - b|^2 - |b|^2)$. After multiplying the entire equation by Δt, the third equation in (143) can be written as:

$$(\|v^{n+\frac{1}{2}}\|^2_{L^2(0,1)} + \|v^{n+\frac{1}{2}} - v^n\|^2_{L^2(0,1)}) + (\|\boldsymbol{V}^{n+\frac{1}{2}}\|^2_{L^2(\Omega_S)} + \|\boldsymbol{V}^{n+\frac{1}{2}} - \boldsymbol{V}^n\|^2_{L^2(\Omega_S)})$$

$$\|\partial_z \eta^{n+\frac{1}{2}}\|^2_{L^2(0,1)} + \|\partial_z(\eta^{n+\frac{1}{2}} - \partial_z \eta^n)\|^2_{L^2(0,1)} + a_S(\boldsymbol{d}^{n+\frac{1}{2}}, \boldsymbol{d}^{n+\frac{1}{2}})$$

$$+a_S(\boldsymbol{d}^{n+\frac{1}{2}} - \boldsymbol{d}^n, \boldsymbol{d}^{n+\frac{1}{2}} - \boldsymbol{d}^n) = \|v^n\|^2_{L^2(0,1)} + \|\boldsymbol{V}^n\|^2_{L^2(\Omega_S)} + \|\partial_z \eta^n\|^2_{L^2(0,1)} + a_S(\boldsymbol{d}^n, \boldsymbol{d}^n).$$

Since in this sub-problem $\mathbf{u}^{n+\frac{1}{2}} = \mathbf{u}^n$, we can add $\rho_f \int_{\Omega_F} (1 + \eta^n) \mathbf{u}^{n+1/2}$ on the left hand-side, and $\rho_f \int_{\Omega_F} (1 + \eta^n) \mathbf{u}^n$ on the right hand-side of the equation. Furthermore, displacements $\boldsymbol{d}^{n+\frac{1}{2}}$ and $\eta^{n+\frac{1}{2}}$ do not change in Problem A2 (see (145)), and so we can replace $\boldsymbol{d}^n$ and η^n on the right hand-side of the equation with $\boldsymbol{d}^{n-\frac{1}{2}}$ and $\eta^{n-\frac{1}{2}}$, respectively, to obtain exactly the energy equality (144). □

Semi-discretization of Problem A2

In this step η, $\boldsymbol{d}$ and $\boldsymbol{V}$ do not change, and so

$$\eta^{n+1} = \eta^{n+\frac{1}{2}}, \; \boldsymbol{d}^{n+1} = \boldsymbol{d}^{n+\frac{1}{2}}, \; \boldsymbol{V}^{n+1} = \boldsymbol{V}^{n+\frac{1}{2}}. \tag{1.145}$$

Then, define $(\mathbf{u}^{n+1}, v^{n+1}) \in \mathcal{V}_F^{\eta^n} \times L^2(0,1)$ to be a weak solution of Problem $A2$ (121) if the following holds for each $(\mathbf{q}, \psi) \in \mathcal{V}_F^{\eta^n} \times L^2(0,1)$ such that $\mathbf{q}_{|\Gamma} = \psi \mathbf{e}_r$, velocities $(\mathbf{u}^{n+1}, v^{n+1})$:

$$\int_\Omega (1 + \eta^n) \left(\frac{\mathbf{u}^{n+1} - \mathbf{u}^{n+\frac{1}{2}}}{\Delta t} \cdot \mathbf{q} + \frac{1}{2} \left[(\mathbf{u}^n - v^{n+\frac{1}{2}} r \mathbf{e}_r) \cdot \nabla^{\eta^n} \right] \mathbf{u}^{n+1} \cdot \mathbf{q} \right.$$

$$\left. - \frac{1}{2} \left[(\mathbf{u}^n - v^{n+\frac{1}{2}} r \mathbf{e}_r) \cdot \nabla^{\eta^n} \right] \mathbf{q} \cdot \mathbf{u}^{n+1} \right) + \frac{1}{2} \int_\Omega v^{n+\frac{1}{2}} \mathbf{u}^{n+1} \cdot \mathbf{q}$$

$$+ 2 \int_\Omega (1 + \eta^n) \mathbf{D}^{\eta^n}(\mathbf{u}) : \mathbf{D}^{\eta^n}(\mathbf{q}) \tag{1.146}$$

$$+ \rho_s h \int_0^1 \frac{v^{n+1} - v^{n+\frac{1}{2}}}{\Delta t} \psi = \left(P_{in}^n \int_0^1 (q_z)_{|z=0} - P_{out}^n \int_0^1 (q_z)_{|z=L} \right),$$

$$\text{with } \nabla^{\eta^n} \cdot \mathbf{u}^{n+1} = 0, \quad \mathbf{u}^{n+1}_{|\Gamma} = v^{n+1} \mathbf{e}_r,$$

where $P_{in/out}^n = \dfrac{1}{\Delta t} \displaystyle\int_{n\Delta t}^{(n+1)\Delta t} P_{in/out}(t)dt.$

The existence of a unique weak solution and energy estimate are given by the following proposition.

Proposition 1.6.4. *Let $\Delta t > 0$, and assume that η^n are such that $1 + \eta^n \geq R_{\min} > 0, n = 0, ..., N$. Then:*

1. *The fluid sub-problem defined by (146) has a unique weak solution $(\mathbf{u}^{n+1}, v^{n+1}) \in \mathcal{V}_F^{\eta^n} \times L^2(0,1)$;*

2. *Solution of problem (146) satisfies the following discrete energy inequality:*

$$
\begin{aligned}
E_{kin,N}^{n+1} + \frac{1}{2} \int_{\Omega_F} (1 + \eta^n)|\mathbf{u}^{n+1} - \mathbf{u}^n|^2 + \frac{1}{2}\|v^{n+1} - v^{n+\frac{1}{2}}\|_{L^2(0,1)}^2 \\
+ D_N^{n+1} \leq E_{kin,N}^{n+\frac{1}{2}} + C\Delta t((P_{in}^n)^2 + (P_{out}^n)^2),
\end{aligned}
\tag{1.147}
$$

   where the kinetic energy E_N^n and dissipation D_N^n are defined in (141) and (142), and the constant C depends only on the parameters in the problem, and not on Δt (or N).

The proof of this proposition is identical to the proof presented in [119] which concerns a FSI problem between an incompressible, viscous fluid and a thin elastic structure modeled by a linearly elastic Koiter shell model. The fluid sub-problems presented in [119] and in the present manuscript (Problem A2) are the same, except for the fact that η in this manuscript satisfies the linear wave equation. Since $\eta^{n+1/2}$ satisfies an elliptic problem for the Laplace operator with the right hand-side given in terms of approximate velocities $v^n, v^{n+1/2} \in L^2(0,1)$ (see equation (143)), the approximation $\eta^{n+1/2}$ is $H^2(0,1)$, and so the fluid domain in the semi-discretized Problem A2 is, in fact, Lipschitz. Therefore, the proof of Proposition 0.6.4 is the same as the proof of Proposition 3 [119] (for statement 1) and the proof of Proposition 4 [119] (for statement 2).

We pause for a second, and summarize what we have accomplished so far. For a given $\Delta t > 0$, the time interval $(0, T)$ was divided into $N = T/\Delta t$ sub-intervals $(t^n, t^{n+1}), n = 0, ..., N - 1$. On each sub-interval (t^n, t^{n+1}) we "solved" the coupled FSI problem by applying the Lie splitting scheme. First, Problem A1 was solved for the structure position and velocity, both thick and thin, and then Problem A2 was solved to update fluid velocity and fluid-structure interface velocity. We showed that each sub-problem has a unique solution, provided that $1 + \eta^n \geq R_{\min} > 0, n = 0, ..., N$, and that each sub-problem solution satisfies an energy estimate. When combined, the two energy estimates provide a discrete version of the energy estimate (103). Thus, for each Δt we have designed a time-marching, splitting scheme, which defines an approximate solution on $(0, T)$ of our main FSI problem (111)-(118). Furthermore, the scheme is designed in such a way that for each $\Delta t > 0$ the approximate FSI solution satisfies a discrete version of an energy estimate for the continuous problem.

We would like to ultimately show that, as $\Delta t \to 0$, the sequence of solutions parameterized by N (or Δt), converges to a weak solution of (111)-(118). Furthermore, we also need to show that $1 + \eta^n \geq R_{\min} > 0$ is satisfied for each $n = 0, ..., N - 1$. In order to obtain this result, it is crucial to show that the discrete energy of the approximate FSI solutions defined for each Δt, is *uniformly bounded*, independently of Δt (or N). This result is obtained by the following Lemma.

Lemma 1.6.1. (The uniform energy estimates) *Let $\Delta t > 0$ and $N = T/\Delta t > 0$. Furthermore, let $E_N^{n+\frac{1}{2}}$, E_N^{n+1}, and D_N^j be the total energy and dissipation given by (141) and (142), respectively.*

There exists a constant $C > 0$ independent of Δt (and N) such that the following estimates hold:

1. $E_N^{n+\frac{1}{2}} \leq C$, $E_N^{n+1} \leq C$, for all $n = 0, ..., N - 1$,

2. $\sum_{j=1}^{N} D_N^j \leq C$,

3. $\displaystyle\sum_{n=0}^{N-1} \left(\int_{\Omega_F} (1 + \eta^n)|\mathbf{u}^{n+1} - \mathbf{u}^n|^2 + \|v^{n+1} - v^{n+\frac{1}{2}}\|_{L^2(0,1)}^2 \right.$

$$\left. + \|v^{n+\frac{1}{2}} - v^n\|_{L^2(0,1)}^2 + \|\boldsymbol{V}^{n+1} - \boldsymbol{V}^n\|_{L^2(\Omega_S)}^2 \right) \leq C,$$

4. $\displaystyle\sum_{n=0}^{N-1} \left(\|\partial_z(\eta^{n+1} - \eta^n)\|_{L^2(0,1)}^2 + a_S(\boldsymbol{d}^{n+1} - \boldsymbol{d}^n, \boldsymbol{d}^{n+1} - \boldsymbol{d}^n) \right) \leq C.$

In fact, $C = E_0 + \tilde{C}\left(\|P_{in}\|_{L^2(0,T)}^2 + \|P_{out}\|_{L^2(0,T)}^2 \right)$, where $\tilde{C}$ is the constant from (147), which depends only on the parameters in the problem.

Proof. We begin by adding the energy estimates (144) and (147) to obtain

$$E_N^{n+1} + D_N^{n+1} + \frac{1}{2}\left(\int_{\Omega_F} (1 + \eta^n)|\mathbf{u}^{n+1} - \mathbf{u}^n|^2 + \|v^{n+1} - v^{n+\frac{1}{2}}\|_{L^2(0,1)}^2 \right.$$

$$+ \|v^{n+\frac{1}{2}} - v^n\|_{L^2(0,1)}^2 + \|\boldsymbol{V}^{n+1} - \boldsymbol{V}^n\|_{L^2(\Omega_S)}^2 + \|\partial_z(\eta^{n+\frac{1}{2}} - \eta^n)\|_{L^2(0,1)}^2$$

$$\left. + a_S(\boldsymbol{d}^{n+1} - \boldsymbol{d}^n, \boldsymbol{d}^{n+1} - \boldsymbol{d}^n) \right) \leq E_N^n + \tilde{C}\Delta t((P_{in}^n)^2 + (P_{out}^n)^2), \quad n = 0, \dots, N - 1.$$

Then, we calculate the sum, on both sides, and cancel out like terms in the kinetic energy that appear on both sides of the inequality to obtain

$$E_N^N + \sum_{n=0}^{N-1} D_N^{n+1} + \frac{1}{2} \sum_{n=0}^{N-1} \left(\int_{\Omega_F} (1 + \eta^n)|\mathbf{u}^{n+1} - \mathbf{u}^n|^2 + \|v^{n+1} - v^{n+\frac{1}{2}}\|_{L^2(0,1)}^2 \right.$$

$$\left. + \|v^{n+\frac{1}{2}} - v^n\|_{L^2(0,1)}^2 + \|\boldsymbol{V}^{n+1} - \boldsymbol{V}^n\|_{L^2(\Omega_S)}^2 + \|\partial_z(\eta^{n+\frac{1}{2}} - \eta^n)\|_{L^2(0,1)}^2 \right.$$

$$+a_S\big(\boldsymbol{d}^{n+1} - \boldsymbol{d}^n, \boldsymbol{d}^{n+1} - \boldsymbol{d}^n\big)\big) \le E_0 + \tilde{C}\Delta t \sum_{n=0}^{N-1}\big((P_{in}^n)^2 + (P_{out}^n)^2\big).$$

To estimate the term involving the inlet and outlet pressure, we recall that on every sub-interval (t^n, t^{n+1}) the pressure data is approximated by a constant which is equal to the average value of the pressure over that time interval. Therefore, we have, after using Hölder's inequality:

$$\Delta t \sum_{n=0}^{N-1}(P_{in}^n)^2 = \Delta t \sum_{n=0}^{N-1}\left(\frac{1}{\Delta t}\int_{n\Delta t}^{(n+1)\Delta t} P_{in}(t)dt\right)^2 \le \|P_{in}\|_{L^2(0,T)}^2.$$

By using the pressure estimate to bound the right hand-side in the above energy estimate, we have obtained all the statements in the Lemma, with the constant C given by $C = E_0 + \tilde{C}\|P_{in/out}\|_{L^2(0,T)}^2$.

Notice that Statement 1 can be obtained in the same way by summing from 0 to $n-1$, for each n, instead of from 0 to $N-1$.   □

We will use this Lemma in the next section to show convergence of approximate solutions.

1.6.6   Convergence of approximate solutions

We define approximate solutions of problem (111)-(118) on $(0, T)$ to be the functions which are piece-wise constant on each sub-interval $((n-1)\Delta t, n\Delta t]$, $n = 1\dots N$ of $(0, T)$, such that for $t \in ((n-1)\Delta t, n\Delta t]$, $n = 1\dots N$,

$$\mathbf{u}_N(t, .) = \mathbf{u}_N^n, \ \eta_N(t, .) = \eta_N^n, \ v_N(t, .) = v_N^n, \ v_N^*(t, .) = v_N^{n-\frac{1}{2}}, \ \boldsymbol{d}_N(t, .) = \boldsymbol{d}_N^n, \ \boldsymbol{V}_N(t, .) = \boldsymbol{V}_N^n.$$
$$(1.148)$$

See Figure 10. Notice that functions $v_N^* = v_N^{n-1/2}$ are determined by Problem A1
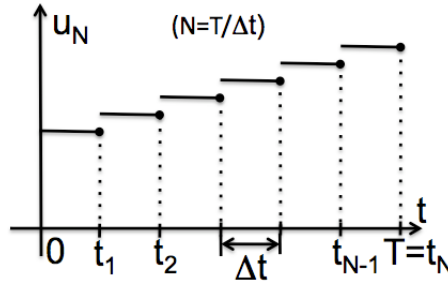
Figure 1.10: A sketch of u_N.

(the elastodynamics sub-problem), while functions $v_N = v_N^n$ are determined by Problem A2 (the fluid sub-problem). As a consequence, functions v_N are equal to

the normal trace of the fluid velocity on Γ, i.e., $\mathbf{u_N} = v_N \mathbf{e_r}$, which may be different from v_N^*. However, we will show later that $\|v_N - v_N^*\|_{L^2(0,1)} \to 0$, as $N \to \infty$.

Using Lemma 0.6.1 we now show that these sequences are uniformly bounded in the appropriate solution spaces.

We begin by showing that $(\eta_N)_{N \in \mathbb{N}}$ is uniformly bounded in $L^\infty(0, T; H_0^1(0, 1))$, and that there exists a $T > 0$ for which $1 + \eta_N^n > 0$ holds independently of N and n.

Proposition 1.6.5. *The sequence* $(\eta_N)_{N \in \mathbb{N}}$ *is uniformly bounded in*

$$L^\infty(0, T; H_0^1(0, 1)).$$

Moreover, for T small enough, we have

$$0 < R_{\min} \leq 1 + \eta_N(t, z) \leq R_{\max}, \ \ \forall N \in \mathbb{N}, z \in (0, 1), t \in (0, T). \qquad (1.149)$$

Proof. From the energy estimate in Lemma 0.6.1 we have

$$\|\eta_N(t)\|_{L^2(0,1)}^2 + \|\partial_z \eta_N(t)\|_{L^2(0,1)}^2, \leq C, \ \forall t \in [0, T],$$

which implies

$$\|\eta_N\|_{L^\infty(0,T;H_0^1(0,1))} \leq C.$$

To show that the radius $1 + \eta_N$ is uniformly bounded away from zero for T small enough, we first notice that the above inequality implies

$$\|\eta_N^n - \eta_0\|_{H_0^1(0,1)} \leq 2C, \ n = 1, \ldots, N, \ N \in \mathbb{N}.$$

Furthermore,

$$\|\eta_N^n - \eta_0\|_{L^2(0,1)} \leq \sum_{i=0}^{n-1} \|\eta_N^{i+1} - \eta_N^i\|_{L^2(0,1)} = \Delta t \sum_{i=0}^{n-1} \|v_N^{i+\frac{1}{2}}\|_{L^2(0,1)},$$

where we recall that $\eta_N^0 = \eta_0$. Lemma 0.6.1 implies that $E_N^{n+\frac{1}{2}} \leq C$, where C is independent of N. Combined with the above inequality this implies

$$\|\eta_N^n - \eta_0\|_{L^2(0,1)} \leq Cn\Delta t \leq CT, \ n = 1, \ldots, N, \ N \in \mathbb{N}.$$

Now, since $\|\eta_N^n - \eta_0\|_{L^2(0,1)}$ and $\|\eta_N^n - \eta_0\|_{H_0^1(0,1)}$ are uniformly bounded, we can use the interpolation inequality for Sobolev spaces, Thm. 4.17, p. 79 in [1], to get

$$\|\eta_N^n - \eta_0\|_{H^s(0,1)} \leq 2CT^{1-s}, \ n = 1, \ldots, N, \ N \in \mathbb{N}, \ \text{for } 0 < s < 1.$$

From Lemma 0.6.1 we see that C depends on T through the norms of the inlet and outlet data in such a way that C is an increasing function of T. Therefore, by choosing T small, we can make $\|\eta_N^n - \eta_0\|_{H^s(0,1)}$ arbitrarily small for $n = 1, \ldots, N$, $N \in \mathbb{N}$. Because of the Sobolev embedding of $H^s(0, 1)$ into $C[0, 1]$, for $s > 1/2$, we

can also make $\|\eta_N^n - \eta_0\|_{C[0,1]}$ arbitrarily small. Since the initial data η_0 is such that $1 + \eta_0(z) > 0$ (due to the conditions listed in (102)), we see that for $T > 0$ small enough, there exist $R_{\min}, R_{\max} > 0$, such that

$$0 < R_{\min} \leq 1 + \eta_N(t, z) \leq R_{\max}, \ \forall N \in \mathbb{N}, z \in (0, 1), t \in (0, T).$$

$\square$

We will show in the end that our existence result holds not only locally in time, i.e., for small $T > 0$, but rather, it can be extended all the way until either $T = \infty$, or until the lateral walls of the channel touch each other.

Proposition 0.6.5 implies, among other things, that the standard L^2-norm, and the following weighted L^2-norm are equivalent: for every $f \in L^2(\Omega_F)$, there exist constants $C_1, C_2 > 0$, which depend only on $R_{\min}, R_{\max}$, and not on f or N, such that

$$C_1 \int_{\Omega_F} (1 + \eta_N) f^2 \leq \|f\|_{L^2(\Omega_F)}^2 \leq C_2 \int_{\Omega_F} (1 + \eta_N) f^2. \qquad (1.150)$$

We will be using this property in the next section to prove strong convergence of approximate solutions.

Next we show that the sequences of approximate solutions for the velocity and its trace on the lateral boundary, as well as the displacement of the thick structure and the thick structure velocity, are uniformly bounded in the appropriate norms. To do that, we introduce the following notation which will be useful in the remainder of this section to prove compactness: denote by τ_h the translation in time by h of a function f

$$\tau_h f(t, .) = f(t - h, .), \ h \in \mathbb{R}. \qquad (1.151)$$

Proposition 1.6.6. *The following statements hold:*

1. *$(v_N)_{N \in \mathbb{N}}$, $(v_N^*)_{N \in \mathbb{N}}$ are uniformly bounded in $L^\infty(0, T; L^2(0, 1))$.*

2. *$(\mathbf{u}_N)_{N \in \mathbb{N}}$ is uniformly bounded in $L^\infty(0, T; L^2(\Omega_F))$.*

3. *$(\nabla^{\tau_{\Delta t} \eta_N} \mathbf{u}_N)_{N \in \mathbb{N}}$ is uniformly bounded in $L^2((0, T) \times \Omega_F)$.*

4. *$(\boldsymbol{d}_N)_{N \in \mathbb{N}}$ is uniformly bounded in $L^\infty(0, T; H^1(\Omega_S))$.*

5. *$(\boldsymbol{V}_N)_{N \in \mathbb{N}}$ is uniformly bounded in $L^\infty(0, T; L^2(\Omega_S))$.*

Proof. The uniform boundedness of $(v_N)_{N \in \mathbb{N}}, (v_N^*)_{N \in \mathbb{N}}, (\boldsymbol{d}_N)_{N \in \mathbb{N}}, (\boldsymbol{V}_N)_{N \in \mathbb{N}}$, and the uniform boundedness of $(\mathbf{u}_N)_{N \in \mathbb{N}}$ in $L^\infty(0, T; L^2(\Omega_F))$ follow directly from Statements 1 and 2 of Lemma 0.6.1, and from the definition of $(v_N)_{n \in \mathbb{N}}, (v_N^*)_{N \in \mathbb{N}}$, $(\boldsymbol{d}_N)_{N \in \mathbb{N}}, (\boldsymbol{V}_N)_{N \in \mathbb{N}}$ and $(\mathbf{u}_N)_{N \in \mathbb{N}}$ as step-functions in t so that

$$\int_0^T \|v_N\|_{L^2(0,1)}^2 dt = \sum_{n=0}^{N-1} \|v_N^n\|_{L^2(0,1)}^2 \Delta t.$$

It remains to show uniform boundedness of $(\nabla^{\tau_{\Delta t}\eta_N}\mathbf{u}_N)_{N\in\mathbb{N}}$ in $L^2((0,T)\times\Omega_F)$. From Lemma 0.6.1 we only know that the *symmetrized gradient* is bounded in the following way:

$$\sum_{n=1}^{N}\int_{\Omega_F}(1+\eta_N^{n-1})|\mathbf{D}_N^{\eta^{n-1}}(\mathbf{u}_N^n)|^2\Delta t \leq C. \tag{1.152}$$

We cannot immediately apply Korn's inequality since estimate (152) is given in terms of the transformed symmetrized gradient. Thus, there are some technical difficulties that need to be overcome due to the fact that our problem involves moving domains. To get around this difficulty we take the following approach. We first transform the problem back to the physical fluid domain $\Omega_F^{\eta_N^{n-1}}$ which is defined by the lateral boundary η_N^{n-1}, on which u_N is defined. There, instead of the transformed gradient, we have the standard gradient, and we can apply Korn's inequality in the usual way. However, since the Korn constant depends on the domain, we will need a result which provides a universal Korn constant, independent of the family of domains under consideration. Indeed, a result of this kind was obtained in [32, 141, 119, 122], assuming certain domain regularity. In particular, a calculation in [122] showed that the following Korn's equality holds for the space $\mathcal{V}_F(t)$:

$$\|\nabla\mathbf{u}^{N,n}\|^2_{L^2(\Omega_F^{\eta_N^{n-1}})} = 2\|\mathbf{D}(\mathbf{u}^{N,n})\|^2_{L^2(\Omega_F^{\eta_N^{n-1}})}. \tag{1.153}$$

Notice that the Korn constant (the number 2) is, indeed, domain independent. The proof of this Korn equality, presented in [122], is similar to the proof in Chambolle et al. [32], Lemma 6, pg. 377, with the slightly different assumptions. By using (153) and by mapping everything back to the fixed domain Ω_F, one recovers the following Korn's equality on Ω_F:

$$2\int_{\Omega_F}(1+\eta_N^{n-1})|\mathbf{D}_N^{\eta^{n-1}}(\mathbf{u}_N^n)|^2 = \int_{\Omega_F}(1+\eta_N^{n-1})|\nabla_N^{\eta^{n-1}}(\mathbf{u}_N^n)|^2. \tag{1.154}$$

By summing equalities (154) for $n=,1\ldots,N$, and by using (150), we get uniform boundedness of $(\nabla^{\tau_{\Delta t}\eta_N}\mathbf{u}_N)_{N\in\mathbb{N}}$ in $L^2((0,T)\times\Omega_F)$. $\qquad\Box$

From the uniform boundedness of approximate sequences, the following weak and weak* convergence results follow.

Lemma 1.6.2. (Weak and weak* convergence results) *There exist subsequences* $(\eta_N)_{N\in\mathbb{N}}$, $(v_N)_{N\in\mathbb{N}}$, $(v_N^*)_{N\in\mathbb{N}}$, $(\boldsymbol{d}_N)_{N\in\mathbb{N}}$, $(\boldsymbol{V}_N)_{N\in\mathbb{N}}$ *and* $(\mathbf{u}_N)_{N\in\mathbb{N}}$, *and the functions* $\eta \in L^\infty(0,T;H_0^1(0,1))$, $v,v^* \in L^\infty(0,T;L^2(0,1))$, $\boldsymbol{d} \in L^\infty(0,T;\mathcal{V}_S)$, $\boldsymbol{V} \in$

$L^\infty(0, T; L^2(\Omega_S))$, $\mathbf{u} \in L^\infty(0, T; L^2(\Omega_F))$ and $\mathbf{G} \in L^2((0, T) \times \Omega_F)$ such that

$$
\begin{aligned}
\eta_N &\rightharpoonup \eta \text{ weakly} * \text{ in } L^\infty(0, T; H_0^1(0, 1)), \\
v_N &\rightharpoonup v \text{ weakly} * \text{ in } L^\infty(0, T; L^2(0, 1)), \\
v_N^* &\rightharpoonup v^* \text{ weakly} * \text{ in } L^\infty(0, T; L^2(0, 1)), \\
\\
\boldsymbol{d}_N &\rightharpoonup \boldsymbol{d} \text{ weakly} * \text{ in } L^\infty(0, T; H^1(\Omega_S)), \\
\boldsymbol{V}_N &\rightharpoonup \boldsymbol{V} \text{ weakly} * \text{ in } L^\infty(0, T; L^2(\Omega_S)), \\
\mathbf{u}_N &\rightharpoonup \mathbf{u} \text{ weakly} * \text{ in } L^\infty(0, T; L^2(\Omega_F)), \\
\nabla^{\tau_{\Delta t} \eta_N} \mathbf{u}_N &\rightharpoonup \mathbf{G} \text{ weakly in } L^2((0, T) \times \Omega_F).
\end{aligned}
\tag{1.155}
$$

Furthermore,

$$
v = v^*. \tag{1.156}
$$

Proof. The only thing left to show is that $v = v^*$. For this purpose, we multiply the second statement in Lemma 0.6.1 by Δt, and notice again that $\|v_N\|_{L^2((0,T)\times(0,1))}^2 = \Delta t \sum_{n=1}^N \|v_N^n\|_{L^2(0,1)}^2$. This implies $\|v_N - v_N^*\|_{L^2((0,T)\times(0,1))} \leq C\sqrt{\Delta t}$, and we have that in the limit, as $\Delta t \to 0$, $v = v^*$. $\qquad\square$

Naturally, our goal is to prove that $\mathbf{G} = \nabla^\eta \mathbf{u}$. However, to achieve this goal we will need some stronger convergence properties of approximate solutions. Therefore, we postpone the proof until Section 0.6.7.

Strong convergence of approximate sequences

Due to the nonlinearity of our FSI problem, to show that the limits obtained in the previous Lemma satisfy the weak form of problem (111)-(118), we will need to show that the approximate sequences converge strongly in the appropriate function spaces. The strong convergence results will be achieved by using the following compactness result by Simon [134]:

Theorem 1.6.1. [134] *Let X be a Banach space and $F \hookrightarrow L^q(0, T; X)$ with $1 \leq q < \infty$. Then F is a relatively compact set in $L^q(0, T; X)$ if and only if*

(i) $\left\{ \int_{t_1}^{t_2} f(t)dt : f \in F \right\}$ *is relatively compact in X, $0 < t_1 < t_2 < T$,*

(ii) $\|\tau_h f - f\|_{L^q(h,T;X)} \to 0$ *as h goes to zero, uniformly with respect to $f \in F$.*

This result was used in [119] to show compactness, but the proof was simpler because of the higher regularity of the lateral boundary of the fluid domain, namely, of the fluid-structure interface. In the present case we need to obtain some additional regularity for the fluid velocity $\mathbf{u}_N$ on Ω_F and its trace $\mathbf{v}_N$ on the lateral boundary, before we can use Theorem 0.6.1 to show strong convergence of approximate sequences. Notice, we only have that our fluid velocity on Ω_F is uniformly bounded in $L^2(\Omega_F)$, plus a condition that the transformed gradient $\nabla^{\tau_{\Delta t} \eta_N} \mathbf{u}_N$ is uniformly bounded in L^2. Since η is not Lipschitz, we cannot get that the gradient

$\nabla \mathbf{u}_N$ is uniformly bounded in L^2 on Ω_F. This lower regularity of η_N causes additional problems in obtaining regularity of $\mathbf{u}_N$ on Ω_F, namely it will imply lower regularity of $\mathbf{u}_N$ in the sense that $\mathbf{u} \in H^s(\Omega_F)$, for $0 < s < 1/2$, and not $H^1(\Omega_F)$. Luckily, according to the trace theorem in [120], this will still allow us to make sense of the trace of $\mathbf{u}_N$ on Γ. More precisely, we prove the following Lemma.

Lemma 1.6.3. *The following statements hold:*

1. *$(\mathbf{u}_N)_{N \in \mathbb{N}}$ is uniformly bounded in $L^2(0,T; H^s(\Omega_F))$, $0 < s < 1/2$;*

2. *$(v_N)_{N \in \mathbb{N}}$ is uniformly bounded in $L^2(0,T; H^{s/2}(0,1))$, $0 < s < 1/2$.*

Proof. We start by mapping the fluid velocity $\mathbf{u}_N$ defined on Ω_F, back to the physical fluid domain with the lateral boundary $\tau_{\Delta t} \eta_N(t, z) = \eta_N(t - \Delta t, z)$. We denote by $\mathbf{u}^N(t, .)$ the fluid velocity on the physical domain $\Omega_{\tau_{\Delta t} \eta_N}$:

$$\mathbf{u}^N(t, .) = \mathbf{u}_N(t, .) \circ A^{-1}_{\tau_{\Delta t} \eta_N}(t), \ N \in \mathbb{N}.$$

As before, we use sub-script N to denote fluid velocity defined on the physical space. From (109) we see that

$$\nabla \mathbf{u}^N = \nabla^{\tau_{\Delta t} \eta_N} \mathbf{u}_N.$$

Proposition 0.6.6, statement 3, implies that the sequence $(\nabla \mathbf{u}^N)_{N \in \mathbb{N}}$ is uniformly bounded in L^2, and so we have that $\|\mathbf{u}^N\|_{L^2(0,T; H^1(\Omega_{\tau_{\Delta t} \eta}))}$ is uniformly bounded.

Now, from the fact that the fluid velocities $\mathbf{u}^N$ defined on the physical domains are uniformly bounded in H^1, we would like to obtain a similar result for the velocities $\mathbf{u}_N$ defined on the reference domain Ω_F. For this purpose, we recall that the functions $\eta_N, N \in \mathbb{N}$ that are involved in the ALE mappings $A_{\tau_{\Delta t} \eta_N}(t)$, $N \in \mathbb{N}$, are uniformly bounded in $H^1(0,1)$. This is, unfortunately, not sufficient to obtain uniform boundedness of the gradients $(\nabla u_N)_{N \in \mathbb{N}}$ in $L^2(\Omega_F)$. However, from the Sobolev embedding $H^1(0,1) \hookrightarrow C^{0,1/2}(0,1)$ we have that the sequence $(\eta_N)_{N \in \mathbb{N}}$ is uniformly bounded in $L^\infty(0,T; C^{0,1/2}(0,1))$. This will help us obtain uniform boundedness of $(\mathbf{u}_N)_{n \in \mathbb{N}}$ in a slightly lower-regularity space, namely in the space $L^2(0,T; H^s(\Omega_F))$, $0 < s < 1/2$. To see this, we first notice that $\mathbf{u}_N$ on Ω_F can be expressed in terms of function $\mathbf{u}^N$ defined on $\Omega_{\tau_{\Delta t} \eta_N}$ as

$$\mathbf{u}_N(t, \tilde{z}, \tilde{r}) = \mathbf{u}^N(t, \tilde{z}, (1 + \tau_{\Delta t} \eta_N)(t, \tilde{z})) \tilde{r}), \ (\tilde{z}, \tilde{r}) \in \Omega_F. \tag{1.157}$$

Therefore, $\mathbf{u}_N$ can be written as an H^1-function $\mathbf{u}^N$ composed with a $C^{0,1/2}$-function η_N, in the way described in (157). The following Lemma, proved in [120], implies that $\mathbf{u}_N$ belongs to a space with asymmetric regularity (more regular in $\tilde{r}$ than in $\tilde{z}$) in the sense that $\mathbf{u}_N \in L^2(0,1; H^s(0,1)), 0 < s < 1/2$, and $\partial_{\tilde{r}} \mathbf{u}_N \in L^2(0,1; L^2(0,1))$. We use notation from Lions and Magenes [112], pg. 10, to denote the corresponding function space by

$$W(0,1; s) = \{f : f \in L^2(0,1; H^s(0,1))), \ \partial_{\tilde{r}} f \in L^2(0,1; L^2(0,1))\}.$$

More precisely, Lemma 3.3 from [120] states the following:

Lemma 1.6.4. [120] *Let $\eta \in C^{0,\alpha}$, $0 < \alpha < 1$, and let $u \in H^1(\Omega_\eta)$. Define*

$$\tilde{u}(\tilde{r}, \tilde{z}) = u(\tilde{z}, (1 + \eta(\tilde{z}))\tilde{r}), \quad (\tilde{z}, \tilde{r}) \in \Omega_F. \qquad (1.158)$$

Then $\tilde{u} \in W(0, 1; s)$ for $0 < s < \alpha$.

Thus, Lemma 0.6.4 implies that $\mathbf{u}_N(t,.) \in W(0, 1; s)$ for $0 < s < 1/2$. Now, using the fact $W(0, 1; s) \hookrightarrow H^s(\Omega_F)$ we get

$$\|\mathbf{u}_N(t,.)\|^2_{H^s(\Omega_F)} \leq C\|\mathbf{u}^N(t,.)\|^2_{H^1(\Omega_{\eta(t-\Delta t)})}, \ a.a. \ t \in (0, T), \ 0 < s < 1/2.$$

By integrating the above inequality w.r.t. t we get the first statement of Lemma 0.6.3.

To prove the second statement of Lemma 0.6.3 we use Theorem 3.1 of [120], which states that the notion of trace for the functions of the form (157) for which $\mathbf{u}^N \in H^1$ and $\eta_N \in C^{0,1/2}$, can be defined in the sense of $H^{s/2}$, $0 < s < 1/2$. For completeness, we state Theorem 3.2 of [120] here.

Theorem 1.6.2. [120] *Let $\alpha < 1$ and let η be such that*

$$\eta \in C^{0,\alpha}(0,1), \ \eta(z) \geq \eta_{min} > -1, \ z \in [0,1], \ \eta(0) = \eta(1) = 1.$$

Then, the trace operator

$$\gamma_\eta : C^1(\overline{\Omega_\eta}) \to C(\Gamma)$$

that associates to each function $u \in C^1(\overline{\Omega_\eta})$ its "Lagrangian trace" $u(\tilde{z}, 1 + \eta(\tilde{z})) \in C(\Gamma)$, defined via (158) for $\tilde{r} = 1$,

$$\gamma_\eta : u \mapsto u(\tilde{z}, 1 + \eta(\tilde{z})),$$

can be extended by continuity to a linear operator from $H^1(\Omega_\eta)$ to $H^s(\Gamma)$ for $0 \leq s < \alpha/2$.

By recalling that $v_N = (\mathbf{u}_N)_{|\Gamma}$, this proves the second statement of Lemma 0.6.3.
□

Notice that the difficulty associated with bounding the gradient of $\mathbf{u}_N$ is somewhat artificial, since the gradient of the fluid velocity $\mathbf{u}^N$ defined on the physical domain is, in fact, uniformly bounded (by Proposition 0.6.6). Namely, the difficulty is imposed by the fact that we decided to work with the problem defined on a fixed domain Ω_F, and not on the family of moving domains. This decision, however, simplifies other parts of the main existence proof. The "expense" that we had to pay for this decision is embedded in the proof of Lemma 0.6.3.

We are now ready to use Theorem 0.6.1 to prove compactness of the sequences $(v_N)_{N\in\mathbb{N}}$ and $(\mathbf{u}_N)_{N\in\mathbb{N}}$.

Theorem 1.6.3. *Sequences $(v_N)_{N\in\mathbb{N}}$ and $(\mathbf{u}_N)_{N\in\mathbb{N}}$ are relatively compact in $L^2(0, T; L^2(0, 1))$ and $L^2(0, T; L^2(\Omega_F))$, respectively.*

Proof. We use Theorem 0.6.1 with $q = 2$, and $X = L^2$. We verify that both assumptions (i) and (ii) hold.

Assumption (i): To show that the sequences $(v_N)_{N \in \mathbb{N}}$ and $(\mathbf{u}_N)_{N \in \mathbb{N}}$ are relatively compact in $L^2(0,1)$ and $L^2(\Omega_F)$, respectively, we use Lemma 0.6.3 and the compactness of the embeddings $H^s(\Omega_F) \hookrightarrow L^2(\Omega_F)$ and $H^{s/2}(0,1) \hookrightarrow L^2(0,1)$, respectively, for $0 < s < 1/2$. Namely, from Lemma 0.6.3 we know that sequences $(\mathbf{u}_N)_{N \in \mathbb{N}}$ and $(v_N)_{N \in \mathbb{N}}$ are uniformly bounded in $L^2(0,T; H^s(\Omega_F))$ and $L^2(0,T; H^{s/2}(0,1))$, respectively, for $0 < s < 1/2$. The compactness of the embeddings $H^s(\Omega_F) \hookrightarrow L^2(\Omega_F)$ and $H^{s/2}(0,1) \hookrightarrow L^2(0,1)$ verify Assumption (i) of Theorem 0.6.1.

Assumption (ii): We prove that the "integral equicontinuity", stated in assumption (ii) of Theorem 0.6.1, holds for the sequence $(v_N)_{N \in \mathbb{N}}$. Analogous reasoning can be used for $(\mathbf{u}_N)_{N \in \mathbb{N}}$. Thus, we want to show that for each $\varepsilon > 0$, there exists a $\delta > 0$ such that

$$\|\tau_h v_N - v_N\|_{L^2(\omega; L^2(0,1))}^2 < \varepsilon, \quad \forall |h| < \delta, \text{ independently of } N \in \mathbb{N}, \quad (1.159)$$

where ω is an arbitrary compact subset of Ω. Indeed, we will show that for each $\varepsilon > 0$, the following choice of δ:

$$\delta := \min\{\text{dist}(\omega, \partial\Omega)/2, \varepsilon/(2C)\}$$

provides the desired estimate, where C is the constant from Lemma 0.6.1 (independent of N).

Let h be an arbitrary real number whose absolute value is less than δ. We want to show that (159) holds for all $\Delta t = T/N$. This will be shown in two steps. First, we will show that (159) holds for the case when $\Delta t \geq h$ (Case 1), and then for the case when $\Delta t < h$ (Case 2).

A short remark is in order: For a given $\delta > 0$, we will have $\Delta t < \delta$ for infinitely many N, and both cases will apply. For a finite number of functions (v_N), we will, however, have that $\Delta t \geq \delta$. For those functions (159) needs to be proved for all Δt such that $|h| < \delta \leq \Delta t$, which falls into Case 1 bellow. Thus, Cases 1 and 2 cover all the possibilities.

Case 1: $\Delta t \geq h$. We calculate the shift by h to obtain (see Figure 11, left):

$$\|\tau_h v_N - v_N\|_{L^2(\omega; L^2(0,1))}^2 \leq \sum_{j=1}^{N-1} \int_{j\Delta t - h}^{j\Delta t} \|v_N^j - v_N^{j+1}\|_{L^2(0,1)}^2 =$$

$$= h \sum_{j=1}^{N-1} \|v_N^j - v_N^{j+1}\|_{L^2(0,1)}^2 \leq hC < \varepsilon/2 < \varepsilon.$$

The last inequality follows from $|h| < \delta \leq \varepsilon/(2C)$.
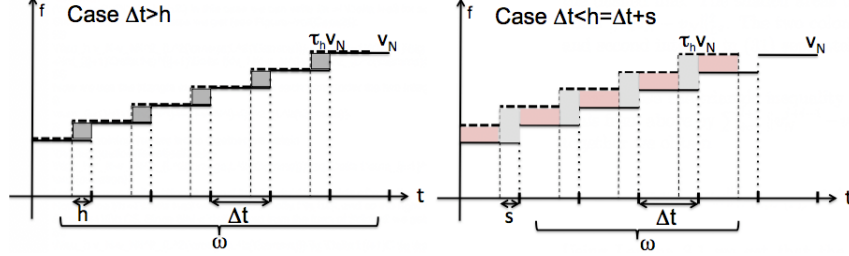
Figure 1.11: Left panel–Case 1: $\Delta t \geq h$. The graph of v_N is shown in solid line, while the graph of the shifted function $\tau_h v_N$ is shown in dashed line. The shaded area denotes the non-zero contributions to the norm $\|\tau_h v_N - v_N\|_{L^2}^2$. Right panel–Case2: $\Delta t < h = \Delta t + s, 0 < s < \Delta t$. The graph of v_N is shown in solid line, while the graph of the shifted function $\tau_h v_N$ is shown in the dashed line. The shaded areas denote non-zero contributions to the norm $\|\tau_h v_N - v_N\|_{L^2}^2$. The two colors represent the contributions to the first and second integral in (160) separately.

Case 2: $\Delta t < h$. In this case we can write $h = l\Delta t + s$ for some $l \in \mathbb{N}$, $0 < s \leq \Delta t$. Similarly, as in the first case, we get (see Figure 11, right):

$$\|\tau_h v_N - v_N\|_{L^2(\omega; L^2(0,1))}^2 = \sum_{j=1}^{N-l-1} \Big(\int_{j\Delta t}^{(j+1)\Delta t - s} \|v_N^j - v_N^{j+l}\|_{L^2(0,1)}^2 \qquad (1.160)$$
$$+ \int_{(j+1)\Delta t - s}^{(j+1)\Delta t} \|v_N^j - v_N^{j+l+1}\|_{L^2(0,1)}^2 \Big).$$

Now we use the triangle inequality to bound each term under the two integrals from above by $\sum_{i=1}^{l+1} \|v_N^{j+i-1} - v_N^{j+i}\|_{L^2(0,1)}^2$. After combining the two terms together one obtains

$$\|\tau_h v_N - v_N\|_{L^2(\omega; L^2(0,1))}^2 \leq \Delta t \sum_{j=1}^{N-l-1} \sum_{i=1}^{l+1} \|v_N^{j+i-1} - v_N^{j+i}\|_{L^2(0,1)}^2. \qquad (1.161)$$

Lemma 0.6.1 now impies that the right hand-side of (161) is bounded by $\Delta t (l+1)C$. Now, since $h = l\Delta t + s$ we see that $\Delta t \leq h/l$, and so the right hand-side of (161) is bounded by $\frac{l+1}{l} hC$. Since $|h| < \delta$ and from the form of δ we get

$$\|\tau_h v_N - v_N\|_{L^2(\omega; L^2(0,1))}^2 \leq \Delta t (l+1)C \leq \frac{l+1}{l} hC \leq \frac{l+1}{l} \frac{\varepsilon}{2} < \varepsilon.$$

Thus, if we set $\omega = [\delta/2, T - \delta/2]$ we have shown:

$$\|\tau_{\delta/2} v_N - v_N\|_{L^2(\delta/2, T-\delta/2; L^2(0,1))}^2 < \varepsilon, \quad N \in \mathbb{N}.$$

To show that condition (ii) from Theorem 0.6.1 holds it remains to estimate $\|\tau_{\delta/2}v_N - v_N\|^2_{L^2(T-\delta/2,T;L^2(0,1))}$. From the first inequality in Lemma 0.6.1 (boundedness of $v_N^{n+\frac{i}{2}}, i = 1, 2$ in $L^2(0,1)$) we have

$$\int_{T-\delta/2}^{T} \|\tau_{\delta/2}v_N - v_N\|^2_{L^2(0,1)} \le \frac{\delta}{2}2C < \varepsilon, \quad N \in \mathbb{N}.$$

Thus, we have verified all the assumptions of Theorem 0.6.1, and so the compactness result for $(v_N)_{N\in\mathbb{N}}$ follows from Theorem 0.6.1. Similar arguments imply compactness of $(\mathbf{u}_N)_{N\in\mathbb{N}}$. □

To show compactness of $(\eta_N)_{N\in\mathbb{N}}$ we use the approach similar to that in [119], except that, due to the weaker regularity properties of η_N, we will have to use different embedding results (Hilbert interpolation inequalities). In the end, compactness of the sequence of lateral boundary approximation will follow due to the Arzelà- Ascoli Theorem.

As in [119], we start by introducing a slightly different set of approximate functions of $\mathbf{u}$, v, η and $\mathbf{V}$. Namely, for each fixed Δt (or $N \in \mathbb{N}$), define $\tilde{\mathbf{u}}_N$, $\tilde{\eta}_N$, $\tilde{v}_N$ and $\tilde{\mathbf{V}}_N$ to be continuous, *linear* on each sub-interval $[(n-1)\Delta t, n\Delta t]$, and such that for $n = 0, \ldots, N$:

$$\begin{aligned}
\tilde{\mathbf{u}}_N(n\Delta t, .) &= \mathbf{u}_N(n\Delta t, .), \ \tilde{v}_N(n\Delta t, .) = v_N(n\Delta t, .), \\
\tilde{\eta}_N(n\Delta t, .) &= \eta_N(n\Delta t, .), \ \tilde{\mathbf{V}}_N(n\Delta t, .) = \mathbf{V}_N(n\Delta t, .),
\end{aligned} \tag{1.162}$$

See Figure 12. A straightforward calculation gives the following inequalities (see
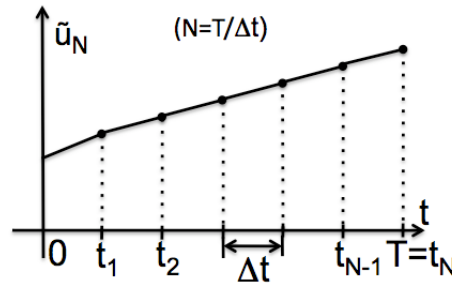
Figure 1.12: A sketch of $\tilde{\mathbf{u}}_N$.

[138], p. 328)

$$\|v_N - \tilde{v}_N\|^2_{L^2(0,T;L^2(0,1))} \leq \frac{\Delta t}{3} \sum_{n=1}^{N} \|v^{n+1} - v^n\|^2_{L^2(0,1)},$$

$$\|\mathbf{u}_N - \tilde{\mathbf{u}}_N\|^2_{L^2(0,T;L^2(\Omega_F))} \leq \frac{\Delta t}{3} \sum_{n=1}^{N} \|\mathbf{u}^{n+1} - \mathbf{u}^n\|^2_{L^2(\Omega_F)},$$

$$\|\eta_N - \tilde{\eta}_N\|^2_{L^2(0,T;L^2(0,1))} \leq \frac{\Delta t}{3} \sum_{n=1}^{N} \|\eta^{n+1} - \eta^n\|^2_{L^2(0,1)}, \quad (1.163)$$

$$\|\boldsymbol{V}_N - \tilde{\boldsymbol{V}}_N\|^2_{L^2(0,T;L^2(\Omega_S))} \leq \frac{\Delta t}{3} \sum_{n=1}^{N} \|\boldsymbol{V}^{n+1} - \boldsymbol{V}^n\|^2_{L^2(\Omega_S)},$$

Now from

$$\partial_t \tilde{\eta}_N(t) = \frac{\eta^{n+1} - \eta^n}{\Delta t} = \frac{\eta^{n+1/2} - \eta^n}{\Delta t} = v^{n+\frac{1}{2}}, \ t \in (n\Delta t, (n+1)\Delta t),$$

since v_N^* was defined in (148) as a piece-wise constant function defined via $v_N^*(t, \cdot) = v^{n+\frac{1}{2}}$, for $t \in (n\Delta t, (n+1)\Delta t]$, we see that

$$\partial_t \tilde{\eta}_N = v_N^* \ a.e. \ \text{on} \ (0, T). \quad (1.164)$$

Lemma 0.6.1 (the boundedness of $E_N^{n+\frac{i}{2}}$) then implies

$(\tilde{\eta}_N)_{N \in \mathbb{N}}$ is bounded in $L^\infty(0, T; H_0^1(0,1)) \cap W^{1,\infty}(0, T; L^2(0,1))$.

We now use the following result on continuous embeddings:

$$L^\infty(0, T; H_0^1(0,1)) \cap W^{1,\infty}(0, T; L^2(0,1)) \hookrightarrow C^{0,1-\alpha}([0,T]; H^\alpha(0,1)), \quad (1.165)$$

for $0 < \alpha < 1$. This result follows from the standard Hilbert interpolation inequalities, see [112]. A slightly different result (assuming higher regularity) was also used in [78] to deal with a set of mollifying functions approximating a solution to a moving-boundary problem between a viscous fluid and an elastic plate. From (165) we see that $(\tilde{\eta}_N)_{N \in \mathbb{N}}$ is also bounded (uniformly in N) in $C^{0,1-\alpha}([0,T]; H^\alpha(0,1))$. Now, from the continuous embedding of $H^\alpha(0,1)$ into $H^{\alpha-\epsilon}$, and by applying the Arzelà-Ascoli Theorem, we conclude that sequence $(\tilde{\eta}_N)_{N \in \mathbb{N}}$ has a convergent subsequence, which we will again denote by $(\tilde{\eta}_N)_{N \in \mathbb{N}}$, such that

$$\tilde{\eta}_N \to \tilde{\eta} \ \text{in} \ C([0,T]; H^s(0,1)), \ 0 < s < 1.$$

Since (163) implies that $(\tilde{\eta}_N)_{N \in \mathbb{N}}$ and $(\eta_N)_{N \in \mathbb{N}}$ have the same limit, we have $\eta = \tilde{\eta} \in C([0,T]; H^s(0,1))$, where η is the weak* limit of $(\eta_N)_{N \in \mathbb{N}}$, discussed in (155). Thus, we have

$$\tilde{\eta}_N \to \eta \ \text{in} \ C([0,T]; H^s(0,1)), \ 0 < s < 1.$$

We can now prove the following Lemma:

Lemma 1.6.5. $\eta_N \to \eta$ in $L^\infty(0, T; H^s(0, 1))$, $0 < s < 1$.

Proof. The proof is similar to the proof of Lemma 3 in [119]. The result follows from the continuity in time of η, and from the fact that $\tilde{\eta}_N \to \eta$ in $C([0, T]; H^s(0, 1))$, for $0 < s < 1$, applied to the inequality

$$\|\eta_N(t) - \eta(t)\|_{H^s(0,1)} = \|\eta_N(t) - \eta(n\Delta t) + \eta(n\Delta t) - \eta(t)\|_{H^s(0,1)}$$

$$= \|\eta_N(n\Delta t) - \eta(n\Delta t) + \eta(n\Delta t) - \eta(t)\|_{H^s(0,1)}$$

$$\leq \|\eta_N(n\Delta t) - \eta(n\Delta t)\| + \|\eta(n\Delta t) - \eta(t)\|_{H^s(0,1)}$$

$$= \|\tilde{\eta}_N(n\Delta t) - \eta(n\Delta t)\|_{H^s(0,1)} + \|\eta(n\Delta t) - \eta(t)\|_{H^s(0,1)}.$$

$\square$

The strong convergence results obtained in Theorem 0.6.3 and Lemma 0.6.5 can be summarized as follows: there exist subsequences $(\mathbf{u}_N)_{N\in\mathbb{N}}$, $(v_N)_{N\in\mathbb{N}}$ and $(\eta_N)_{N\in\mathbb{N}}$ such that

$$
\begin{aligned}
\mathbf{u}_N &\to \mathbf{u} \text{ in } L^2(0, T; L^2(\Omega_F)), \\
v_N &\to v \text{ in } L^2(0, T; L^2(0, 1)), \\
\tau_{\Delta t}\mathbf{u}_N &\to u \text{ in } L^2(0, T; L^2(\Omega_F)), \\
\tau_{\Delta t}v_N &\to v \text{ in } L^2(0, T; L^2(0, 1)), \\
\eta_N &\to \eta \text{ in } L^\infty(0, T; H^s(0, 1)), \ 0 \leq s < 1.
\end{aligned}
\tag{1.166}
$$

Because of the uniqueness of derivatives, we also have $v = \partial_t \eta$ in the sense of distributions. The statements about the convergence of $(\tau_{\Delta t}\mathbf{u}_N)_{N\in\mathbb{N}}$ and $(\tau_{\Delta t}v_N)_{N\in\mathbb{N}}$ follow directly from

$$\|\tau_{\Delta t}\mathbf{u}_N - \mathbf{u}_N\|^2_{L^2((0,T)\times\Omega_F)} + \|\tau_{\Delta t}v_N - v_N\|^2_{L^2((0,T)\times(0,1))} \leq C\Delta t, \tag{1.167}$$

which is obtained after multiplying the third equality of Lemma 0.6.1 by Δt.

Furthermore, one can also show that subsequences $(\tilde{v}_N)_N$, $(\tilde{\mathbf{u}}_N)_N$ and $(\tilde{\mathbf{V}}_N)_N$ also converge to v, $\mathbf{u}$ and $\mathbf{V}$ respectively. More precisely,

$$
\begin{aligned}
\tilde{\mathbf{u}}_N &\to \mathbf{u} \text{ in } L^2(0, T; L^2(\Omega_F)), \\
\tilde{v}_N &\to v \text{ in } L^2(0, T; L^2(0, 1)), \\
\tilde{\mathbf{V}}_N &\rightharpoonup \mathbf{V} \text{ weakly* in } L^\infty(0, T; L^2(\Omega_S))
\end{aligned}
\tag{1.168}
$$

This statement follows directly from the inequalities (163) and Lemma 0.6.1, which provides uniform boundedness of the sums on the right hand-sides of the inequalities.

We conclude this section by showing one last convergence result that will be used in the next section to prove that the limiting functions satisfy weak formulation of the FSI problem. Namely, we want to show that

$$
\begin{aligned}
\eta_N &\to \eta \text{ in } L^\infty(0, T; C[0, 1]), \\
\tau_{\Delta t}\eta_N &\to \eta \text{ in } L^\infty(0, T; C[0, 1]).
\end{aligned}
\tag{1.169}
$$

The first statement is a direct consequence of Lemma 0.6.5 in which we proved that $\eta_N \to \eta$ in $L^\infty(0,T; H^s(0,1))$, $0 < s < 1$. For $s > \frac{1}{2}$ this implies

$$\eta_N \to \eta \text{ in } L^\infty(0,T; C[0,1]). \tag{1.170}$$

To show convergence of the shifted displacements $\tau_{\Delta t}\eta_N$ to the same limiting function η, we recall that

$$\tilde{\eta}_N \quad \to \quad \eta \text{ in } C([0,T]; H^s[0,L]), \ 0 < s < 1,$$

and that $(\tilde{\eta}_N)_{N \in \mathbb{N}}$ is uniformly bounded in $C^{0,1-\alpha}([0,T]; H^\alpha(0,1))$, $0 < \alpha < 1$. Uniform boundedness of $(\tilde{\eta}_N)_{N \in \mathbb{N}}$ in $C^{0,1-\alpha}([0,T]; H^\alpha(0,1))$ implies that there exists a constant $C > 0$, independent of N, such that

$$\|\tilde{\eta}_N((n-1)\Delta t) - \tilde{\eta}_N(n\Delta t)\|_{H^\alpha(0,1)} \leq C|\Delta t|^{1-\alpha}.$$

This means that for each $\varepsilon > 0$, there exists an $N_1 > 0$ such that

$$\|\tilde{\eta}_N((n-1)\Delta t) - \tilde{\eta}_N(n\Delta t)\|_{H^\alpha(0,1)} \leq \frac{\varepsilon}{2}, \text{for all } N \geq N_1.$$

Here, N_1 is chosen by recalling that $\Delta t = T/N$, and so the right hand-side implies that we want an N_1 such that

$$C\left(\frac{T}{N}\right)^{1-\alpha} < \frac{\varepsilon}{2} \text{ for all } N \geq N_1.$$

Now, convergence $\tilde{\eta}_N \to \eta$ in $C([0,T]; H^s[0,1])$, $0 < s < 1$, implies that for each $\varepsilon > 0$, there exists an $N_2 > 0$ such that

$$\|\tilde{\eta}_N(n\Delta t) - \eta(t)\|_{H^s(0,1)} < \frac{\varepsilon}{2}, \text{ for all } N \geq N_2.$$

We will use this to show that for each $\varepsilon > 0$ there exists an $N^* \geq \max\{N_1, N_2\}$, such that

$$\|\tau_{\Delta t}\tilde{\eta}_N(t) - \eta(t)\|_{H^s(0,1)} < \varepsilon, \text{ for all } N \geq N^*.$$

Indeed, let $t \in (0,T)$. Then there exists an n such that $t \in ((n-1)\Delta t, n\Delta t]$. We calculate

$$\|\tau_{\Delta t}\tilde{\eta}_N(t) - \eta(t)\|_{H^s(0,1)} = \|\tau_{\Delta t}\tilde{\eta}_N(t) - \tilde{\eta}_N(n\Delta t) + \tilde{\eta}_N(n\Delta t) - \eta(t)\|_{H^s(0,1)}$$
$$= \|\tilde{\eta}_N((n-1)\Delta t) - \tilde{\eta}_N(n\Delta t) + \tilde{\eta}_N(n\Delta t) - \eta(t)\|_{H^s(0,1)}$$
$$\leq \|\tilde{\eta}_N((n-1)\Delta t) - \tilde{\eta}_N(n\Delta t)\|_{H^s(0,1)} + \|\tilde{\eta}_N(n\Delta t) - \eta(t)\|_{H^s(0,1)}.$$

The first term is less than $\varepsilon/2$ by the uniform boundedness of $(\tilde{\eta}_N)_{N \in \mathbb{N}}$ in $C^{0,1-\alpha}([0,T]; H^\alpha(0,1))$, while the second term is less than $\varepsilon/2$ by the convergence of $\tilde{\eta}_N$ to η in $C([0,T]; H^s[0,1])$, $0 < s < 1$.

Now, since $\tau_{\Delta t}\tilde{\eta}_N = \widetilde{(\tau_{\Delta t}\eta_N)}$, we can use the same argument as in Lemma 0.6.5 to show that sequences $\widetilde{(\tau_{\Delta t}\eta_N)}$ and $\tau_{\Delta t}\eta_N$ both converge to the same limit η in $L^\infty(0,T; H^s(0,1))$, for $0 < s < 1$.

1.6.7 The limiting problem and weak solution

Next we want to show that the limiting functions satisfy the weak form (139) of the full fluid-structure iteration problem. In this vein, one of the things that needs to be considered is what happens in the limit as $N \to \infty$, i.e., as $\Delta t \to 0$, of the weak form of the fluid sub-problem (146). Before we pass to the limit we must observe that, unfortunately, the velocity test functions in (146) depend of N! More precisely, they depend on η_N^n because of the requirement that the transformed divergence-free condition $\nabla^{\eta_N^n} \cdot \mathbf{q} = 0$ must be satisfied. This is a consequence of the fact that we mapped our fluid sub-problem onto a fixed domain Ω_F. Therefore, we need to take special care when constructing suitable velocity test functions and passing to the limit in (146).

1.6.8 Construction of the appropriate test functions

We begin by recalling that test functions $(\mathbf{q}, \psi, \boldsymbol{\psi})$ for the limiting problem are defined by the space $\mathcal{Q}$, given in (133), which depends on η. Similarly, the test spaces for the approximate problems depend on N through the dependence on η_N.

   To deal with the dependence of test functions on N, we follow the same ideas as those presented in [32, 119]. We restrict ourselves to a dense subset $\mathcal{X}$ of all test functions in $\mathcal{Q}$ that is independent of η_N even for the approximate problems. We construct the set $\mathcal{X}$ to consist of the test functions $(\mathbf{q}, \psi, \boldsymbol{\psi}) \in \mathcal{X} = \mathcal{X}_F \times \mathcal{X}_W \times \mathcal{X}_S$, such that the velocity components $\mathbf{q} \in \mathcal{X}_F$ are smooth, independent of N, and $\nabla \cdot \mathbf{q} = 0$. Such functions can be constructed as an algebraic sum of the functions $\mathbf{q}_0$ that have compact support in $\Omega_\eta \cup \Gamma_{in} \cup \Gamma_{out} \cup \Gamma_b$, plus a function $\mathbf{q}_1$, which captures the behavior of the solution at the boundary Γ_η. More precisely, let Ω_{min} and Ω_{max} denote the fluid domains associated with the radii R_{min} and R_{max}, respectively.

1. **Definition of test functions $(\mathbf{q}_0, 0, \mathbf{0})$ on $(0,T) \times \Omega_{max} \times \Omega_S$:** Consider all smooth functions $\mathbf{q}$ with compact support in $\Omega_\eta \cup \Gamma_{in} \cup \Gamma_{out} \cup \Gamma_b$, and such that $\nabla \cdot \mathbf{q} = 0$. Then we can extend $\mathbf{q}$ by 0 to a divergence-free vector field on $(0,T) \times \Omega_{max}$. This defines $\mathbf{q}_0$.

   Notice that since η_N converge uniformly to η, there exists an $N_q > 0$ such that $\mathrm{supp}(\mathbf{q}_0) \subset \Omega_{\tau_{\Delta t} \eta_N}$, $\forall N \geq N_q$. Therefore, $\mathbf{q}_0$ is well defined on infinitely many approximate domains $\Omega_{\tau_{\Delta t} \eta_N}$.

2. **Definition of test functions $(\mathbf{q}_1, \psi, \boldsymbol{\psi})$ on $(0,T) \times \Omega_{max} \times \Omega_S$:** Consider $\psi \in C_c^1([0,T]; H_0^2(0,1))$. Define

$$
\mathbf{q}_1 := \begin{cases} \begin{array}{l} \text{A constant extension in the vertical} \\ \text{direction of } \psi \mathbf{e}_r \text{ on } \Gamma_\eta : \mathbf{q}_1 := (0, \psi(z))^T; \\ \text{Notice div} \mathbf{q}_1 = 0. \end{array} \left.\begin{array}{} \\ \\ \\ \end{array}\right\} \text{on } \Omega_{max} \setminus \Omega_{min}, \\[2em] \begin{array}{l} \text{A divergence} - \text{free extension to } \Omega_{min} \\ \text{(see, e.g. [75], p. 127).} \end{array} \left.\begin{array}{} \\ \\ \end{array}\right\} \text{on } \Omega_{min}. \end{cases}
$$

From the construction it is clear that $\mathbf{q}_1$ is also defined on $\Omega_{\tau_{\Delta t}\eta_N}$ for each N, and so it can be mapped onto the reference domain Ω by the transformation $A_{\tau_{\Delta t}\eta_N}$. We take $\boldsymbol{\psi} \in H^1(\Omega_S)$ such that $\boldsymbol{\psi}(t, z, 1) = \psi(t, z)$.

For any test function $(\mathbf{q}, \psi, \boldsymbol{\psi}) \in \mathcal{Q}$ it is easy to see that the velocity component $\mathbf{q}$ can then be written as $\mathbf{q} = \mathbf{q} - \mathbf{q}_1 + \mathbf{q}_1$, where $\mathbf{q} - \mathbf{q}_1$ can be approximated by divergence-free functions $\mathbf{q}_0$ that have compact support in $\Omega_\eta \cup \Gamma_{in} \cup \Gamma_{out} \cup \Gamma_b$. Therefore, one can easily see that functions $(\mathbf{q}, \psi) = (\mathbf{q}_0 + \mathbf{q}_1, \psi)$ in $\mathcal{X}$ satisfy the following properties:

- $\mathcal{X}$ is dense in the space $\mathcal{Q}$ of all test functions defined on the physical, moving domain Ω_η, defined by (133); furthermore, $\nabla \cdot \mathbf{q} = 0, \forall \mathbf{q} \in \mathcal{X}_F$.

- For each $\mathbf{q} \in \mathcal{X}_F$, define
  $$\tilde{\mathbf{q}} = \mathbf{q} \circ A_\eta.$$
  The set $\{(\tilde{\mathbf{q}}, \psi, \boldsymbol{\psi}) | \tilde{\mathbf{q}} = \mathbf{q} \circ A_\eta, \mathbf{q} \in \mathcal{X}_F, \psi \in \mathcal{X}_S, \boldsymbol{\psi} \in \mathcal{X}_S\}$ is dense in the space $\mathcal{Q}_\eta$ of all test functions defined on the fixed, reference domain Ω_F, defined by (138).

- For each $\mathbf{q} \in \mathcal{X}_F$, define
  $$\mathbf{q}_N := \mathbf{q} \circ A_{\tau_{\Delta t}\eta_N}.$$
  Functions $\mathbf{q}_N$ are defined on the fixed domain Ω_F, and they satisfy $\nabla^{\tau_{\Delta t}\eta_N} \cdot \mathbf{q_N} = 0$.

Functions $\mathbf{q}_N$ will serve as test functions for approximate problems associated with the sequence of domains $\Omega_{\tau_{\Delta t}\eta_N}$, while functions $\tilde{\mathbf{q}}$ will serve as test functions associated with the domain Ω_η. Both sets of test functions are defined on Ω_F.

Lemma 1.6.6. *For every $(\mathbf{q}, \psi, \boldsymbol{\psi}) \in \mathcal{X}$ we have $\mathbf{q}_N \to \tilde{\mathbf{q}}$ uniformly in $L^\infty(0, T; C(\Omega_F))$.*

Proof. By the Mean-Value Theorem we get:

$$\begin{aligned}
|\mathbf{q}_N(t, z, r) - \tilde{\mathbf{q}}(t, z, r)| &= |\mathbf{q}(t, z, (1 + \tau_{\Delta t}\eta_N)r) - \mathbf{q}(t, z, (1 + \eta)r)| \\
&= |\partial_r \mathbf{q}(t, z, \zeta)r| \, |\eta(t, z) - \eta_N(t - \Delta t, z)|.
\end{aligned}$$

The uniform convergence of $\mathbf{q}_N$ follows from the uniform convergence of η_N, since $\mathbf{q}$ are smooth. $\qquad \square$

We are now ready to identify the weak limit $\mathbf{G}$ from Lemma 0.6.2.

Proposition 1.6.7. $\mathbf{G} = \nabla^\eta \mathbf{u}$, *where $\mathbf{G}$, $\mathbf{u}$ and η are the weak and weak* limits given by Lemma 0.6.2.*

Proof. As in Lemma 0.6.3, it will be helpful to map the approximate fluid velocities and the limiting fluid velocity onto the physical domains. For this purpose, we introduce the following functions

$$\mathbf{u}^N(t, .) = \mathbf{u}_N(t, .) \circ A_{\tau_{\Delta t}\eta_N}^{-1}(t), \qquad \tilde{\mathbf{u}}(t, .) = \mathbf{u}(t, .) \circ A_\eta^{-1}(t),$$

$$\chi^N \mathbf{f}(t, \mathbf{x}) = \begin{cases} \mathbf{f}, & \mathbf{x} \in \Omega_{\tau_{\Delta t}\eta_N}(t) \\ 0, & \mathbf{x} \notin \Omega_{\tau_{\Delta t}\eta_N}(t) \end{cases}, \quad \chi \mathbf{f}(t, \mathbf{x}) = \begin{cases} \mathbf{f}, & \mathbf{x} \in \Omega_\eta(t) \\ 0, & \mathbf{x} \notin \Omega_\eta(t) \end{cases},$$

where A is the ALE mapping defined by (106), η is the weak* limit $\eta_N \rightharpoonup \eta$ in $L^\infty(0, T; H_0^1(0,1))$ satisfying the uniform convergence property (169), and $\mathbf{f}$ is an arbitrary function defined on the physical domain. Notice, again, that superscript N is used to denote a function defined on the physical domain, while subscript N is used denote a function defined on the fixed domain Ω_F.

The proof consists of three main steps: (1) we will first show that $\chi^N \mathbf{u}^N \to \chi\tilde{\mathbf{u}}$ strongly in $L^2((0, T) \times \Omega_{max})$, then, by using step (1), we will show (2) $\chi^N \nabla \mathbf{u}^N \to \chi \nabla \tilde{\mathbf{u}}$ weakly in $L^2((0, T) \times \Omega_{max})$, and, finally by using (2) we will show (3) $\int_0^T \int_{\Omega_F} \mathbf{G} : \tilde{\mathbf{q}} = \int_0^T \int_{\Omega_F} \nabla^\eta \mathbf{u} : \tilde{\mathbf{q}}$ for every test function $\tilde{\mathbf{q}} = \mathbf{q} \circ A_\eta$.

STEP 1. We will show that $\|\chi^N \mathbf{u}^N - \chi\tilde{\mathbf{u}}\|_{L^2((0,T) \times \Omega_{max})} \to 0$. To achieve this goal, we introduce the following auxiliary functions

$$\tilde{\mathbf{u}}^N(t, .) = \mathbf{u}_N(t, .) \circ A_\eta^{-1}(t),$$

which will be used in the following estimate

$$\|\chi^N \mathbf{u}^N - \chi\tilde{\mathbf{u}}\|_{L^2((0,T) \times \Omega_{max})} \le \|\chi^N \mathbf{u}^N - \chi\tilde{\mathbf{u}}^N\|_{L^2((0,T) \times \Omega_{max})} + \|\chi\tilde{\mathbf{u}}^N - \chi\tilde{\mathbf{u}}\|_{L^2((0,T) \times \Omega_{max})}.$$

The second term on the right-hand side converges to zero because of the strong convergence of $\mathbf{u}_N$ to $\mathbf{u}$ on the reference domain Ω_F, namely,

$$\|\chi\tilde{\mathbf{u}}^N - \chi\tilde{\mathbf{u}}\|_{L^2(\Omega_{max})}^2 = \int_{\Omega_F} (1+\eta)|\mathbf{u}_N - \mathbf{u}|^2 \to 0.$$
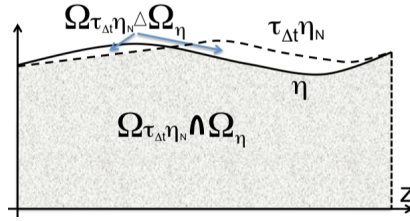
Figure 1.13: A sketch of the fluid domains in STEP 1.

To show that the first term on the right-hand side converges to zero, first notice that

$$\int_0^T \int_{\Omega_{max}} |\chi\tilde{\mathbf{u}}^N - \chi^N \mathbf{u}^N|^2 = \left(\int_0^T \int_{\Omega_\eta(t) \triangle \Omega_{\tau_{\Delta t} \eta_N}(t)} + \int_0^T \int_{\Omega_\eta(t) \cap \Omega_{\tau_{\Delta t} \eta_N}(t)} \right) |\chi\tilde{\mathbf{u}}^N - \chi^N \mathbf{u}^N|^2.$$

Here $A\triangle B := (A \cup B) \setminus (A \cap B)$. See Figure 13. Because of the uniform convergence (169) we can make the measure $|\Omega_\eta(t) \triangle \Omega_{\tau_{\Delta t} \eta_N}(t)|$ arbitrary small. Furthermore, by Propostions 0.6.5 and 0.6.6 we have that the sequence $(\chi\tilde{\mathbf{u}}^N - \chi^N \mathbf{u}^N)_{N \in \mathbb{N}}$ is

uniformly bounded in $L^2((0,T) \times \Omega_{max})$. Therefore, for every $\varepsilon > 0$, there exists an $N_0 \in \mathbb{N}$ such that for every $N \geq N_0$ we have

$$\int_0^T \int_{\Omega_\eta(t) \triangle \Omega_{\tau_{\Delta t} \eta_N}(t)} |\chi \tilde{\mathbf{u}}^N - \chi^N \mathbf{u}^N|^2 < \frac{\varepsilon}{2}. \tag{1.171}$$

To estimate the second term, we need to measure the relative difference between the function $\mathbf{u}_N$ composed with $A_\eta^{-1}(t)$, denoted by $\tilde{\mathbf{u}}^N$, and the same function $\mathbf{u}_N$ composed with $A_{\tau_{\Delta t} \eta_N(t)}^{-1}$, denoted by $\mathbf{u}^N$. We will map them both on the same domain and work with one function $\mathbf{u}_N$, while the convergence of the L^2-integral will be obtained by estimating the difference in the ALE mappings. More precisely, we introduce the set $\omega = A_\eta^{-1}(\Omega_\eta(t) \cap \Omega_{\tau_{\Delta t} \eta_N}(t)) \subset \Omega_F$. Now, we use the properties of the ALE mapping A_η and the definitions of $\tilde{\mathbf{u}}^N$, $\mathbf{u}^N$ to get

$$\int_0^T \int_{\Omega_\eta(t) \cap \Omega_{\tau_{\Delta t} \eta_N}(t)} |\chi \tilde{\mathbf{u}}^N - \chi^N \mathbf{u}^N|^2 = \int_0^T \int_\omega \frac{1}{1+\eta} |\mathbf{u}_N - \mathbf{u}_N \circ A_{\tau_{\Delta t} \eta_N(t)}^{-1} \circ A_{\eta(t)}|^2$$

$$= \int_0^T \int_\omega \frac{1}{1+\eta(t,z)} |\mathbf{u}_N(t,z,r) - \mathbf{u}_N(t,z, \frac{1+\eta(t,z)}{1+\tau_{\Delta t}\eta_N(t,z)} r)|^2$$

$$= \int_0^T \int_\omega \left| \partial_r \mathbf{u}_N(t,z,\zeta) r \left(1 - \frac{1+\eta(t,z)}{1+\tau_{\Delta t}\eta_N(t,z)}\right) \right|^2$$

Now because of the uniform convergence (169) of the sequence $(\tau_{\Delta t} \eta_N)_{N \in \mathbb{N}}$, and the uniform boundedness of $(\|\partial_r \mathbf{u}_N\|_{L^2(\Omega_F)})_{N \in \mathbb{N}}$, which is consequence of Proposition 0.6.6, we can take $N_1 \geq N_0$ such that

$$\int_0^T \int_{\Omega_\eta(t) \cap \Omega_{\tau_{\Delta t} \eta_N}(t)} |\chi \tilde{\mathbf{u}}^N - \chi^N \mathbf{u}^N|^2 < \frac{\varepsilon}{2}, \ N \geq N_1.$$

This inequality, together with (171) proofs that $\chi^N \mathbf{u}^N \to \chi \tilde{\mathbf{u}}$ strongly in $L^2((0,T) \times \Omega_{max})$.

STEP 2. We will now show that $\chi^N \nabla \mathbf{u}^N \rightharpoonup \chi \nabla \tilde{\mathbf{u}}$ weakly in $L^2((0,T) \times \Omega_{max})$. First notice that from

$$\nabla \mathbf{u}^N = \nabla^{\tau_{\Delta t} \eta_N} \mathbf{u}_N$$

and from uniform boundedness of $(\nabla^{\tau_{\Delta t} \eta_N} \mathbf{u}_N)_{N \in \mathbb{N}}$ in $L^2((0,T) \times \Omega_F)$, established in Proposition 0.6.6, we get that the sequence $(\chi^N \nabla \mathbf{u}^N)_{N \in \mathbb{N}}$ converges weakly in $L^2((0,T) \times \Omega_{max})$. Let us denote the weak limit of $(\chi^N \nabla \mathbf{u}^N)_{N \in \mathbb{N}}$ by $\tilde{\mathbf{G}}$. Therefore,

$$\int_0^T \int_{\Omega_{max}} \tilde{\mathbf{G}} \cdot \phi = \lim_{N \to \infty} \int_0^T \int_{\Omega_{max}} \chi^N \nabla \mathbf{u}^N \cdot \phi, \quad \phi \in C_c^\infty((0,T) \times \Omega_{max}).$$

We want to show that $\tilde{\mathbf{G}} = \chi \nabla \tilde{\mathbf{u}}$.

For this purpose, we first consider the set $(\Omega_{max} \setminus \Omega_\eta(t))$ and show that $\tilde{\mathbf{G}} = 0$ there, and then the set $\Omega_\eta(t)$ and show that $\tilde{\mathbf{G}} = \nabla \tilde{\mathbf{u}}$ there.

Let ϕ be a test function such that $\text{supp}\phi \subset (0,T) \times \left(\Omega_{max} \setminus \Omega_\eta(t) \right)$. Using the uniform convergence of the sequence $\tau_{\Delta t} \eta_N$, obtained in (169), there exists an N_ϕ such that $\chi^N(\mathbf{x}) = 0$, $N \geq N_\phi$, $\mathbf{x} \in \text{supp}\phi$. Therefore, we have

$$\int_0^T \int_{\Omega_{max}} \tilde{\mathbf{G}} \cdot \phi = \lim_{N \to \infty} \int_0^T \int_{\Omega_{max}} \chi^N \nabla \mathbf{u}^N \cdot \phi = 0.$$

Thus, $\tilde{\mathbf{G}} = 0$ on $(0,T) \times \left(\Omega_{max} \setminus \Omega_\eta(t) \right)$.

Now, let us take a test function ψ such that $\text{supp}\psi \subset (0,T) \times \Omega_\eta(t)$. Again using the same argument as before, as well as the uniform convergence of the sequence $\tau_{\Delta t} \eta_N$, obtained in (169), we conclude that there exists an N_ψ such that $\chi^N(\mathbf{x}) = 1$, $N \geq N_\psi$, $\mathbf{x} \in \text{supp}\psi$. Therefore, we have

$$\int_0^T \int_{\Omega_{max}} \tilde{\mathbf{G}} \cdot \psi = \lim_{N \to \infty} \int_0^T \int_{\Omega_{max}} \chi^N \nabla \mathbf{u}^N \cdot \psi = \lim_{N \to \infty} \int_0^T \int_{\Omega_\eta(t)} \nabla \mathbf{u}^N \cdot \psi.$$

From the strong convergence $\chi^N \mathbf{u}^N \to \chi \tilde{\mathbf{u}}$ obtained in STEP 1, we have that on the set $\text{supp}\psi$, $\mathbf{u}^N \to \tilde{\mathbf{u}}$ in the sense of distributions, and so, on the same set $\text{supp}\psi$, $\nabla \mathbf{u}^N \to \nabla \tilde{\mathbf{u}}$ in the sense of distributions. Therefore we have

$$\int_0^T \int_{\Omega_{max}} \tilde{\mathbf{G}} \cdot \psi = \lim_{N \to \infty} \int_0^T \int_{\Omega_\eta(t)} \nabla \mathbf{u}^N \cdot \psi = \int_0^T \int_{\Omega_\eta(t)} \nabla \tilde{\mathbf{u}} \cdot \psi.$$

Since this conclusion holds for all the test functions ψ supported in $(0,T) \times \Omega_{\eta(t)}$, from the uniqueness of the limit, we conclude $\tilde{\mathbf{G}} = \nabla \tilde{\mathbf{u}}$ in $(0,T) \times \Omega_{\eta(t)}$.

Therefore, we have shown that

$$\chi^N \nabla \mathbf{u}^N \quad \rightharpoonup \quad \chi \nabla \tilde{\mathbf{u}} \text{ weakly in } L^2((0,T) \times \Omega_{max}).$$

STEP 3. We want to show that $\int_0^T \int_{\Omega_F} \mathbf{G} : \tilde{\mathbf{q}} = \int_0^T \int_{\Omega_F} \nabla^\eta \mathbf{u} : \tilde{\mathbf{q}}$ for every test function $\tilde{\mathbf{q}} = \mathbf{q} \circ A_\eta$, $\mathbf{q} \in \mathcal{X}_F$. This will follow from STEP 2, the uniform boundedness and convergence of the gradients $\nabla^{\tau_{\Delta t} \eta_N} \tilde{\mathbf{u}}_N$ provided by Lemma 0.6.2, and from the strong convergence of the test functions $\mathbf{q}_N \to \tilde{\mathbf{q}}$ provided by Lemma 0.6.6. More precisely, we have that for every $\tilde{\mathbf{q}} = \mathbf{q} \circ A_\eta$, $\mathbf{q} \in \mathcal{X}_F$

$$\int_0^T \int_{\Omega_F} \mathbf{G} : \tilde{\mathbf{q}} = \lim_{N \to \infty} \int_0^T \int_{\Omega_F} \nabla^{\tau_{\Delta t} \eta_N} \mathbf{u}_N : \mathbf{q}_N$$

$$= \lim_{N \to \infty} \int_0^T \int_{\Omega_{max}} \frac{1}{1 + \tau_{\Delta t} \eta_N} \chi^N \nabla \mathbf{u}^N : \mathbf{q} = \int_0^T \int_{\Omega_\eta} \frac{1}{1 + \eta} \nabla \tilde{\mathbf{u}} : \mathbf{q} = \int_0^T \int_{\Omega_F} \nabla^\eta \mathbf{u} : \tilde{\mathbf{q}}.$$

Here, we have used from (110) that $\nabla \mathbf{u}^N = \nabla^{\tau_{\Delta t} \eta_N} \mathbf{u}_N$, and $\nabla \tilde{\mathbf{u}} = \nabla^\eta \mathbf{u}$. This completes proof. $\square$

Corollary 1.6.1. *For every* $(\mathbf{q}, \psi, \boldsymbol{\psi}) \in \mathcal{X}$ *we have*

$$\nabla^{\tau_{\Delta t}\eta_N}\mathbf{q}_N \to \nabla^{\eta}\tilde{\mathbf{q}}, \text{ in } L^2((0,T)\times\Omega_F).$$

Proof. Since $\tau_{\Delta t}\eta_N\mathbf{q}_N$ and $\tilde{\mathbf{q}}$ are the test functions for the velocity fields, the same arguments as in Proposition 0.6.7 provide weak convergence of $(\nabla^{\tau_{\Delta t}\eta_N}\mathbf{q}_N)_{N\in\mathbb{N}}$. To prove strong convergence it is sufficient to prove the convergence of norms $\|\nabla^{\tau_{\Delta t}\eta_N}\mathbf{q}_N\|_{L^2(\Omega_F)} \to \|\nabla^{\eta}\tilde{\mathbf{q}}\|_{L^2(\Omega_F)}$. This can be done, by using the uniform convergence of $(\tau_{\Delta t}\eta_N)_{N\in\mathbb{N}}$, in the following way:

$$\|\nabla^{\tau_{\Delta t}\eta_N}\mathbf{q}_N\|^2_{L^2(\Omega_F)} = \int_0^T \int_{\Omega_{max}} \chi^N \frac{1}{1+\tau_{\Delta t}\eta_N}|\nabla\mathbf{q}|^2 \to \int_0^T \int_{\Omega_{max}} \chi\frac{1}{1+\eta}|\nabla\mathbf{q}|^2$$

$$= \int_0^T \int_{\Omega_F} |\nabla^{\eta}\tilde{\mathbf{q}}|^2 = \|\nabla^{\eta}\tilde{\mathbf{q}}\|^2_{L^2(\Omega_F)}.$$

The notation used here is analogous to that used in the proof of Proposition 0.6.7. $\square$

Before we can pass to the limit in the weak formulation of the approximate problems, there is one more useful observation that we need. Namely, notice that although $\mathbf{q}$ are smooth functions both in the spatial variables and in time, the functions $\mathbf{q}_N$ are discontinuous at $n\Delta t$ because $\tau_{\Delta t}\eta_N$ is a step function in time. As we shall see below, it will be useful to approximate each discontinuous function $\mathbf{q}_N$ in time by a piece-wise constant function, $\bar{\mathbf{q}}_N$, so that

$$\bar{\mathbf{q}}_N(t,.) = \mathbf{q}(n\Delta t-,.), \quad t \in [(n-1)\Delta t, n\Delta t), \ n = 1,\dots,N,$$

where $\mathbf{q}_N(n\Delta t-)$ is the limit from the left of $\mathbf{q}_N$ at $n\Delta t$, $n = 1,\dots,N$. By using Lemma 0.6.6, and by applying the same arguments in the proof of Lemma 0.6.5, we get

$$\bar{\mathbf{q}}_N \to \tilde{\mathbf{q}} \text{ uniformly on } [0,T]\times\Omega.$$

Passing to the limit

To get to the weak formulation of the coupled problem, take the test functions $(\psi(t), \boldsymbol{\psi}(t)) \in \mathcal{X}_W \times \mathcal{X}_S$ as the test functions in the weak formulation of the structure sub-problem (143) and integrate the weak formulation (143) with respect to t from $n\Delta t$ to $(n+1)\Delta t$. Notice that the construction of the test functions is done in such a way that $(\psi(t), \boldsymbol{\psi}(t))$ do not depend on N, and are continuous. Then, consider the weak formulation (146) of the fluid sub-problem and take the test functions $(\mathbf{q}_N(t), \psi(t))$ (where $\mathbf{q}_N = \mathbf{q} \circ A_{\tau_{\Delta t}\eta_N}$, $\mathbf{q} \in \mathcal{X}_F$). Integrate the fluid sub-problem (146) with respect to t from $n\Delta t$ to $(n+1)\Delta t$. Add the two weak formulations together, and take the sum from $n = 0,\dots,N-1$ to get the time

integrals over $(0, T)$ as follows:

$$
\int_0^T \int_{\Omega_F} (1 + \tau_{\Delta t}\, \eta_N)\Big(\partial_t \tilde{\mathbf{u}}_N \cdot \mathbf{q}_N + \frac{1}{2}(\tau_{\Delta t}\mathbf{u}_N - \mathbf{w}_N) \cdot \nabla^{\tau_{\Delta t}\eta_N} \mathbf{u}_N \cdot \mathbf{q}_N
$$

$$
- \frac{1}{2}(\tau_{\Delta t}\mathbf{u}_N - \mathbf{w}_N) \cdot \nabla^{\tau_{\Delta t}\eta_N} \mathbf{q}_N \cdot \mathbf{u}_N\Big) + \frac{1}{2}\int_0^T \int_{\Omega_F} v_N^* \mathbf{u}_N \cdot \mathbf{q}_N
$$

$$
+ \int_0^T \int_{\Omega_F} (1 + \tau_{\Delta t}\eta_N)2\mathbf{D}^{\tau_{\Delta t}\eta_N}(\mathbf{u_N}) : \mathbf{D}^{\tau_{\Delta t}\eta_N}(\mathbf{q}_N) + \int_0^T \int_0^1 \partial_t \tilde{v}_N \psi \qquad (1.172)
$$

$$
+ \int_0^T \int_0^1 \partial_z \eta_N \partial_z \psi + \int_0^T \int_{\Omega_S} \partial_t \tilde{\boldsymbol{V}}_N \cdot \boldsymbol{\psi} + \int_0^T \int_{\Omega_S} a_S(\boldsymbol{d}_N, \boldsymbol{\psi})
$$

$$
= \int_0^T P_{in}^N dt \int_0^1 q_z(t, 0, r)dr - \int_0^T P_{out}^N dt \int_0^1 q_z(t, L, r)dr,
$$

with

$$
\nabla^{\tau_{\Delta t}\eta} \cdot \mathbf{u}_N = 0, \quad v_N = ((u_r)_N)_{|\Gamma},\ \eta_N = (\boldsymbol{d}_N)_{|\Gamma},
$$

$$
\mathbf{u}_N(0,.) = \mathbf{u}_0,\ \eta(0,.)_N = \eta_0,\ v_N(0,.) = v_0. \qquad (1.173)
$$

Here $\tilde{\mathbf{u}}_N$, $\tilde{v}_N$ and $\tilde{\boldsymbol{V}}_N$ are the piecewise linear functions defined in (162), $\tau_{\Delta t}$ is the shift in time by Δt to the left, defined in (151), $\nabla^{\tau_{\Delta t}\eta_N}$ is the transformed gradient via the ALE mapping $A_{\tau_{\Delta t}\eta_N}$, defined in (110), and v_N^*, $\mathbf{u}_N$, v_N, η_N, $\boldsymbol{d}_N$ and $\boldsymbol{V}_N$ are defined in (148).

Using the convergence results obtained for the approximate solutions in Section 0.6.6, and the convergence results just obtained for the test functions $\mathbf{q}_N$, we can pass to the limit directly in all the terms except in the term that contains $\partial_t \tilde{\mathbf{u}}_N$. To deal with this term we notice that, since $\mathbf{q}_N$ are smooth on sub-intervals $(j\Delta t, (j+1)\Delta t)$, we can use integration by parts on these sub-intervals to obtain:

$$
\int_0^T \int_{\Omega_F} (1 + \tau_{\Delta t}\eta_N)\partial_t \tilde{\mathbf{u}}_N \cdot \mathbf{q}_N = \sum_{j=0}^{N-1} \int_{j\Delta t}^{(j+1)\Delta t} \int_{\Omega_F} (1 + \eta_N^j)\partial_t \tilde{\mathbf{u}}_N \cdot \mathbf{q}_N
$$

$$
= \sum_{j=0}^{N-1} \Big(- \int_{j\Delta t}^{(j+1)\Delta t} \int_{\Omega_F} (1 + \tau_{\Delta t}\eta_N)\tilde{\mathbf{u}}_N \cdot \partial_t \mathbf{q}_N
$$

$$
+ \int_{\Omega_F} (1 + \eta^{j+1} - \eta^{j+1} + \eta^j)\mathbf{u}_N^{j+1} \cdot \mathbf{q}_N((j+1)\Delta t-) - \int_{\Omega_F} (1 + \eta^j)\mathbf{u}_N^j \cdot \mathbf{q}_N(j\Delta t+)\Big).
$$

$$
(1.174)
$$

Here, we have denoted by $\mathbf{q}_N((j+1)\Delta t-)$ and $\mathbf{q}_N(j\Delta t+)$ the limits from the left and right, respectively, of $\mathbf{q}_N$ at the appropriate points.

The integral involving $\partial_t \mathbf{q}_N$ can be simplified by recalling that $\mathbf{q}_N = \mathbf{q} \circ A_{\eta_N}$, where η_N are constant on each sub-interval $(j\Delta t, (j+1)\Delta t)$. Thus, by the chain rule, we see that $\partial_t \mathbf{q}_N = \partial_t \mathbf{q}$ on $(j\Delta t, (j+1)\Delta t)$. After summing over all $j = 0, ..., N-1$ we obtain

$$-\sum_{j=0}^{N-1} \int_{j\Delta t}^{(j+1)\Delta t} \int_{\Omega_F} (1 + \tau_{\Delta t}\eta_N)\tilde{\mathbf{u}}_N \cdot \partial_t \mathbf{q}_N = -\int_0^T \int_{\Omega_F} (1 + \tau_{\Delta t}\eta_N)\tilde{\mathbf{u}}_N \cdot \partial_t \mathbf{q}.$$

To deal with the last two terms in (174) we calculate

$$\sum_{j=0}^{N-1} \left(\int_{\Omega_F} (1+\eta_N^{j+1}-\eta_N^{j+1}+\eta_N^j)\mathbf{u}_N^{j+1}\cdot\mathbf{q}_N((j+1)\Delta t-) - \int_{\Omega_F} (1+\eta_N^j)\mathbf{u}_N^j\cdot\mathbf{q}_N(j\Delta t+) \right)$$

$$= \sum_{j=0}^{N-1} \int_{\Omega_F} \left((1+\eta_N^{j+1})\mathbf{u}_N^{j+1}\cdot\mathbf{q}_N((j+1)\Delta t-) - (\eta_N^{j+1}-\eta_N^j)\mathbf{u}_N^{j+1}\cdot\mathbf{q}_N((j+1)\Delta t-) \right)$$

$$- \int_\Omega (1+\eta_0)\mathbf{u}_0\cdot\mathbf{q}(0) - \sum_{j=1}^{N-1}\int_{\Omega_F}(1+\eta_N^j)\mathbf{u}_N^j\cdot\mathbf{q}_N(j\Delta t+) \Big)$$

Now, we can write $(\eta^{j+1} - \eta^j)$ as $v^{j+\frac{1}{2}}\Delta t$, and rewrite the summation indexes in the first term to obtain that the above expression is equal to

$$= \sum_{j=1}^{N}\int_{\Omega_F}(1+\eta_N^j)\mathbf{u}_N^j\cdot\mathbf{q}_N(j\Delta t-) - \int_0^T\int_{\Omega_F}v_N^*\mathbf{u}_N\cdot\bar{\mathbf{q}}_N - \int_{\Omega_F}(1+\eta_0)\mathbf{u}_0\cdot\mathbf{q}(0) - \sum_{j=1}^{N-1}\int_{\Omega_F}(1+\eta_N^j)\mathbf{u}_N^j\cdot\mathbf{q}_N(j\Delta t+).$$

Since the test functions have compact support in $[0, T)$, the value of the first term at $j = N$ is zero, and so we can combine the two sums to obtain

$$= \sum_{j=1}^{N}\int_{\Omega_F}(1+\eta_N^j)\mathbf{u}_N^j\cdot(\mathbf{q}_N(j\Delta t-) - \mathbf{q}_N(j\Delta t+)) - \int_{\Omega_F}(1+\eta_0)\mathbf{u}_0\cdot\mathbf{q}(0) - \int_0^T\int_{\Omega_F}v_N^*\mathbf{u}_N\cdot\bar{\mathbf{q}}_N.$$

Now we know how to pass to the limit in all the terms expect the first one. We continue to rewrite the first expression by using the Mean Value Theorem to obtain:

$$\mathbf{q}_N(j\Delta t-, z, r) - \mathbf{q}_N(j\Delta t+, z, r) = \mathbf{q}(j\Delta t, z, (1+\eta_N^j)r) - \mathbf{q}(j\Delta t, z, (1+\eta_N^{j+1})r) =$$

$$= \partial_r\mathbf{q}(j\Delta t, z, \zeta)r(\eta_N^j - \eta_N^{j+1}) = -\Delta t\partial_r\mathbf{q}(j\Delta t, z, \zeta)v_N^{j+\frac{1}{2}}r.$$

Therefore we have:

$$\sum_{j=1}^{N-1}\int_{\Omega_F}(1+\eta_N^j)\mathbf{u}_N^j\big(\mathbf{q}(j\Delta t-)-\mathbf{q}(j\Delta t+)\big) = -\int_0^{T-\Delta t}\int_{\Omega_F}(1+\eta_N)\mathbf{u}_N r\tau_{-\Delta t}v_N^*\partial_r\bar{\mathbf{q}}.$$

We can now pass to the limit in this last term to obtain:

$$\int_0^{T-\Delta t}\int_{\Omega_F}(1+\eta_N)\mathbf{u}_N r\tau_{-\Delta t}v_N^*\partial_r\bar{\mathbf{q}}\rightarrow\int_0^T\int_{\Omega_F}(1+\eta)\mathbf{u}r\partial_t\eta\partial_r\mathbf{q}.$$

Therefore, by noticing that $\partial_t\tilde{\mathbf{q}}=\partial_t\mathbf{q}+r\partial_t\eta\partial_r\mathbf{q}$ we have finally obtained

$$\int_0^T\int_{\Omega_F}(1+\tau_{\Delta t}\eta_N)\partial_t\tilde{\mathbf{u}}_N\cdot\mathbf{q}_N\rightarrow-\int_0^T\int_{\Omega_F}(1+\eta)\mathbf{u}\cdot\partial_t\tilde{\mathbf{q}}-\int_0^T\int_{\Omega_F}\partial_t\eta\mathbf{u}\cdot\tilde{\mathbf{q}}$$

$$-\int_{\Omega_F}(1+\eta_0)\mathbf{u}_0\cdot\tilde{\mathbf{q}}(0),$$

where we recall that $\tilde{\mathbf{q}}=\mathbf{q}\circ A_\eta$.

Thus, we have shown that the limiting functions $\mathbf{u}$, η and $\boldsymbol{d}$ satisfy the weak form of problem (111)-(118) in the sense of Definition 0.6.2, for all test functions that belong to a dense subset of $\mathcal{Q}^\eta$. By density arguments, we have, therefore, shown the main result of this manuscript:

Theorem 1.6.4. (Main Theorem) *Suppose that the initial data $v_0\in L^2(0,1)$, $\mathbf{u}_0\in L^2(\Omega_{\eta_0})$, $\boldsymbol{V}_0\in L^2(\Omega_S)$, $\boldsymbol{d}_0\in H^1(\Omega_S)$, and $\eta_0\in H_0^1(0,1)$ are such that $1+\eta_0(z)>0$, $z\in[0,1]$ and compatibility conditions (102) are satisfied. Furthermore, let P_{in}, $P_{out}\in L_{loc}^2(0,\infty)$.*

Then, there exist a $T>0$ and a weak solution $(\mathbf{u},\eta,\boldsymbol{d})$ of problem (111)-(118) (or equivalently problem (91)-(102)) on $(0,T)$ in the sense of Definition 0.6.2 (or equivalently Definition 0.6.1), such that the following energy estimate is satisfied:

$$E(t)+\int_0^t D(\tau)d\tau\leq E_0+C(\|P_{in}\|_{L^2(0,t)}^2+\|P_{out}\|_{L^2(0,t)}^2),\quad t\in[0,T],\quad(1.175)$$

where C depends only on the coefficients in the problem, E_0 is the kinetic energy of initial data, and $E(t)$ and $D(t)$ are given by

$$E(t)=\frac{1}{2}\|\mathbf{u}\|_{L^2(\Omega_F)}^2+\frac{1}{2}\|\partial_t\eta\|_{L^2(0,1)}^2+\frac{1}{2}\|\boldsymbol{d}\|_{L^2(\Omega_S)}^2+\frac{1}{2}(\|\partial_z\eta\|_{L^2(0,1)}^2+a_S(\boldsymbol{d},\boldsymbol{d})),$$
$$D(t)=\|\mathbf{D}(\mathbf{u})\|_{L^2(\Omega_\eta(t)))}^2.$$

Furthermore, one of the following is true:

$$either\ T=\infty\ \ or\ \lim_{t\rightarrow T}\min_{z\in[0,1]}(1+\eta(z))=0.\qquad(1.176)$$

Proof. It only remains to prove the last assertion, which states that our result is either global in time, or, in case the walls of the cylinder touch each other, our existence result holds until the time of touching. However, the proof of this argument follows the same reasoning as the proof of the Main Theorem in [119], and the proof of the main result in [32], p. 397-398. We avoid repeating those arguments here, and refer the reader to references [119, 32]. □

1.7   Numerical Simulation

In this section we show how the Kinematically-Coupled β-Scheme can be applied to FSI problems with multiple structural layers. We also present numerical arguments showing that the presence of a thin fluid-structure interface with mass, regularizes solutions of the related FSI problems.

We first summarize the FSI problem that will be solved numerically, then present the numerical algorithm, and finally show the numerical results. The problem, the numerical method, and the results will be shown on an example in 2D.

1.7.1   Problem Definition

We consider the flow of an incompressible, viscous fluid in a two-dimensional channel of reference length L, and reference width $2R$, see Figure 9. The channel is bounded by a two-layered deformable wall, which consists of a thin elastic layer with thickness h, and a thick elastic layer with thickness H. The thin structural layer serves as a fluid-structure interface with mass.

We are interested in simulating the normal stress-driven fluid flow through a deformable 2D channel with two-way coupling between the fluid and structure. Without loss of generality, we consider only the upper half of the fluid domain supplemented by a symmetry condition at the axis of symmetry. Thus, as before, the reference fluid and structure domains in our problem are given, respectively, by

$$
\begin{aligned}
\Omega_F &:= \{(z,r)|0 < z < L, 0 < r < R\}, \\
\Omega_S &:= \{(z,r)|0 < z < L, R < r < R+H\}.
\end{aligned}
$$

Here z and r denote the horizontal and vertical Cartesian coordinates, respectively (see Figure 9).

The flow of an incompressible, viscous fluid is modeled by the Navier-Stokes equations:

$$
\rho_F\left(\frac{\partial \mathbf{u}}{\partial t} + \mathbf{u}\cdot\nabla\mathbf{u}\right) = \nabla\cdot\boldsymbol{\sigma}(\mathbf{u},p) \qquad \text{in } \Omega_F(t)\times(0,T), \qquad (1.177)
$$

$$
\nabla\cdot\mathbf{u} = 0 \qquad\qquad\qquad \text{in } \Omega_F(t)\times(0,T), \qquad (1.178)
$$

where $\mathbf{u} = (u_z, u_r)$ is the fluid velocity, p is the fluid pressure, ρ_F is the fluid density, and $\boldsymbol{\sigma}$ is the fluid Cauchy stress tensor. For a Newtonian fluid the Cauchy stress tensor is given by $\boldsymbol{\sigma}(\mathbf{u},p) = -p\boldsymbol{I} + 2\mu_F\boldsymbol{D}(\mathbf{u})$, where μ_F is the fluid viscosity and $\boldsymbol{D}(\mathbf{u}) = (\nabla\mathbf{u} + (\nabla\mathbf{u})^\tau)/2$ is the rate-of-strain tensor.

Denote the inlet and outlet fluid boundaries by $\Gamma_{in} = \{0\}\times(0,R)$ and $\Gamma_{out} = \{L\}\times(0,R)$, respectively. At the inlet and outlet boundary we prescribe the normal stress:

$$
\boldsymbol{\sigma}\boldsymbol{n}_{in} = -p_{in}(t)\boldsymbol{n}_{in} \qquad\qquad \text{on } \Gamma_{in}\times(0,T), \qquad (1.179)
$$

$$
\boldsymbol{\sigma}\boldsymbol{n}_{out} = -p_{out}(t)\boldsymbol{n}_{out} \qquad\qquad \text{on } \Gamma_{out}\times(0,T), \qquad (1.180)
$$

where $\boldsymbol{n}_{in}$ and $\boldsymbol{n}_{out}$ are the outward normals to the inlet and outlet fluid boundaries, respectively. Even though not physiologically optimal, these boundary conditions are common in blood flow modeling [9, 126].

At the bottom fluid boundary $r = 0$ we impose the symmetry conditions:

$$\frac{\partial u_z}{\partial r}(z, 0, t) = 0, \quad u_r(z, 0, t) = 0 \quad \text{on } (0, L) \times (0, T). \tag{1.181}$$

The lateral fluid boundary is bounded by a deformable, thin wall. We assume that the wall is linearly elastic, whose dynamics is modeled by the linearly elastic Koiter membrane model, specified in (25), Section 92:

$$\rho_K h \frac{\partial^2 \eta_z}{\partial t^2} - C_2 \frac{\partial \eta_r}{\partial z} - C_1 \frac{\partial^2 \eta_z}{\partial z^2} = f_z \qquad \text{on } \Gamma \times (0, T), \tag{1.182}$$

$$\rho_K h \frac{\partial^2 \eta_r}{\partial t^2} + C_0 \eta_r + C_2 \frac{\partial \eta_z}{\partial z} = f_r \qquad \text{on } \Gamma \times (0, T), \tag{1.183}$$

where $\boldsymbol{\eta}(z, t) = (\eta_x(z, t), \eta_r(z, t))$ denotes the axial and radial displacement, $\boldsymbol{f} = (f_z, f_r)$ is the force surface density, ρ_K denotes the shell density and (see (25))

$$C_0 = \frac{hE}{R^2(1 - \sigma^2)}, \quad C_1 = \frac{hE}{1 - \sigma^2}, \quad C_2 = \frac{hE\sigma}{R(1 - \sigma^2)}.$$

The thick layer of the wall will be modeled by the equations of linear elasticity (59), with an added extra term $\gamma \mathbf{d}$ to account for circumferential strain whose effects are lost in the transition from 3D to 2D. This term corresponds to the non-differentiated term in the Koiter membrane equations (183) containing the coefficient C_0, which appears in these equations due to the cylindrical geometry of the domain. Adding the non-differentiated term $\gamma \mathbf{d}$ to the thick structure problem in 2D has been done by several authors, see [8, 9, 114, 14]. If the structure is not fixed at the end points, this term helps keep the top and bottom portions of the structure domain together. The model reads:

$$\rho_S \frac{\partial^2 \mathbf{d}}{\partial t^2} + \gamma \mathbf{d} = \nabla \cdot \boldsymbol{S}(\mathbf{d}) \quad \text{in } \Omega_S \times (0, T), \tag{1.184}$$

with the first Piola-Kirschhoff stress tensort $\boldsymbol{S}$ given by

$$\boldsymbol{S}(\mathbf{d}) = 2\mu \boldsymbol{D}(\mathbf{d}) + \lambda(\nabla \cdot \mathbf{d})\boldsymbol{I},$$

where $\mathbf{d} = (d_z, d_r)$ is the structure displacement and ρ_S is the structure density.

As before, the structure is assumed to be fixed at the inlet and outlet boundaries:

$$\mathbf{d}(0, r, t) = \mathbf{d}(L, r, t) = 0 \quad \text{on } [R, R + H] \times (0, T), \tag{1.185}$$

and the external structure boundary $\Gamma_{ext} = \{R + H\} \times (0, L)$ is exposed to zero external ambient pressure, while the axial displacement remains fixed:

$$\boldsymbol{S}\boldsymbol{n}_{ext} \cdot \boldsymbol{n}_{ext} = 0 \qquad \qquad \text{on } \Gamma_{ext} \times (0, T), \tag{1.186}$$

$$d_z = 0 \qquad \qquad \text{on } \Gamma_{ext} \times (0, T), \tag{1.187}$$

where $\boldsymbol{n}_{ext}$ is the outward unit normal vector on Γ_{ext}.

Initially, the fluid and the structure are assumed to be at rest, with zero displacement from the reference configuration

$$\boldsymbol{v} = 0, \quad \boldsymbol{\eta} = 0, \quad \frac{\partial \boldsymbol{\eta}}{\partial t} = 0, \quad \mathbf{d} = 0, \quad \frac{\partial \mathbf{d}}{\partial t} = 0, \quad \text{at } t = 0. \tag{1.188}$$

The fluid and the multilayered structure are coupled via the kinematic and dynamic boundary conditions (62), (63):
Continuity of the velocity:

$$\mathbf{u}(z + \eta_z(z,t), R + \eta_r(z,t), t) = \frac{\partial \boldsymbol{\eta}}{\partial t}(z,t) \quad \text{on } (0, L) \times (0, T), \tag{1.189}$$

Continuity of displacement:

$$\boldsymbol{\eta}(z,t) = \mathbf{d}(z, R, t) \quad \text{on } (0, L) \times (0, T). \tag{1.190}$$

Balance of forces:

$$\begin{pmatrix} \rho_K h \dfrac{\partial^2 \eta_z}{\partial t^2} - C_2 \dfrac{\partial \eta_r}{\partial z} - C_1 \dfrac{\partial^2 \eta_z}{\partial z^2} \\ \rho_K h \dfrac{\partial^2 \eta_r}{\partial t^2} + C_0 \eta_r + C_2 \dfrac{\partial \eta_z}{\partial z} \end{pmatrix} = \boldsymbol{S}\mathbf{e}_r|_\Gamma - J \, \boldsymbol{\sigma} \boldsymbol{n}|_{\Gamma(t)} \quad \text{on } (0, L) \times (0, T), \tag{1.191}$$

where J is the Jacobian of the transformation from the Eulerian to Lagrangian framework, $\boldsymbol{n}$ is the outward unit normal to the deformed fluid domain, and $\mathbf{e}_r$ is the unit vector pointing in the vertical direction.

1.7.2   The Energy of the Coupled Problem

The coupled problem (177)-(191) satisfies the following energy equality:

$$\frac{1}{2}\frac{d}{dt}\Big\{\rho_F\|\mathbf{u}\|^2_{\Omega_F(t)} + \rho_K h\|\partial_t\boldsymbol{\eta}\|^2_{L^2(\Gamma)} + \rho_S\|\partial_t\mathbf{d}\|^2_{L^2(\Omega_S)} + E^{mem}_{el}(\boldsymbol{\eta})$$

$$+ \gamma\|\mathbf{d}\|^2_{L^2(\Omega_S)} + 2\mu\|\mathbf{D}(\mathbf{d})\|^2_{L^2(\Omega_S)} + \lambda\|\nabla\cdot\mathbf{d}\|^2_{L^2(\Omega_S)}\Big\} + \mu_F\|\mathbf{D}(\mathbf{u})\|^2_{\Omega_F(t)}$$

$$= \int_0^R p_{in}(t)u_z|_{z=0} - \int_0^R p_{out}(t)u_z|_{z=L}$$

where

$$E^{mem}_{el}(\boldsymbol{\eta}) = \frac{h}{2}\int_0^L \mathcal{A}\mathbf{G}(\boldsymbol{\eta}) : \mathbf{G}(\boldsymbol{\eta})$$

$$= \frac{h}{2}\left[\frac{4E}{1+\sigma}\left\|\frac{\eta_r}{R}\right\|^2_{L^2(0,L)} + \frac{4E}{1+\sigma}\left\|\frac{\partial\eta_z}{\partial z}\right\|^2_{L^2(0,L)} + \frac{4E\sigma}{1-\sigma^2}\left\|\frac{\partial\eta_z}{\partial z} + \frac{\eta_r}{R}\right\|^2_{L^2(0,L)}\right]$$

If the inlet and outlet data are the *dynamic pressure data* (64), then the following energy estimate holds:

$$\frac{1}{2}\frac{d}{dt}\Big\{\rho_F\|\mathbf{u}\|^2_{\Omega_F(t)} + \rho_K h\|\partial_t\boldsymbol{\eta}\|^2_{L^2(\Gamma)} + \rho_S\|\partial_t\mathbf{d}\|^2_{L^2(\Omega_S)} + E^{mem}_{el}(\boldsymbol{\eta})$$
$$+ \gamma\|\mathbf{d}\|^2_{L^2(\Omega_S)} + 2\mu\|\mathbf{D}(\mathbf{d})\|^2_{L^2(\Omega_S)} + \lambda\|\nabla\cdot\mathbf{d}\|^2_{L^2(\Omega_S)}\Big\} + \mu_F\|\mathbf{D}(\mathbf{u})\|^2_{\Omega_F(t)}$$
$$\leq C(P_{in}(t), P_{out}(t)).$$

1.7.3 The ALE Formulation

As mentioned in Section 0.3, to deal with the motion of the fluid domain we use the ALE approach. An ALE mapping $\mathcal{A}$ maps the reference domain Ω_F into the current domain $\Omega_F(t)$:

$$\mathcal{A}:\Omega_F\to\Omega_F(t)\subset\mathbb{R}^2,\quad \boldsymbol{x}=\mathcal{A}(\boldsymbol{x})\in\Omega_F(t),\quad\text{for }\boldsymbol{x}\in\Omega_F.$$

We will use ALE mapping to deal with the deformation of the mesh, and to resolve the issues related to the approximation of the time-derivative $\partial\boldsymbol{v}/\partial t\approx(\boldsymbol{v}(t^{n+1})-\boldsymbol{v}(t^n))/\Delta t,$, which due to the fact that $\Omega_F(t)$ depends on time, is not well defined. In particular, we will be using the ALE mapping which is defined as the harmonic extension of the boundary, determined by the current position of $\boldsymbol{\eta}$, to the entire fluid domain:

$$\begin{aligned}\Delta\mathcal{A} &= 0,\ \text{in }\Omega_{\mathrm{F}},\\ \mathcal{A}|_\Gamma &= \boldsymbol{\eta},\\ \mathcal{A}|_{\partial\Omega_F\setminus\Gamma} &= 0.\end{aligned}$$

To solve the Navier-Stokes equations numerically on a moving domain, we transform the time derivative of the fluid velocity using the chain rule

$$\frac{\partial\mathbf{u}}{\partial t}\Big|_{\Omega_F} = \frac{\partial\mathbf{u}}{\partial t} + \mathbf{w}\cdot\nabla\mathbf{u}, \tag{1.192}$$

where $\mathbf{w} = \dfrac{\partial\mathcal{A}}{\partial t}$ denotes the domain velocity, and consider the rest of the problem defined on the moving domain $\Omega_F(t)$. See Section 0.5.2. Therefore, with a slight abuse of notation, the Navier-Stokes problem (177)-(178) that will be solved numerically, can be written in ALE formulation as follows: find $\mathbf{u} = (u_z, u_r)$ and p such that

$$\rho_F\left(\frac{\partial\mathbf{u}}{\partial t}\Big|_{\Omega_F} + (\mathbf{u}-\mathbf{w})\cdot\nabla\mathbf{u}\right) = \nabla\cdot\boldsymbol{\sigma}(\boldsymbol{v},p),\qquad\text{in }\Omega_F(t)\times(0,T), \tag{1.193}$$

$$\nabla\cdot\mathbf{u} = 0\qquad\qquad\qquad\qquad\qquad\quad\text{in }\Omega_F(t)\times(0,T), \tag{1.194}$$

satisfying the corresponding initial and boundary conditions.

The structure problems remain the same since the equations are defined on the reference, fixed domains Ω_S and Γ.

To perform the Lie splitting, described in Section 0.5.3, the coupled problem is re-written as a first order system in time. For this purpose, the trace of the fluid velocity on $\Gamma(t)$ will be denoted by $\mathbf{v} := \mathbf{u}|_{\Gamma(t)}$, while the trace of the thick structure velocity on Γ will be denoted by $\mathbf{V} = \partial\mathbf{d}/\partial t$. The kinematic coupling condition $\partial\boldsymbol{\eta}/\partial t = \mathbf{v}$ is then used to rewrite the system.

Notice again that $\mathbf{u}|_{\Gamma(t)}$ is defined on $\Gamma(t)$, namely, at $R + \eta(z,t)$. More precisely, $\mathbf{u}|_{\Gamma(t)} = \mathbf{u}(R + \eta(z,t), z, t)$. Therefore, $\mathbf{v}$, which is defined on Γ is equal to

$$\mathbf{v}(z,t) := \mathbf{u}(R + \eta(z,t), z, t).$$

The resulting problem is given by the following:

$$\rho_f\left(\left.\frac{\partial\mathbf{u}}{\partial t}\right|_{\Omega_F} + (\mathbf{u} - \mathbf{w})\cdot\nabla\mathbf{u}\right) = \nabla\cdot\boldsymbol{\sigma} \qquad \text{in } \Omega_F(t)\times(0,T), \qquad (1.195a)$$

$$\nabla\cdot\mathbf{u} = 0 \qquad \text{in } \Omega_F(t)\times(0,T), \qquad (1.195b)$$

$$\rho_K h\frac{\partial v_z}{\partial t} - C_2\frac{\partial\eta_r}{\partial z} - C_1\frac{\partial^2\eta_z}{\partial z^2} = f_z \qquad \text{on } \Gamma\times(0,T), \qquad (1.195c)$$

$$\rho_K h\frac{\partial v_r}{\partial t} + C_0\eta_r + C_2\frac{\partial\eta_z}{\partial z} = f_r \qquad \text{on } \Gamma\times(0,T), \qquad (1.195d)$$

$$\frac{\partial\boldsymbol{\eta}}{\partial t} = \mathbf{v} \qquad \text{on } \Gamma\times(0,T), \qquad (1.195e)$$

$$\rho_S\frac{\partial\boldsymbol{V}}{\partial t} + \gamma\mathbf{d} = \nabla\cdot\boldsymbol{S}(\mathbf{d}) \qquad \text{in } \Omega_S\times(0,T), \qquad (1.195f)$$

$$\frac{\partial\mathbf{d}}{\partial t} = \boldsymbol{V} \qquad \text{in } \Omega_S\times(0,T), \qquad (1.195g)$$

with the coupling conditions at the fluid-structure interface

$$\mathbf{v} = \mathbf{u}|_{\Gamma(t)}, \quad \boldsymbol{\eta} = \mathbf{d}|_\Gamma, \qquad (1.196)$$

$$\rho_K h\frac{\partial v_z}{\partial t} - C_2\frac{\partial\eta_r}{\partial z} - C_1\frac{\partial^2\eta_z}{\partial z^2} + J\,\boldsymbol{\sigma n}|_{\Gamma(t)}\cdot\boldsymbol{e}_z + \boldsymbol{S}\mathbf{e}_z|_\Gamma\cdot\boldsymbol{e}_z = 0, \quad (1.197)$$

$$\rho_K h\frac{\partial v_r}{\partial t} + C_0\eta_r + C_2\frac{\partial\eta_z}{\partial z} + J\,\boldsymbol{\sigma n}|_{\Gamma(t)}\cdot\boldsymbol{e}_r + \boldsymbol{S}\mathbf{e}_r|_\Gamma\cdot\boldsymbol{e}_r = 0. \qquad (1.198)$$

Notice, again, that $\mathbf{v} = \mathbf{u}|_{\Gamma(t)}$ means $\mathbf{v}(z,t) = \mathbf{u}(R + \eta(z,t), z, t)$ on $(0,L)\times(0,T)$. This problem is supplemented with the boundary and initial conditions presented in Section 0.7.1.

Before we continue with the Lie splitting algorithm applied to the problem in ALE form (195a)-(198), we introduce the notion of weak solutions for the problem studied in this section, namely, for problem (177)-(191). The corresponding function spaces on domains $\Omega_F(t)$ will be defined in terms of the functions defined on the fixed, reference domain Ω_F, where the association between the two is done via the ALE mapping, defined above.

1.7.4 Weak Formulation of FSI Problem (177)-(191)

For $t \in [0, T)$ introduce the following test function spaces: the fluid velocity space is defined by

$$\mathcal{V}_F(t) = \{\boldsymbol{\varphi} : \Omega_F(t) \to \mathbb{R}^2 | \ \boldsymbol{\varphi} = \hat{\boldsymbol{\varphi}} \circ (\mathcal{A})^{-1}, \hat{\boldsymbol{\varphi}} \in (H^1(\Omega_F))^2,$$
$$\varphi_r|_{r=0} = 0, \ \boldsymbol{\varphi}|_{z=0,L} = 0\},,$$

the fluid pressure:

$$Q(t) = \{q : \Omega_F(t) \to \mathbb{R} | \ q = \hat{q} \circ (\mathcal{A})^{-1}, \hat{q} \in L^2(\Omega_F)\},,$$

the test space for the thin structure problem:

$$\mathcal{V}_K = \{\boldsymbol{\zeta} : (0, L) \to \mathbb{R}^2 | \ \boldsymbol{\zeta} \in (H_0^1(\Gamma))^2\},$$

and the test space for the thick structure problem

$$\mathcal{V}_S \quad = \quad \{\boldsymbol{\psi} : \Omega_S \to \mathbb{R}^2 | \ \boldsymbol{\psi} \in (H^1(\Omega_S))^2, \boldsymbol{\psi}|_{z=0,L} = 0, \psi_z|_{\Gamma_{S_{ext}}} = 0\}.$$

The test space for the coupled FSI problem is given by:

$$\mathcal{Q}(t) = \{(\boldsymbol{\varphi}, \boldsymbol{\zeta}, \boldsymbol{\psi}) \in \mathcal{V}_F(t) \times \mathcal{V}_K \times \mathcal{V}_S \ | \ \boldsymbol{\varphi}|_{\Gamma(t)} = \boldsymbol{\zeta}, \ \boldsymbol{\zeta} = \boldsymbol{\psi}|_\Gamma\}, \tag{1.199}$$

The variational formulation of the coupled fluid-structure interaction problem now reads: for $t \in (0, T)$, find $(\mathbf{u}, p, \boldsymbol{\eta}, \mathbf{d}) \in \mathcal{V}_F(t) \times Q(t) \times \mathcal{V}_K \times \mathcal{V}_S$ such that the kinematic coupling conditions (189) and (190) hold, and such that for all $(\boldsymbol{\varphi}, \boldsymbol{\zeta}, \boldsymbol{\psi}, q) \in \mathcal{Q}(t) \times Q(t)$ the following equations are satisfied:

$$\rho_F \int_{\Omega_F(t)} \frac{\partial \mathbf{u}}{\partial t} \cdot \boldsymbol{\varphi} + \int_{\Omega_F(t)} (\mathbf{u} \cdot \nabla)\mathbf{u} \cdot \boldsymbol{\varphi} + 2\mu_F \int_{\Omega_F(t)} \boldsymbol{D}(\mathbf{u}) : \boldsymbol{D}(\boldsymbol{\varphi})$$

$$- \int_{\Omega_F(t)} p\nabla \cdot \boldsymbol{\varphi} \int_{\Omega_F(t)} q\nabla \cdot \mathbf{u} + \rho_K h \int_0^L \frac{\partial^2 \eta_z}{\partial t^2} \zeta_z + \rho_K h \int_0^L \frac{\partial^2 \eta_r}{\partial t^2} \zeta_r$$

$$- C_2 \int_0^L \frac{\partial \eta_r}{\partial z} \zeta_z + C_1 \int_0^L \frac{\partial \eta_z}{\partial z} \frac{\partial \zeta_z}{\partial z} + C_0 \int_0^L \eta_r \zeta_r + C_2 \int_0^L \frac{\partial \eta_z}{\partial z} \zeta_r$$

$$+ \rho_S \int_{\Omega_S} \frac{\partial^2 \mathbf{d}}{\partial t^2} \cdot \boldsymbol{\psi} + 2\mu \int_{\Omega_S} \boldsymbol{D}(\mathbf{d}) : \boldsymbol{D}(\boldsymbol{\psi}) + \lambda \int_{\Omega_S} (\nabla \cdot \mathbf{d})(\nabla \cdot \boldsymbol{\psi}) \tag{1.200}$$

$$+ \gamma \int_{\Omega_S} \mathbf{d} \cdot \boldsymbol{\psi} = \int_0^R p_{in}(t)\varphi_z|_{z=0} dr - \int_0^R p_{out}(t)\varphi_z|_{z=L} dr.$$

$$\int_{\Omega_F} q\nabla \cdot \mathbf{u} = 0.$$

1.7.5   Numerical Implementation of the Splitting Scheme

The splitting is performed on the first-order system written in ALE form (195a)-(198). System (195a)-(198) is split into two sub-problems, the fluid and the structure sub-problem, as described in Section 0.5.4. We notice that in this splitting, we also separated the viscous part of the structure problem from the purely elastic part of the structure problem, so that in the final structure sub-problem, denoted by Problem A1 in Section 0.5.4, we only solve non-dissipative, hyperbolic part of the structure problem using appropriate solvers. Namely, it has been our experience that for the stability and accuracy of the splitting scheme, it is beneficial to separate the parabolic from the hyperbolic features of the coupled FSI problem, and apply non-dissipative solvers to the non-dissipative, hyperbolic sub-problems. While in the example studied in this section we do not have viscous dissipation in the structure problem, we, however, use the same logic to numerically solve the fluid sub-problem, which contains, in itself, dissipative and non-dissipative features. More precisely, we will split the fluid sub-problem into the pure advection sub-problem (non-dissipative), and the remaining, time-dependent Stokes problem capturing viscous dissipation. This will give rise to a splitting algorithm with three main steps:

A1.   An elastodynamics sub-problem for the structure;

A2(a). A time-dependent Stokes problem for the fluid;

A2(b). A fluid and ALE advection problem.

To achieve higher accuracy, we implement the Kinematically-Coupled β-Scheme, described in Section 0.5.4, in which the normal fluid stress is further split into two parts:

$$\boldsymbol{\sigma n} = \underbrace{\boldsymbol{\sigma n} + \beta p \boldsymbol{n}}_{(Part\ I)}\ \underbrace{-\beta p \boldsymbol{n}}_{(Part\ II)}\ ,$$

where $\beta \in [0, 1]$. It was shown in [19] that the accuracy of the scheme increases as the value of β increases from 0 to 1. Part I of the fluid stress will be taken into account in the fluid sub-problem, while Part II of the fluid stress will be used as loading to the structure in the structure sub-problem, and will appear as a Robin boundary condition for the thick structure equations. Details of the scheme are as follows:

Problem A1: The Elastodynamics Problem.
     This step involves solving the thick structure problem together with membrane elastodynamics. The membrane elastodynamics problem appears in this step as a Robin boundary condition on Γ for the thick structure problem defined on Ω_S, where we have used continuity of displacement (kinematic coupling condition) to write the problem this way. The Robin boundary condition also includes Part II of the normal fluid stress, which enters explicitly in the sense that the pressure is taken from the fluid sub-problem at the time step n (Problem A1(a)). The

Jacobian of the transformation from the Eulerian to Lagrangian framework J is calculated based on the data obtained in the previous time step.

In this step we also compute the domain velocity $\mathbf{w}$ and use it in Problem A2(b) below to solve the fluid and ALE advection problem. The initial data for the structure velocity on Γ is taken to be the trace of the fluid velocity $\mathbf{v}$ calculated in the previous time step. Thus, the structure communicates with the fluid sub-problem through this initial data and through the pressure exerted by the fluid onto the fluid-structure interface. In turn, the updated structure velocity is then taken in Problem A2(a) as the initial data for the trace of the fluid velocity on $\Gamma(t)$.

In this step the fluid velocity $\mathbf{u}$ and fluid pressure p remain unchanged, and so

$$\mathbf{u}^{n+1/3} = \mathbf{u}^n, p^{n+1/3} = p^n.$$

The structure sub-problem reads: Find $\boldsymbol{\eta}, \mathbf{d}, \mathbf{v}$, and $\boldsymbol{V}$, such that for $t \in (t^n, t^{n+1})$

$$\rho_S \frac{\partial \boldsymbol{V}}{\partial t} + \gamma \mathbf{d} = \nabla \cdot \boldsymbol{S}(\mathbf{d}) \qquad\qquad \text{in } \Omega_S \times (t^n, t^{n+1}),$$

$$\frac{\partial \mathbf{d}}{\partial t} = \boldsymbol{V} \qquad\qquad \text{in } \Omega_S \times (t^n, t^{n+1}),$$

$$\rho_K h \frac{\partial v_z}{\partial t} - C_2 \frac{\partial \eta_r}{\partial z} - C_1 \frac{\partial^2 \eta_z}{\partial z^2} + \boldsymbol{S}\mathbf{e}_r \cdot \mathbf{e}_z = J^n \beta p^n \boldsymbol{n}|_{\Gamma(t)} \cdot \mathbf{e}_z \quad \text{on } \Gamma \times (t^n, t^{n+1}),$$

$$\rho_K h \frac{\partial v_r}{\partial t} + C_0 \eta_r + C_2 \frac{\partial \eta_z}{\partial z} + \boldsymbol{S}\mathbf{e}_r \cdot \mathbf{e}_r = J^n \beta p^n \boldsymbol{n}|_{\Gamma(t)} \cdot \boldsymbol{e}_r \qquad \text{on } \Gamma \times (t^n, t^{n+1}),$$

$$\frac{\partial \boldsymbol{\eta}}{\partial t} = \mathbf{v} \qquad\qquad \text{on } \Gamma \times (t^n, t^{n+1}),$$

$$\boldsymbol{\eta} = \mathbf{d}|_\Gamma \qquad\qquad \text{on } \Gamma \times (t^n, t^{n+1}),$$

$$\boldsymbol{V}|_\Gamma = \mathbf{v} \qquad\qquad \text{on } \Gamma \times (t^n, t^{n+1}),$$

with the following boundary conditions:

$$\mathbf{d}|_{z=0,L} = 0, \text{ and } d_z = 0, \quad \boldsymbol{n}_{ext}^s \cdot \boldsymbol{S}\boldsymbol{n}_{ext}^s = 0 \quad \text{on } \Gamma_{ext} \times (t^n, t^{n+1}).$$

The initial conditions are given by:

$$\mathbf{d}(t^n) = d^n, \boldsymbol{\eta}(t^n) = \boldsymbol{\eta}^n, \mathbf{v}(t^n) = \mathbf{v}^n, \boldsymbol{V}(t^n) = \boldsymbol{V}^n.$$

Then set

$$\mathbf{d}^{n+1/3} = \mathbf{d}(t^{n+1}), \boldsymbol{\eta}^{n+1/3} = \boldsymbol{\eta}(t^{n+1}), \mathbf{v}^{n+1/3} = \mathbf{v}(t^{n+1}), \boldsymbol{V}^{n+1/3} = \boldsymbol{V}(t^{n+1}).$$

After the new position of the structure has been calculated, and the new fluid domain updated, we calculate the ALE mapping $\mathcal{A}^{n+1}$ as the harmonic extension of the structure displacement $\boldsymbol{\eta}^{n+1}$ onto the whole domain Ω_F

$$\begin{aligned}
\Delta \mathcal{A}^{n+1} &= 0 \quad \text{in } \Omega_F, \\
\mathcal{A}^{n+1}|_\Gamma &= \boldsymbol{\eta}^{n+1}, \\
\mathcal{A}^{n+1}|_{\partial \Omega_F \setminus \Gamma} &= 0.
\end{aligned}$$

From here we calculate the domain velocity $\mathbf{w}^{n+1} = \dfrac{\partial \mathcal{A}^{n+1}}{\partial t}$, based on the updated location of the structure, and use it in the advection problem, Problem A2(b) below.

Remark 1. Note that in Problem A1, we can rewrite the membrane equations by using the kinematic coupling conditions in the following way:

$$\rho_K h \frac{\partial V_z}{\partial t} - C_2 \frac{\partial d_r}{\partial z} - C_1 \frac{\partial^2 d_z}{\partial z^2} + \boldsymbol{S}\mathbf{e}_r \cdot \mathbf{e}_z = 0 \qquad \text{on } \Gamma \times (t^n, t^{n+1}),$$

$$\rho_K h \frac{\partial V_r}{\partial t} + C_0 d_r + C_2 \frac{\partial d_z}{\partial z} + \boldsymbol{S}\mathbf{e}_r \cdot \mathbf{e}_r = 0 \qquad \text{on } \Gamma \times (t^n, t^{n+1}).$$

In this way the membrane equations serve as Robin boundary conditions for the thick structure problem.

Problem A2(a): The Stokes Problem.
 This step involves solving a time-dependent Stokes problem on (t^n, t^{n+1}), with a Robin-type boundary condition involving the thin structure inertia and Part I of the fluid stress. This problem is solved on the fixed fluid domain $\Omega_F(t^n)$, determined by the structure position in the previous time step. Using the updated fluid domain calculated in Problem A1 is also an option. In the proof of stability of this scheme, using $\Omega_F(t^n)$ is more covenient for the proof. In this step the structure position and the velocity of the thick structure do not change, and so

$$\boldsymbol{\eta}^{n+2/3} = \boldsymbol{\eta}^{n+1/3}, \mathbf{d}^{n+2/3} = \mathbf{d}^{n+1/3}, \boldsymbol{V}^{n+2/3} = \boldsymbol{V}^{n+1/3}.$$

The problem reads as follows:
 Find $\mathbf{u}, p$, and $\mathbf{v}$ such that for $t \in (t^n, t^{n+1})$, with p^n denoting the pressure obtained at the previous time step, the following holds:

$$\rho_F \frac{\partial \mathbf{u}}{\partial t} \bigg|_{\Omega_F} = \nabla \cdot \boldsymbol{\sigma}, \quad \nabla \cdot \mathbf{u} = 0 \qquad \qquad \text{in } \Omega_F(t^n) \times (t^n, t^{n+1}),$$

$$\rho_K h \frac{\partial (\mathbf{u}|_{\Gamma(t)})}{\partial t} + J\big(\boldsymbol{\sigma}\boldsymbol{n}|_{\Gamma(t)} + \beta p^n \boldsymbol{n}|_{\Gamma(t)} \big) = 0 \qquad \text{on } \Gamma \times (t^n, t^{n+1}),$$

$$\mathbf{v} = \mathbf{u}|_{\Gamma(t)} \qquad \qquad \text{on } \Gamma \times (t^n, t^{n+1}),$$

where $\mathbf{v} = \mathbf{u}|_{\Gamma(t)}$ means $\mathbf{v}(z,t) = \mathbf{u}(R + \eta(z,t), z, t)$ on Γ. This is supplemented with the following boundary conditions:

$$\frac{\partial u_z}{\partial r}(z,0,t) = \quad u_r(z,0,t) = 0 \quad \text{on } (0,L), \quad \mathbf{u}(0,R,t) = \mathbf{u}(L,R,t) = 0,$$

$$\boldsymbol{\sigma}\boldsymbol{n}_{in} = -p_{in}(t)\boldsymbol{n}_{in} \text{ on } \Gamma_{\text{in}}, \quad \boldsymbol{\sigma}\boldsymbol{n}_{out} = -p_{out}(t)\boldsymbol{n}_{out} \text{ on } \Gamma_{\text{out}},$$

and initial conditions: $\mathbf{u}(t^n) = \mathbf{u}^n$, $\mathbf{v}(t^n) = \mathbf{v}^{n+1/3}$. Then set

$$\mathbf{u}^{n+2/3} = \mathbf{u}(t^{n+1}), \ p^{n+2/3} = p(t^{n+1}), \ \mathbf{v}^{n+2/3} = \mathbf{v}(t^{n+1}).$$

Problem A2(b): The Advection Problem.
Solve the fluid and ALE advection sub-problem defined on the fixed domain $\Omega(t^n)$, with the domain velocity $\mathbf{w}^{n+1}$ just calculated in Problem A1. The displacement of the structure, the velocity of the thick structure, the velocity of the thin structure, and the fluid pressure do not change in this step, so that

$$\boldsymbol{\eta}^{n+1} = \boldsymbol{\eta}^{n+2/3}, \mathbf{d}^{n+1} = \mathbf{d}^{n+2/3}, \boldsymbol{V}^{n+1} = \boldsymbol{V}^{n+2/3}, \mathbf{v}^{n+1} = \mathbf{v}^{n+2/3}, p^{n+1} = p^{n+2/3}.$$

The advection problem reads: Find $\mathbf{u}$ such that for $t \in (t^n, t^{n+1})$

$$\left.\frac{\partial \mathbf{u}}{\partial t}\right|_{\Omega_F} + (\mathbf{u}^{n+2/3} - \mathbf{w}^{n+1}) \cdot \nabla \mathbf{u} = 0, \qquad \text{in } \Omega_F(t^n) \times (t^n, t^{n+1}),$$

$$\mathbf{u} = \mathbf{v}^{n+2/3}, \qquad\qquad\qquad\qquad\qquad \text{on } \Gamma \times (t^n, t^{n+1}),$$

with the inlet/outlet conditions:

$$\mathbf{u} = \mathbf{u}^{n+2/3} \quad \text{on} \quad \Gamma_-^{n+2/3} = \{\boldsymbol{x} \in \mathbb{R}^2 | \boldsymbol{x} \in \partial\Omega_F(t^n), (\mathbf{u}^{n+2/3} - \mathbf{w}^{n+1}) \cdot \boldsymbol{n} < 0\},$$

and initial conditions $\mathbf{u}(t^n) = \mathbf{u}^{n+2/3}$. Then set

$$\mathbf{u}^{n+1} = \mathbf{u}(t^{n+1}).$$

Set $n = n + 1$ and return to Problem A1.

1.7.6   Discretized Scheme in Weak Form

To discretize the problem in time, sub-divide the time interval $(0, T)$ into N sub-intervals of width Δt, and let $t^n = n\Delta t$, where $n \leq N$. The Backward Euler scheme is implemented to discretize the time-derivatives. For the space discretization, we use the finite element method approach. Thus, we define the finite element spaces $\mathcal{V}_F^h(t^n) \subset \mathcal{V}_F(t^n), Q^h(t^n) \subset Q(t^n), \mathcal{V}_K^h \subset \mathcal{V}_K$ and $\mathcal{V}_S^h \subset \mathcal{V}_S$, and introduce the following bilinear forms

$$a_F^n(\mathbf{u}, \boldsymbol{\varphi}) \quad := \quad 2\mu_F \int_{\Omega_F(t^n)} \boldsymbol{D}(\mathbf{u}) : \boldsymbol{D}(\boldsymbol{\varphi}),$$

$$b_F^n(p, \boldsymbol{\varphi}) \quad := \quad \int_{\Omega_F(t^n)} p\nabla \cdot \boldsymbol{\varphi},$$

$$a_K(\eta_r, \zeta_r) \quad := \quad C_0 \int_0^L \eta_r \zeta_r,$$

$$a_S(\mathbf{d}, \boldsymbol{\psi}) \quad := \quad 2\mu \int_{\Omega_S} \boldsymbol{D}(\mathbf{d}) : \boldsymbol{D}(\boldsymbol{\psi}) + \lambda \int_{\Omega_S} (\nabla \cdot \mathbf{d})(\nabla \cdot \boldsymbol{\psi}).$$

A weak formulation of the fully discrete loosely coupled algorithm applied to the simplified problem is given as follows:

Problem A1. (The structure problem) To discretize the structure problem in time we use the second order Newmark scheme. The problem reads as follows: Find $(\mathbf{d}_h^{n+1/3}, \boldsymbol{V}_h^{n+1/3}) \in \mathcal{V}_S^h \times \mathcal{V}_S^h$ such that for all $(\boldsymbol{\psi}_h, \boldsymbol{\phi}_h) \in \mathcal{V}_S^h \times \mathcal{V}_S^h$

$$\rho_S \int_{\Omega_S} \frac{\boldsymbol{V}_h^{n+1/3} - \boldsymbol{V}_h^n}{\Delta t} \cdot \boldsymbol{\psi}_h + \gamma \int_{\Omega_S} \frac{\mathbf{d}_h^n + \mathbf{d}_h^{n+1/3}}{2} \cdot \boldsymbol{\psi}_h$$

$$+\rho_K h \int_\Gamma \frac{V_{r,h}^{n+1/3} - V_{r,h}^n}{\Delta t} \psi_{r,h} + a_K \left(\frac{d_{r,h}^n + d_{r,h}^{n+1/3}}{2}, \psi_{r,h} \right) + a_S \left(\frac{\mathbf{d}_h^n + \mathbf{d}_h^{n+1/3}}{2}, \boldsymbol{\psi}_h \right)$$

$$+\rho_S \int_{\Omega_S} \left(\frac{\boldsymbol{V}_h^n + \boldsymbol{V}_h^{n+1/3}}{2} - \frac{\mathbf{d}_h^{n+1/3} - \mathbf{d}_h^n}{\Delta t} \right) \cdot \boldsymbol{\phi}_h$$

$$+\rho_K h \int_\Gamma \left(\frac{V_{r,h}^n + V_{r,h}^{n+1/3}}{2} - \frac{d_{r,h}^{n+1/3} - d_{r,h}^n}{\Delta t} \right) \cdot \phi_{r,h} = 0. \qquad (1.201)$$

Note that in this step we take all the kinematic coupling conditions into account. More precisely:

1. Initially we set $V_{r,h}^n|_\Gamma = v_{r,h}^n = u_{r,h}^n|_{\Gamma(t^n)}$;

2. Once $\mathbf{d}_h^{n+1/3}$ and $\boldsymbol{V}_h^{n+1/3}$ are computed, $\eta_{r,h}^{n+1/3}, v_{r,h}^{n+1/3}$ and $u_{r,h}^{n+1/3}|_{\Gamma(t^n)}$ are recovered via

$$\eta_{r,h}^{n+1/3} = d_{r,h}^{n+1/3}|_\Gamma, \ v_{r,h}^{n+1/3} = u_{r,h}^{n+1/3}|_{\Gamma(t^n)} = V_{r,h}^{n+1/3}|_\Gamma.$$

In this step the fluid velocity does not change, and so

$$\mathbf{u}_h^{n+1/3} = \mathbf{u}_h^n.$$

In this step we also update the fluid domain velocity $\mathbf{w}$. As mentioned earlier, after the new position of the structure has been calculated, we calculate the ALE mapping $\mathcal{A}^{n+1} : \Omega_F \to \Omega_F(t^{n+1})$ as the harmonic extension of the structure displacement $\boldsymbol{\eta}_h^{n+1/3} = \boldsymbol{\eta}_h^{n+1}$ onto the whole fluid domain, and obtain the domain velocity $\mathbf{w}_h^{n+1}$ as the difference quotient between the new location of points associated with $\mathcal{A}^{n+1}$, minus the old location of points associated with $\mathcal{A}^n$, divided by Δt. This will be used it in the advection problem, i.e., Problem A2(b) below.

Problem A2(a). (The time dependent Stokes problem) Find $(\mathbf{u}_h^{n+2/3}, p_h^{n+2/3}) \in \mathcal{V}_F^h(t^n) \times Q^h(t^n)$ such that for all $(\boldsymbol{\varphi}_h, q_h) \in \mathcal{V}_F^h(t^n) \times Q^h(t^n)$

$$\rho_F \int_{\Omega_F(t^n)} \frac{\mathbf{u}_h^{n+2/3} - \mathbf{u}_h^{n+1/3}}{\Delta t} \cdot \boldsymbol{\varphi}_h + a_F^n(\mathbf{u}_h^{n+1}, \boldsymbol{\varphi}_h) - b_F^n(p_h^{n+2/3}, \boldsymbol{\varphi}_h)$$

$$+\rho_K h \int_0^L \frac{u_{r,h}^{n+2/3}|_{\Gamma(t^n)} - u_{r,h}^{n+1/3}|_{\Gamma(t^n)}}{\Delta t} \varphi_{r,h} dx + b_F^n(q_h, \mathbf{u}_h^{n+2/3})$$

$$= \int_0^R p_{in}(t^{n+1})\varphi_{z,h}|_{z=0}dr - \int_0^R p_{out}(t^{n+1})\varphi_{z,h}|_{z=L}dr. \qquad (1.202)$$

This step is computed on the fixed domain $\Omega^f(t^n)$. The only updated variables are the fluid velocity and pressure. For higher accuracy, this step can be computed on the updated domain $\Omega(t^{n+1})$.

Problem A2(b) (The advection problem) As mentioned earlier, it is convenient to write the fluid and ALE advection term in symmetric form, giving rise to the following weak formulation: Find $\mathbf{u}_h^{n+1} \in \mathcal{V}_F^h(t^n)$ such that for all $\boldsymbol{\varphi}_h \in \mathcal{V}_F^h(t^n)$

$$\rho_F \int_{\Omega_F(t^n)} \frac{\mathbf{u}_h^{n+1} - \mathbf{u}_h^{n+2/3}}{\Delta t} \cdot \boldsymbol{\varphi}_h + \frac{\rho_F}{2} \int_{\Omega_F(t^n)} (\nabla \cdot \boldsymbol{w}_h^{n+1})\mathbf{u}_h^{n+1} \cdot \boldsymbol{\varphi}_h$$

$$+\frac{\rho_F}{2} \int_{\Omega_F(t^n)} \left((\mathbf{u}_h^n - \boldsymbol{w}_h^{n+1}) \cdot \nabla)\mathbf{u}_h^{n+1} \cdot \boldsymbol{\varphi}_h - ((\mathbf{u}_h^n - \boldsymbol{w}_h^{n+1}) \cdot \nabla)\boldsymbol{\varphi}_h \cdot \mathbf{u}_h^{n+1} \right) = 0.$$

$$(1.203)$$

In this step all the other variables, except for the fluid velocity, remain unchanged so that

$$\mathbf{d}_h^{n+1} = \mathbf{d}_h^{n+2/3}, \boldsymbol{V}_h^{n+1} = \boldsymbol{V}_h^{n+2/3}, \eta_{r,h}^{n+1} = \eta_{r,h}^{n+2/3}, \mathbf{v}_{r,h}^{n+1} = \mathbf{v}_{r,h}^{n+2/3},$$

with

$$u_{r,h}^{n+1}|_{\Gamma(t^n)} = u_{r,h}^{n+2/3}|_{\Gamma(t^n)} = v_{r,h}^{n+2/3}.$$

In was shown in [22] that an energy estimate associated with unconditional stability of this scheme, holds for the full nonlinear FSI problem. Therefore, we expect that this scheme in unconditionally stable for all the parameters in the problem.

1.7.7 Numerical Examples

We present two numerical examples. One is a simplified problem for which there exists and exact solution against which we can test our numerical scheme. The other one if a fully nonlinear FSI problem with a thin and thick structural layer. Since there are no numerical results in literature on FSI problems with multiple structural layers against which we could test our solution, in this second example we calculated solutions to a sequence of problems for which the thickness of the thin structure converges to zero, and showed that the limiting solution is the same as the solution of the FSI problem in which the structure consists of only one thick structural layer. This was proved using analytical methods in [22]. The solution of the limiting problem was then numerically tested against the solution of the FSI problem with only one thick structural layer, which was obtained using a different solver. We show below that the two solutions, obtained with two different solvers, are in good agreement.

Example 1.

We consider a simplified FSI problem with multiple structural layers that satisfies the following simplifying assumptions:

1. The fluid problem is defined on the fixed, reference domain of width R, and length L (the coupling is linear).

2. The fluid problem is driven by the constant inlet and outlet pressure data p_{in} and $p_{out} = 0$ (the pressure drop is constant).

3. Only radial displacement of the thin and thick structure is assumed to be different from zero.

Assumption 3 implies that the thin structure membrane model takes the form:

$$\rho_K h \frac{\partial^2 \eta_r}{\partial t} + C_0 \eta_r = f_r,$$

while the thick structure problem simplifies as follows:

$$\rho_s \frac{\partial^2 d_r}{\partial t^2} = \mu \frac{\partial^2 d_r}{\partial x^2} + (\mu + \lambda) \frac{\partial^2 d_r}{\partial y^2}.$$

Finally, the coupling conditions between the fluid and the multilayered structure are given by

$$f_r = p + (\lambda + \mu) \frac{\partial d_r}{\partial y} \qquad\qquad \text{on } \Gamma \times (0, T),$$

$$\frac{\partial \eta_r}{\partial t} = u_r \qquad\qquad \text{on } \Gamma \times (0, T),$$

$$\eta_r = U_r \qquad\qquad \text{on } \Gamma \times (0, T).$$

The exact solution to this problem is given by the following. The fluid flow through the fixed cylinder with constant pressure drop is given by the Poiseuille velocity profile:

$$u_z^e(z, r) = u_z^e(r) = \frac{p_{in} - p_{out}}{2\mu_F L}(R^2 - r^2), \quad u_r^e = 0,$$

and the fluid pressure is linear within the channel:

$$p^e(z, r) = p^e(z) = \frac{p_{out} z + p_{in}(L - z)}{L}, \ \ z \in (0, L), \ r \in (0, R).$$

The radial displacements of the thin and thick structure are given by:

$$\eta_r^e(z) = \frac{p^e(z)}{C_0}, \quad d_r^e(z, r) = d_r^e(z) = \eta_r^e(z).$$

Parameters	Values	Parameters	Values
Radius R (cm)	0.5	**Length** L (cm)	6
In. press. p_{in} (dyne/cm^2)	250	**Out. press.** p_{out} (dyne/cm^2)	0
Fluid density ρ_f (g/cm^3)	1	**Dyn. viscosity** μ (g/cm s)	0.35
Thin wall:			
Density ρ_m (g/cm^3)	1.1	**Thickness** h (cm)	0.02
Lamé coeff. μ_m (dyne/cm^2)	1.07×10^6	**Lamé coeff.** λ_m (dyne/cm^2)	4.29×10^6
Thick wall:			
Density ρ_s (g/cm^3)	1.1	**Thickness** H (cm)	0.1
Lamé coeff. μ_s (dyne/cm^2)	1.07×10^6	**Lamé coeff.** λ_s (dyne/cm^2)	4.29×10^6
Spring coeff. γ (dyne/cm^4)	0		

Table 1.5: Geometry, fluid and structure parameters used in Example 1.

We solve this problem numerically using the parameters given in Table 5. The initial data was taken to be

$$\mathbf{u} = 0, p = p_{out}, \eta_r = 0, d_r = 0, \text{ at } t = 0,$$

while at the inlet and outlet boundaries we kept both structures fixed, with the inlet and outlet displacement data tailored so that the final solution does not exhibit a boundary layer:

$$\eta_r|_{z=0} = d_r|_{z=0} = \frac{p_{in}}{C_0}, \quad \eta_r|_{z=L} = d_r|_{z=L} = \frac{p_{out}}{C_0} = 0, \forall t > 0.$$

The numerical scheme with $\beta = 1$ was implemented, and the problem was solved until the steady state was achieved. With the time step $\Delta t = 10^{-5}$ it took 200 iterations to achieve the accuracy of less than 0.08%. Namely, the maximum relative error between the computed and exact solution was less than 0.08% (namely, 0.000778).
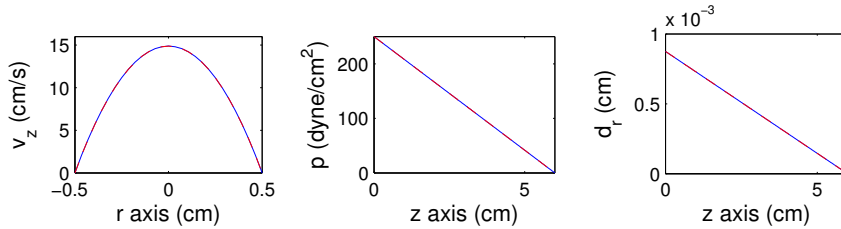
Figure 1.14: Comparison between the computed solution (in blue) and the exact solution (in red). The two are superimposed. Left: Axial velocity. Middle: Fluid pressure. Right: Radial displacement.

Figure 14 shows a comparison between the computed (blue) and the exact solution (red) for axial velocity (left), fluid pressure (middle), and radial displace-

ment (right), showing excellent agreement. The corresponding relative errors are given by the following:

$$\frac{||\mathbf{u}^e - \mathbf{u}||_{L^2(\Omega^f)}}{||\mathbf{u}^e||_{L^2(\Omega^f)}} = 7.78 \times 10^{-4}, \quad \frac{||p^e - p||_{L^2(\Omega^f)}}{||p^e||_{L^2(\Omega^f)}} = 1.17 \times 10^{-4},$$

$$\frac{||\eta_r^e - \eta_r||_{L^2(0,L)}}{||\eta_r^e||_{L^2(0,L)}} = 3.82 \times 10^{-5}, \quad \frac{||d_r^e - d_r||_{L^2(\Omega^s)}}{||d_r^e||_{L^2(\Omega^s)}} = 3.82 \times 10^{-5}.$$

We conclude that the scheme behaves well for this simplified FSI problem with multiple structural layers.

Example 2.

In this example we solve the full, nonlinear FSI problem (177)-(191) with the structure consisting of two layers, using the data that correspond to a benchmark problem in FSI with a single thick structure. Moreover, we solve a sequence of FSI problems (177)-(191) in which the thickness of the thin layer converges to zero. The limiting solution is then compared with the solution of the benchmark problem with a single, thick structure, obtained using a different solver. In the sequence of FSI problem with two structural layers, the combined thickness of the entire structure is set to be constant, and equal to the thickness of the thick structure from the benchmark problem. Furthermore, the elastic properties (i.e., the Young's modulus of elasticity and the Poisson ratio) of the thin and thick structure, are all set to be equal to the elastic properties of the thick structure in the benchmark problem.

The elastodynamics of the thin structural layer is modeled using the linearly elastic Koiter membrane equations with both radial and longitudinal displacement (182), (183), while the elastodynamics of the thick structure is modeled using the equations of 2D linear elasticity (184). The same 2D linear elasticity model (184) is used to capture the elastodynamics of the thick structure in the FSI benchmark problem. In both cases the flow is driven by the time-dependent pressure data:

$$p_{in}(t) = \begin{cases} \frac{p_{max}}{2}\left[1 - \cos\left(\frac{2\pi t}{t_{max}}\right)\right] & \text{if } t \leq t_{max} \\ 0 & \text{if } t > t_{max} \end{cases}, \quad p_{out}(t) = 0 \ \forall t \in (0, T),$$

where $p_{max} = 1.333 \times 10^4$ (dyne/cm^2) and $t_{max} = 0.003$ (s). The values of the parameters used in this example are given in Table 6. The same parameters were used to test partitioned FSI schemes in [9].

We assume that the combined thickness of the two-layered structure is fixed, and equal to $h + H = 0.12$cm, which is set to be the same as the thickness of the single thick structure in the benchmark problem. Our kinematically-coupled β scheme, described in Section 0.7.5, was used to solve the multi-layered FSI problem

Parameters	Values	Parameters	Values
Radius R (cm)	0.5	**Length** L (cm)	6
Fluid density ρ_f (g/cm^3)	1	**Dyn. viscosity** μ (g/cm s)	0.035
Thin wall:			
Density ρ_m(g/cm^3)	1.1	**Thickness** h (cm)	0.02
Lamé coeff. μ_m(dyne/cm^2)	5.75×10^5	**Lamé coeff.** λ_m(dyne/cm^2)	1.7×10^6
Thick wall:			
Density ρ_s(g/cm^3)	1.1	**Thickness** H (cm)	0.1
Lamé coeff. μ_s(dyne/cm^2)	5.75×10^5	**Lamé coeff.** λ_s(dyne/cm^2)	1.7×10^6
Spring coeff. γ(dyne/cm^4)	4×10^6		

Table 1.6: Geometry, fluid and structure parameters that are used in Example 2.
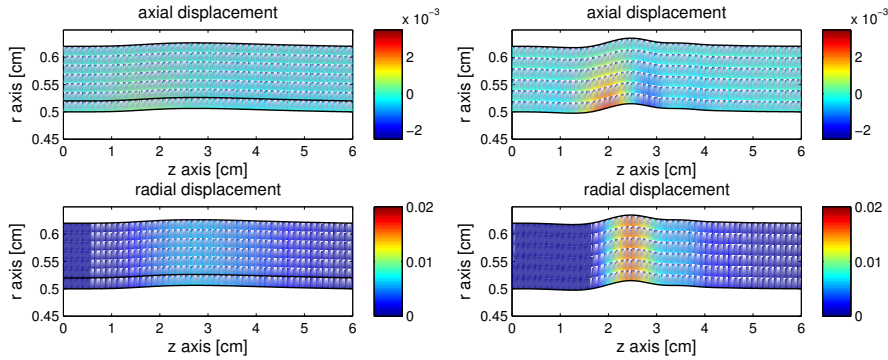
Figure 1.15: Axial displacement (top) and radial displacement (bottom) at time $t = 8$ ms obtained using the model capturing two structural layers (left), and the model capturing FSI with a single thick structural layer [21] (right).

with $\beta = 1$, while the scheme presented in [21] was used to solve the single-layered FSI benchmark problem. The problem was solved over the time interval $[0, 0.012]$s, using the time step $\Delta t = 5 \times 10^{-5}$. Figure 15 shows the axial and radial displacement at time $t = 8$ ms obtained using the multilayered model (left) and the single-layered model (right) for the arterial wall. We further compared the results of the multilayered model with the single layered model as the thickness of the thin structure h goes to zero. As we decreased h, we increased H to maintain the constant combined thickness $h + H = 0.12$ cm. Figures 16, 17 and 18 show the flowrate, mean pressure and displacement of the fluid-structure interface obtained using different values of h. The results obtained using the single layered wall model correspond to the label $h = 0$. Indeed, we can see that as we decrease the thickness of the fluid-structure interface, the numerical results obtained using our multilayered model approach the results obtained using the single-layered FSI model! Notice how for $h = 0.025$cm the solutions obtained using the multilayered
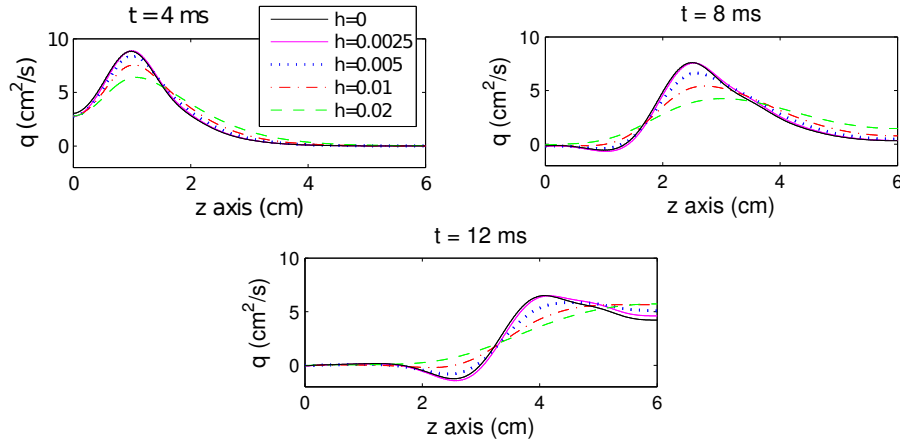
Figure 1.16: Flowrate computed using two different models: the model in [21] containing a single thick structural layer ($h = 0$), and the model considered in this chapter, consisting of two layers. The thickness of the thin membrane layer was decreased from $h = 0.02$ to $h = 0.0025$ cm. The combined thickness of the two-layered structure was kept constant at $h + H = 0.12$cm. Convergence of the solutions to the FSI solution containing a single, thick layered model ($h = 0$) can be observed.
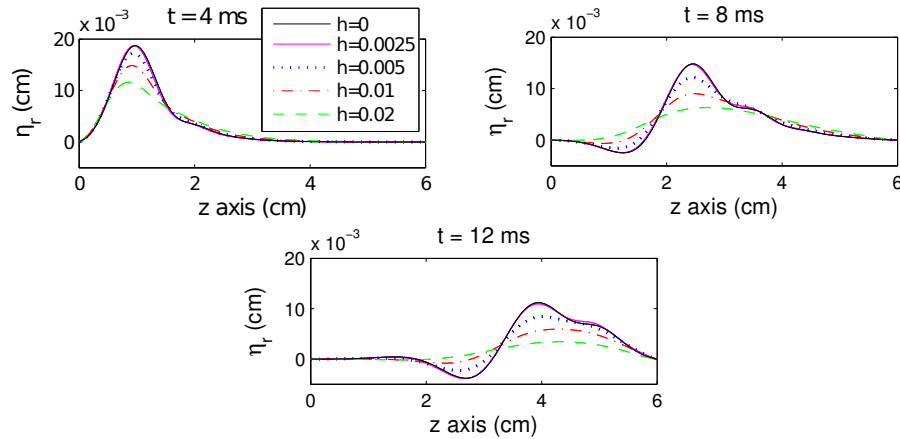
Figure 1.17: Displacement of the fluid-structure interface obtained under the same conditions as those described in Figure 16.

model and the single thick structure model ($h = 0$ in Figures 16, 17, 18) are almost identical.
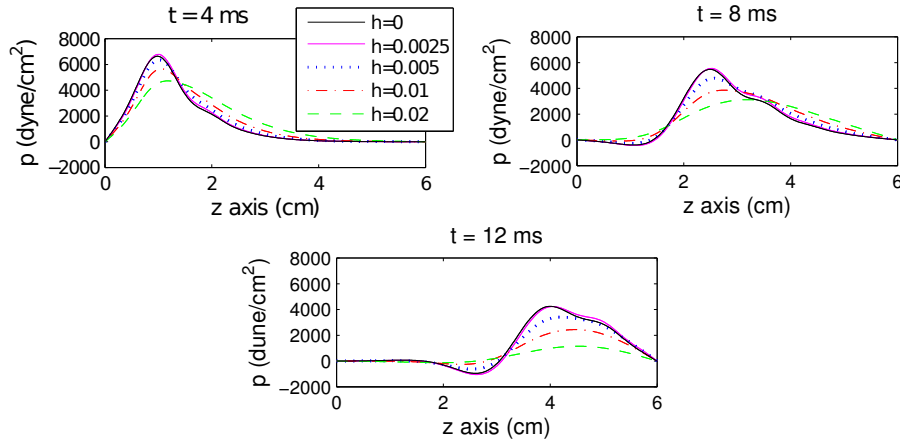
Figure 1.18: Mean pressure obtained under the same conditions as those described in Figure 16.

Regularizing Effects by Thin Fluid-Structure Interface with Mass

We conclude this section with a remark on the regularizing effects of the thin fluid-structure interface with mass. Figures 16, 17, 18 indicate that as we increase inertia of the thin fluid-structure interface with mass by increasing its thickness, the solution of the entire FSI problem is damped, or regularized. More precisely, if one looks at the FSI problem with a single thick structural layer, the fluid-structure interface is simply the massless trace of the thick structure that is in contact with the fluid. Mathematically, in that case the trace of the structure displacement is not well-defined (assuming regularity of the data consistent with weak solutions), and using energy estimates it is not possible to even show that the fluid-structure interface is continuous. In the case when the fluid-structure interface has mass, we showed in Proposition 73 that not only is the fluid-structure interface continuous, but its evolution can be controlled by the energy norm of the time derivative of its displacement. We see effects of this in the solutions presented in Figures 16, 17, 18, and in Figures 19 below. In Figure 19 below we focus on the displacement and displacement velocity of the fluid-structure interface, which measures the effects of inertia. In the first row of Figure 19 three snap-shots of the fluid-structure interface are shown as the inlet pressure wave travels down the tube. In the second row of Figure 19 the same three snap-shots are shown, but for the fluid-structure interface velocity. The red solid line in these figures corresponds to the massless fluid-structure interface in the FSI problem with a single thick structural layer. The black dashed line correspond to the fluid-structure interface with mass in the FSI problem with two structural layers. We see significant damping of the traveling wave in the case when the fluid-structure interface has mass. This indicates that inertia of the fluid-structure interface with
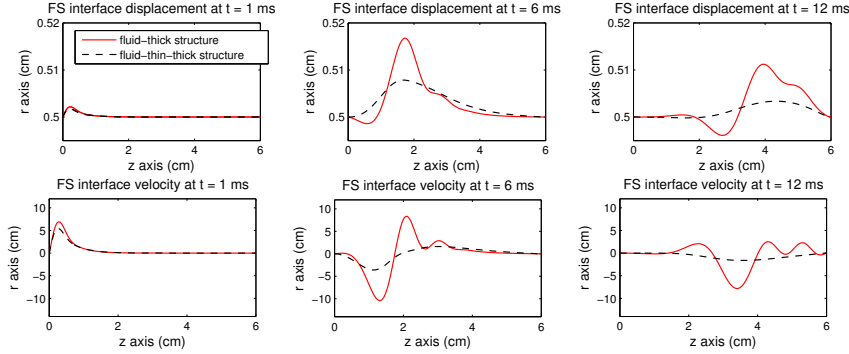
Figure 1.19: Fluid-structure interface displacement (top) and velocity (bottom) obtained using a multilayered wall model and the single layered model from [21], shown at times $t = 1$ ms, $t = 6$ ms, and $t = 12$ ms.

mass regularizes solutions of FSI problems.

This is reminiscent of the results by Hansen and Zuazua [89] in which the presence of a point mass at the interface between two linearly elastic strings with solutions in asymmetric spaces (different regularity on each side) allowed the proof of well-posedness due to the regularizing effects by the point mass. In particular, in [89] two linearly elastic strings were considered, meeting at a point mass. The elastodynamics of each string was modeled by the linear wave equation. It was shown that as the wave with the displacement in $H^1(0, L)$ and velocity in $L^2(0, L)$ passes through the point mass, a reflected and a transmitted waves form. The transmitted wave, which passes through the point mass, gets smoothed out to $H^2(0, L)$ regularity in displacement, and $H^1(0, L)$ regularity in velocity. A numerical simulation of this phenomenon was shown in [105]. Figure 20 shows one of the results
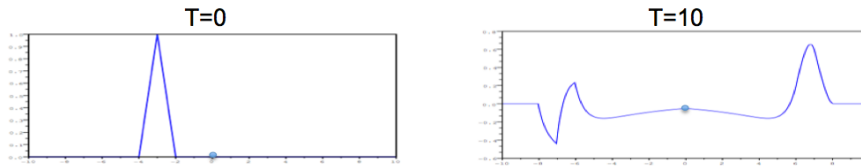
Figure 1.20: Regularizing effects of point mass. The figure is taken from [105]. The initial data (left panel) is smoothed out as the transmitted wave traveling to the right, passes through the point mass (right panel).

from [105]. The panel on the left show the initial displacement in $H^1(0, L)$ with zero initial velocity, located just left from the point mass. The panel on the right shows the solution at time $T = 10s$ at which the reflected and transmitted waves have formed, with the displacement of the reflected wave on the left of the point

mass still in $H^1(0, L)$, but with the displacement of the transmitted wave, shown to the right of the point mass, belonging to $H^2(0, L)$. For a reader with further interest in the area of simplified coupled problems we mention [90, 132, 143].

1.8 Conclusions

This chapter addresses an operator splitting approach to study multi-physics problems related to fluid-structure interaction. The methodology is based on the Lie splitting scheme, also known as the Marchuk-Yanenko scheme. The splitting discussed in this chapter deals successfully with the added mass effect which is known to be responsible for instabilities in loosely-coupled Dirichlet-Neumann schemes for FSI problems in which the density of the structure is comparable to that of the fluid. Particular attention was payed to a multi-physics FSI problem in which the structure is composed of multiple structural layers. Problems if this kind arise, for example, in modeling blood flow through human arteries which are composed of several layers, each with different mechanical characteristics and thickness. A benchmark problem was studied in which the structure consists of two layers: a think layer which is in contact with the fluid, and a thick layer which sits on top of the thin layer. The thin layer serves as a fluid-structure interface with mass. Both analytical (existence of a weak solution) as well as numerical results were studied for the underlying benchmark problem. In particular, it was shown that the proposed scheme converges to a weak solution to the full nonlinear fluid-multi-layered structure interaction problem. Two academic examples were considered to test the performance of the numerical scheme.

The analytical and numerical methods presented here apply with slight modifications to a larger class of problems. They include, for example, a study of FSI with one structural layer (thin [85, 19, 20], or thick [21]), FSI with poroelastic structures [23], FSI between a mechanical device called stent, arterial wall and fluid [123], and FSI involving a non-Newtonian fluid [92, 94, 95].

Bibliography

[1] R. A. Adams. *Sobolev spaces.* Academic Press [A subsidiary of Harcourt Brace Jovanovich, Publishers], New York-London, 1975. Pure and Applied Mathematics, Vol. 65.

[2] Å.R. Ahlgren, M. Cinthio, S. Steen, H.W. Persson, T. Sjöberg, and K. Lindström. Effects of adrenaline on longitudinal arterial wall movements and resulting intramural shear strain: a first report. *Clin. Physiol. Funct. Imaging,* **29** (2009), 353–359.

[3] R. L. Armentano, J.G. Barra, J. Levenson, A. Simon, R.H. Pichel. *Arterial wall mechanics in conscious dogs: assessment of viscous, inertial, and elastic moduli to characterize aortic wall behavior.* Circ. Res. 76 (1995), pp. 468–478.

[4] R. L. Armentano, J.L. Megnien, A. Simon, F. Bellenfant, J.G. Barra, J. Levenson. *Effects of hypertension on viscoelasticity of carotid and femoral arteries in humans.* Hypertension 26 (1995), pp. 48–54.

[5] M. Astorino, F. Chouly, and M.A. Fernández. An added-mass free semi-implicit coupling scheme for fluid-structure interaction. *Comptes Rendus Mathematique*, 347(1-2):99–104, 2009.

[6] M. Astorino, F. Chouly, and M.A. Fernández Varela. Robin based semi-implicit coupling in fluid-structure interaction: Stability analysis and numerics. *SIAM J. Sci. Comput.*, 31:4041–4065, 2009.

[7] F.P.T. Baaijens, A fictitious domain/mortar element method for fluid-structure interaction, *Int. J. Numer. Meth. Fluids*, 35 (2001), 743–761.

[8] S. Badia, A. Quaini, A. Quarteroni. Splitting methods based on algebraic factorization for fluid-structure interaction, *SIAM J. Sci. Comput.*, 30(4):1778-1805, 2008.

[9] S. Badia, F. Nobile, C. Vergara. Fluid-structure partitioned procedures based on Robin transmission conditions. *J. Comput. Phys.* 227:7027–7051, 2008.

[10] S. Badia, F.. Nobile, and C. Vergara. Robin-robin preconditioned Krylov methods for fluid-structure interaction problems. *Comput. Methods Appl. Mech. Eng.*, 198(33-36):2768–2784, 2009.

[11] R. D. Bauer, R. Busse, A. Shabert, Y. Summa, E. Wetterer. *Separate determination of the pulsatile elastic and viscous forces developed in the arterial wall in vivo.* Pflugers Arch. 380 (1979), pp. 221-226.

[12] V. Barbu, Z. Grujić, I. Lasiecka, and A. Tuffaha. Existence of the energy-level weak solutions for a nonlinear fluid-structure interaction model. In *Fluids and waves*, volume 440 of *Contemp. Math.*, pages 55–82. Amer. Math. Soc., Providence, RI, 2007.

[13] V. Barbu, Z. Grujić, I. Lasiecka, and A. Tuffaha. Smoothness of weak solutions to a nonlinear fluid-structure interaction model. *Indiana Univ. Math. J.*, 57(3):1173–1207, 2008.

[14] A.T. Barker and X.C. Cai. Scalable parallel methods for monolithic coupling in fluid-structure interaction with application to blood flow modeling, *Journal of Computational Physics*, 229(3):642–659, 2010.

[15] Y. Bazilevs, V.M. Calo, T.J.R. Hughes, Y. Zhang. Isogeometric fluid-structure interaction: theory algorithms and computations. *Comput. Mech.* 43:3-37, 2008.

[16] Y. Bazilevs, V.M. Calo, Y. Zhang, T.J.R. Hughes. Isogeometric fluid-structure interaction analysis with applications to arterial blood flow *Comput. Mech.* 38 (4-5): 310–322, 2006.

[17] H. Beirão da Veiga. On the existence of strong solutions to a coupled fluid-structure evolution problem. *J. Math. Fluid Mech.*, 6(1):21–52, 2004.

[18] M. Boulakia. Existence of weak solutions for the motion of an elastic structure in an incompressible viscous fluid. *C. R. Math. Acad. Sci. Paris*, 336(12):985–990, 2003.

[19] M. Bukač, S. Čanić, R. Glowinski, J. Tambača, and A. Quaini. Fluid-structure interaction in blood flow allowing non-zero longitudinal structure displacement. *Journal of Comp. Phys.* 235:515–541, 2013.

[20] M. Bukač and S. Čanić. Longitudinal displacement in viscoelastic arteries: a novel fluid-structure interaction computational model, and experimental validation. *Journal of Mathematical Biosciences and Engineering.* 10(2), pp. 258-388, 2013.

[21] M. Bukač, S. Čanić, R. Glowinski, B. Muha, A. Quaini. An Operator Splitting Scheme for Fluid-Structure Interaction Problems with Thick Structures. . The International Journal for Numerical Methods in Fluids. Under revision, 2013.

[22] M. Bukač, S. Čanić, B. Muha. The kinematically-coupled β-scheme for fluid-structure interaction problems with multi-layered structures. In preparation.

[23] Bukač, M., Zunino, P., Yotov, I. Explicit partitioning strategies for interaction of the fluid with a multilayered poroelastic structure: An operator-splitting approach. Submitted 2013.

[24] E. Burman and M. A. Fernández. Stabilization of explicit coupling in fluid-structure interaction involving fluid incompressibility. *Comput. Methods Appl. Mech. Eng.*, 198:766–784, 2009.

[25] S. Čanić, E.H. Kim. Mathematical Analysis of the Quasilinear Effects in a Hyperbolic Model of Blood Flow through Compliant Axisymmetric Vessels. *Mathematical Methods in Applied Sciences* 26 (14) (2003), 1161-1186.

[26] S. Canic, J. Tambaca, G. Guidoboni, A. Mikelic, C. J. Hartley, and D. Rosenstrauch. Modeling viscoelastic behavior of arterial walls and their interaction with pulsatile blood flow. *SIAM J. Appl. Math.*, 67(1):164–193, 2006.

[27] S. Canic, C.J. Hartley, D. Rosenstrauch, J. Tambaca, G. Guidoboni, A. Mikelic. Blood Flow in Compliant Arteries: An Effective Viscoelastic Reduced Model, Numerics and Experimental Validation. *Annals of Biomedical Engineering.* 34:575–592, 2006.

[28] S. vCanić and B. Muha. A nonlinear moving-boundary problem of parabolic-hyperbolic-hyperbolic type arising in fluid-multi-layered structure interaction problems. Submitted.

[29] S. Canic, B. Muha, M. Bukac. Stability of the kinematically coupled β-scheme for fluid-structure interaction problems in hemodynamics. arXiv:1205.6887v1. Submitted.

[30] P. Causin, J. Gerbeau, and F. Nobile. Added-mass effect in the design of partitioned algorithms for fluid-structure problems. *Comput. Methods Appl. Mech. Eng.*, 194(42-44):4506–4527, 2005.

[31] M. Cervera, R. Codina, M. Galindo, On the computational efficiency and implementation of block-iterative algorithms for nonlinear coupled problems, *Engrg. Comput.*, 13 (1996), 4–30.

[32] A. Chambolle, B. Desjardins, M. J. Esteban, and C. Grandmont. Existence of weak solutions for the unsteady interaction of a viscous fluid with an elastic plate. *J. Math. Fluid Mech.*, 7(3):368–404, 2005.

[33] C. H. A. Cheng, D. Coutand, and S. Shkoller. Navier-Stokes equations interacting with a nonlinear elastic biofluid shell. *SIAM J. Math. Anal.*, 39(3):742–800 (electronic), 2007.

[34] C. H. A. Cheng and S. Shkoller. The interaction of the 3D Navier-Stokes equations with a moving nonlinear Koiter elastic shell. *SIAM J. Math. Anal.*, 42(3):1094–1155, 2010.

[35] P. G. Ciarlet. A two-dimensional nonlinear shell model of Koiter type. *C.R. Acad. Sci. Paris. Ser I Math.* 331, 405-410 (2000)

[36] C. H. Ciarlet, D. Cautnad. An existence theorem for nonlinearly elastic "flexural" shells. *J. Elasticity* 50(3), 261-277 (1998)

[37] C.R. Ciarlet, A. Roquefort. Justification of a two-dimensional shell model of Koiter type. *C.R. Acad. Sci. Paris*, Ser I Math. 331(5), 411-416 (2000)

[38] P. G. CIARLET. *Mathematical elasticity. Vol. III. Theory of shells.* Studies in Mathematics and its Applications, 29. North-Holland Publishing Co., Amsterdam, 2000.

[39] P. G. CIARLET AND V. LODS. *Asymptotic analysis of linearly elastic shells. III. Justification of Koiter's shell equations.* Arch. Rational Mech. Anal. 136 (1996), pp. 191–200.

[40] P. G. CIARLET AND V. LODS. *Asymptotic analysis of linearly elastic shells. Generalized membrane shells.* J. Elasticity 43 (1996), pp. 147–188.

[41] M. Cinthio, A. Ahlgren, J. Bergkvist, T. Jansson, H.W. Persson, K. Lindstrom. Longitudinal movements and resulting shear strain of the arterial wall. *Am. J. Physiol. Heart Circ. Physiol.* 291(1): H394–H402 (2006).

[42] M. Cinthio, Ahlgren, A.R. Jansson, T. Eriksson, A. Persson, H.W. Lindstrom, K. Evaluation of an ultrasonic echo-tracking method for measurements of arterial wall movements in two dimensions. *IEEE Trans. Ultrason. Ferroelectr. Freq. Control*, 52(8):1300–1311, 2005.

[43] C. Conca, J. San Martín H., and M. Tucsnak. Motion of a rigid body in a viscous fluid. *C. R. Acad. Sci. Paris Sér. I Math.*, 328(6):473–478, 1999.

[44] G.H. Cottet,E. Maitre and T. Milcent. Eulerian Formulation and Level Set Models for Incompressible Fluid-Structure Interaction. *Mathematical Modelling and Numerical Analysis.* 42(3): 471-492, 2008.

[45] D. Coutand and S. Shkoller. Motion of an elastic solid inside an incompressible viscous fluid. *Arch. Ration. Mech. Anal.*, 176(1):25–102, 2005.

[46] D. Coutand and S. Shkoller. The interaction between quasilinear elastodynamics and the Navier-Stokes equations. *Arch. Ration. Mech. Anal.*, 179(3):303–352, 2006.

[47] H. DEMIRAY *Small but Finite Amplitude Waves in a Prestressed Viscoelastic Thin Tube Filled with an Inviscid Fluid* Int. J. Engng Sci., 35(4) (1997), pp. 353–363.

[48] P. Cumsille and T. Takahashi. Wellposedness for the system modelling the motion of a rigid body of arbitrary form in an incompressible viscous fluid. *Czechoslovak Math. J.*, 58(133)(4):961–992, 2008.

[49] S. Deparis, M.A. Fernández, L. Formaggia, Acceleration of a fixed point algorithm for a fluid-structure interaction using transpiration condition, *Math. Model. Numer. Anal.*, 37 (2003), 601–616.

[50] S. Deparis, M. Discacciati, G. Fourestey, and A. Quarteroni, Fluid-structure algorithms based on Steklov-Poincaré operators, *Comput. Methods Appl. Mech. Engrg.*, 195 (2006) 5797–5812.

[51] B. Desjardins and M. J. Esteban. Existence of weak solutions for the motion of rigid bodies in a viscous fluid. *Arch. Ration. Mech. Anal.*, 146(1):59–71, 1999.

[52] B. Desjardins, M. J. Esteban, C. Grandmont, and P. Le Tallec. Weak solutions for a fluid-elastic structure interaction model. *Rev. Mat. Complut.*, 14(2):523–538, 2001.

[53] P. DESTUYNDER, *A classification of thin shell theories*, Acta Applicandae Mathematicae, 4,. 1985, pp. 15-63.

[54] J. Donea, Arbitrary Lagrangian-Eulerian finite element methods, in: Computational methods for transient analysis, North-Holland, Amsterdam,1983.

[55] Q. Du, M. D. Gunzburger, L. S. Hou, and J. Lee. Analysis of a linear fluid-structure interaction problem. *Discrete Contin. Dyn. Syst.*, 9(3):633–650, 2003.

[56] Q. Du, M.D. Gunzburger, L.S. Hou, J. Lee. Semidiscrete finite element approximations of a linear fluid-structure interaction problem. *SIAM J. Numer. Anal* 42(1): 1–29 (2004)

[57] Q. Du, M.D. Gunzburger, L.S. Hou, J. Lee. Analysis of Linear Fluid-Structure Interaction Problem. *Disc. Cont. Dyn. Sys.* 9: 633–650 (2003)

[58] A. C . ERINGEN. *Mechanics of continua.* Wiley New York 1967.

[59] H. Fang, Z. Wang, Z. Lin, M. Liu, Lattice Boltzmann method for simulating the viscous flow in large distensible blood vessels, *Phys. Rev. E*, 65 (2002), 051925.

[60] L.J. Fauci, R. Dillon, Biofluidmechanics of reproduction, *Ann. Rev. Fluid Mech.*, 38 (2006), 371–394.

[61] E. Feireisl. On the motion of rigid bodies in a viscous compressible fluid. *Arch. Ration. Mech. Anal.*, 167(4):281–308, 2003.

[62] Z.-G. Feng, E.E. Michaelides, The immersed boundary-lattice Boltzmann method for solving fluid-particles interaction problem, *J. Comp. Phys.*, 195 (2004), 602–628.

[63] M. A. Fernández. Incremental displacement-correction schemes for incompressible fluid-structure interaction : stability and convergence analysis. Numer. Math. 123 (1):21-65, 2013.

[64] M. A. Fernández and M. Moubachir. A Newton method using exact Jacobians for solving fluid-structure coupling. *Computers and Structures*, 83(2-3):127–142, 2005.

[65] M.A. Fernández, J.F. Gerbeau, and C. Grandmont. A projection algorithm for fluid-structure interaction problems with strong added-mass effect. *Comptes Rendus Mathematique*, 342(4):279–284, 2006.

[66] M. A. Fernández. Incremental displacement-correction schemes for the explicit coupling of a thin structure with an incompressible fluid. *C. R. Math. Acad. Sci. Paris*, 349(7-8):473–477, 2011.

[67] M. A. Fernández and J. Mullaert. Displacement-velocity correction schemes for incompressible fluid-structure interaction. *C. R. Math. Acad. Sci. Paris*, 349(17-18):1011–1015, 2011.

[68] M. A. Fernández. Incremental displacement-correction schemes for incompressible fluid-structure interaction: stability and convergence analysis. *Numerische Mathematik*, 2012.

[69] C. Figueroa, I. Vignon-Clementel, K.E. Jansen, T. Hughes, C. Taylor. A coupled momentum method for modeling blood flow in three-dimensional deformable arteries. *Comput. Methods Appl. Mech. Eng.* 195: 5685–5706, 2006.

[70] A.L. Fogelson, R.D. Guy, Platelet-wall interactions in continuum models of platelet thrombosis: Formulation and numerical solution, *Math. Med. Biol.*, 21 (2004), 293–334.

[71] L. Formaggia, J.F. Gerbeau, F. Nobile, A. Quarteroni. On the coupling of 3D and 1D Navier-Stokes equations for flow problems in compliant vessels. *Comput. Methods Appl. Mech. Eng.*, 191 (6-7):561–582,2001.

[72] Y. C. Fung, "Biomechanics: Circulation," Second Edition. Springer-Verlag, New York, 1984.

[73] Y. C. Fung, "Biomechanics:Mechanical Properties of Living Tissues," Second Edition. Springer-Verlag, New York, 1993.

[74] G. P. Galdi. Mathematical problems in classical and non-Newtonian fluid mechanics. In *Hemodynamical flows*, volume 37 of *Oberwolfach Semin.*, pages 121–273. Birkhäuser, Basel, 2008.

[75] G. P. Galdi. *An introduction to the mathematical theory of the Navier-Stokes equations. Vol. I*, volume 38 of *Springer Tracts in Natural Philosophy*. Springer-Verlag, New York, 1994. Linearized steady problems.

[76] J.F. Gerbeau, M. Vidrascu, A quasi-Newton algorithm based on a reduced model for fluid-structure interactions problems in blood flows, *Math. Model. Numer. Anal.*, 37 (2003), 631–648.

[77] R. Glowinski. *Finite element methods for incompressible viscous flow, in: P.G.Ciarlet, J.-L.Lions (Eds), Handbook of numerical analysis*, volume 9. North-Holland, Amsterdam, 2003.

[78] C. Grandmont. Existence of weak solutions for the unsteady interaction of a viscous fluid with an elastic plate. *SIAM J. Math. Anal.*, 40(2):716–737, 2008.

[79] B.E. Griffith. On the volume conservation of the immersed boundary method. *Commun Comput Phys.* 12: 401-432, 2012.

[80] B.E. Griffith. Immersed boundary model of aortic heart valve dynamics with physiological driving and loading conditions. *Int J Numer Meth Biomed Eng.* 28: 317-345, 2012.

[81] B.E. Griffith, X. Luo, D.M. McQueen, and C.S. Peskin. Simulating the fluid dynamics of natural and prosthetic heart valves using the immersed boundary method. *Int J Appl Mech.* 1: 137-177, 2009.

[82] B.E. Griffith, R.D. Hornung, D.M. McQueen, and C.S. Peskin. An adaptive, formally second order accurate version of the immersed boundary method. *J Comput Phys.* 223: 10-49, 2007.

[83] B.E. Griffith and X. Luo. Hybrid finite difference/finite element version of the immersed boundary method. Submitted.

[84] G. Guidoboni, M. Guidorzi, and M. Padula. Continuous dependence on initial data in fluid-structure motions. *J. Math. Fluid Mech.*, 14(1):1–32, 2012.

[85] G. Guidoboni, R. Glowinski, N. Cavallini, and S. Čanić. Stable loosely-coupled-type algorithm for fluid-structure interaction in blood flow. *J. Comput. Phys.*, 228(18):6916–6937, 2009.

[86] G. Guidoboni, N. Cavallini, R. Glowinski, S. Čanić and S. Lapin. A kinematically coupled time-splitting scheme for fluid-structure interaction in blood flow. *Applied Mathematics Letters* 22 (5), 684–688, 2009.

[87] J. D. HAMPHREY, *Mechanics of the Arterial Wall: Review and Directions*, Critical Reviews in Biomedical Engineering Vol. 23 (1&2) 1995.

[88] P. Hansbo. Nitsche's method for interface problems in computational mechanics. *GAMM-Mitt.*, 28(2):183–206, 2005.

[89] S. Hansen and E. Zuazua. Exact controllability and stabilization of a vibrating string with an interior point mass. *SIAM J. Control Optim.*, 33(5):1357–1391, 1995.

[90] H. Koch and E. Zuazua. A hybrid system of PDE's arising in multi-structure interaction: coupling of wave equations in n and $n - 1$ space dimensions. In *Recent trends in partial differential equations*, volume 409 of *Contemp. Math.*, pages 55–77. Amer. Math. Soc., Providence, RI, 2006.

[91] M. Heil. An efficient solver for the fully coupled solution of large-displacement fluid-structure interaction problems. *Comput. Methods Appl. Mech. Eng.* 193(1-2): 1-23, 2004.

[92] A. Hundertmark-Zaušková, M. Lukáčová-Medvidová, and Š. Nečasová. On the existence of weak solution to the coupled fluid-structure interaction problem for non-newtonian shear-dependent fluid. Submitted, 2013.

[93] T.J.R. Hughes, W.K Liu, T.K. Zimmermann. Lagrangian-Eulerian finite element formulation for incompressible viscous flows. *Comput. Methods Appl. Mech. Eng.* 29(3): 329-349, 1981.

[94] A. Hundertmark-Zauskova, M. Lukacova-Medvidova, G. Rusnakova. Kinematic splitting algorithm for fluid-structure interaction in hemodynamics. Computer Methods in Appl. Mech. Engi., To appear., 2013.

[95] A. Hundertmark-Zauskova, M. Lukacova-Medvidova, G. Rusnakova. Fluid-structure interaction for shear-dependent non-Newtonian fluids. Topics in mathematical modeling and analysis. Necas Center for Mathematical Modeling. Lecture notes, Volume 7, pp. 109-158, 2012.

[96] W. T. KOITER, *A consistent first approximation in the general theory of thin elastic shells. Part 1: Foundations and linear theory.* Technological University, Delft, August 5. 1959.

[97] W. T. KOITER. *On the foundations of the linear theory of thin elastic shells. I, II.* Nederl. Akad. Wetensch. Proc. Ser. B 73 (1970), pp. 169-182.

[98] M. Krafczyk, M. Cerrolaza, M. Schulz, E. Rank, Analysis of 3D transient blood flow passing through an artificial aortic valve by Lattice-Boltzmann methods, *J Biomech.*, 31 (1998), 453–462.

[99] M. Krafczyk, J. Tolke, E. Rank, M. Schulz, Two-dimensional simulation of fluid-structure interaction using Lattice-Boltzmann methods, *Comput. Struct.*, 79 (2001), 2031–2037.

[100] I. Kukavica, A. Tuffaha, and M. Ziane. Strong solutions for a fluid structure interaction system. *Adv. Differential Equations*, 15(3-4):231–254, 2010.

[101] I. Kukavica and A. Tuffaha. Solutions to a fluid-structure interaction free boundary problem. *DCDS-A*, 32(4):1355–1389, 2012.

[102] I. Kukavica and A. Tuffaha. Well-posedness for the compressible Navier-Stokes-Lamé system with a free interface. *Nonlinearity*, 25(11):3111–3137, 2012.

[103] D. Lengeler and M. Ružička. Global weak solutions for an incompressible newtonian fluid interacting with a linearly elastic Koiter shell. arXiv:1207.3696v1, 2012.

[104] D. Lengeler Global weak solutions for an incompressible, generalized Newtonian fluid interacting with a linearly elastic Koiter shell arXiv:1212.3435, 2012.

[105] V. Lescarret and E. Zuazua. Numerical approximation schemes for multi-dimensional wave equations in asymmetric spaces. Preprint. http://www.bcamath.org/documentos_public/archivos/publicaciones/assym_discret_rev.pdf

[106] R. van Loon, P. Anderson, J. de Hart, F. Baaijens, A combined fictitious domain/adaptive meshing method for fluid-structure interaction in heart valves, *Int. J. Num. Meth. Fluids*, 46 (2004), 533–544.

[107] P. Le Tallec, J. Mouro. Fluid structure interaction with large structural displacements. *Comput. Methods Appl. Mech. Eng.* 190(24-25):3039-3067, 2001.

[108] A. Leuprecht, K. Perktold, M. Prosi, T. Berk, W. Trubel, H. Schima. Numerical study of hemodynamics and wall mechanics in distal end-to-side anastomoses of bypass grafts. *J. Biomech.* 35(2):225-236, 2002.

[109] J. Lequeurre. Existence of strong solutions to a fluid-structure system. *SIAM J. Math. Anal.*, 43(1):389–410, 2011.

[110] J. Lequeurre. Existence of strong solutions for a system coupling the Navier-Stokes equations and a damped wave equation. *Journal of Mathematical Fluid Mechanics*, pages 1–23, 2012.

[111] S. Lim, C.S. Peskin, Simulations of the whirling instability by the immersed boundary method, *SIAM J. Sci. Comput.*, 25 (2004), 2066–2083.

[112] J.-L. Lions and E. Magenes. *Non-homogeneous boundary value problems and applications. Vol. I.* Springer-Verlag, New York, 1972. Translated from the French by P. Kenneth, Die Grundlehren der mathematischen Wissenschaften, Band 181.

[113] P. Luchini, M. Lupo and A. Pozzi, *Unsteady Stokes flow in a distensible pipe*, Z. angew. Math. Mech. 71 (1991), pp. 367–378.

[114] X. Ma, G.C. Lee and S.G. Lu. *Numerical Simulation for the ropagation of Nonlinear Pulsatile Waves in Arteries,* ASME J. Biomech. Eng. **114** (1992), pp. 490–496.

[115] H. Matthies, J. Steindorf, Numerical efficiency of different partitioned methods for fluid-structure interaction, *Z. Angew. Math. Mech.*, 2 (2000), 557–558.

[116] C. Michler, S.J. Hulshoff, E.H. van Brummelen, R. de Borst A monolithic approach to fluid-structure interaction *Computers and Fluids* 33(5-6), 839-848, 2004.

[117] L.A. Miller, C.S. Peskin, A computational fluid dynamics study of 'clap and fling' in thesmallest insects, *J. Exp. Biol.*, 208 (2005), 195–212.

[118] C.M. Murea and S. Sy. A fast method for solving fluid-structure interaction problems numerically. *Int. J. Numer. Meth. Fl.*, 60(10):1149–1172, 2009.

[119] B. Muha and S. Čanić. Existence of a Weak Solution to a Nonlinear Fluid–Structure Interaction Problem Modeling the Flow of an Incompressible, Viscous Fluid in a Cylinder with Deformable Walls. *Arch. Ration. Mech. Anal.*, 207(3):919–968, 2013.

[120] B. Muha. A note on the trace theorem for domains which are locally subgraph of a Hölder continuous function. Networks and Heterogeneous Media, Accepted 2013.

[121] B. Muha and S. Čanić. Existence of a Weak Solution to a Nonlinear Fluid Structure Interaction Problem in a 3D Cylinder. Journal of Differential Equations. In print 2013. arXiv:1305.5310

[122] B. Muha and S. Čanić. Existence of a solution to a fluid-multi-layered-structure interaction problem. Submitted.

[123] B. Muha and S. Čanić. Existence of a solution to a fluid-stent-artery interaction problem. In preparation.

[124] B. Muha and S. Čanić. Regularization by point mass coupling the 1D heat equation with the 1D wave equation. In preparation.

[125] F. Nobile, C. Vergara. An effective fluid-structure interaction formulation for vascular dynamics by generalized Robin conditions. *SIAM J. Sci. Comput.* 30 (2):731–763, 2008.

[126] F. Nobile. Numerical approximation of fluid-structure interaction problems with application to haemodynamics. *PhD Thesis, EPFL Switzerland, 2001.*

[127] C. Peskin. Numerical analysis of blood flow in the heart. *J. Comput. Phys.* 25: 220–252, 1977.

[128] C. Peskin, D.M. McQueen. A three-dimensional computational method for blood flow in the heart I. Immersed elastic fibers in a viscous incompressible fluid. *J. Comput. Phys.* 81(2): 372–405, 1989.

[129] M. Persson, R. Ahlgren, T. Jansson, A. Eriksson, H.W. Persson, K Lindstrom. A new non-invasive ultrasonic method for simultaneous measurements of longitudinal and radial arterial wall movements: first in vivo trial. *Clin. Physiol. Funct. Imaging* 23(5):247–251, 2003.

[130] G. PONTRELLI. *A mathematical model of flow through a viscoelastic tube.* Med. Biol. Eng. Comput, 2002.

[131] A. Quaini and A Quarteroni. A semi-implicit approach for fluid-structure interaction based on an algebraic fractional step method. *Math. Models Methods Appl. Sci.*, 17(6):957–985, 2007.

[132] J. Rauch, X. Zhang, and E. Zuazua. Polynomial decay for a hyperbolic-parabolic coupled system. *J. Math. Pures Appl. (9)*, 84(4):407–470, 2005.

[133] J. A. San Martín, V. Starovoitov, and M. Tucsnak. Global weak solutions for the two-dimensional motion of several rigid bodies in an incompressible viscous fluid. *Arch. Ration. Mech. Anal.*, 161(2):113–147, 2002.

[134] J.Simon. Compact sets in the space $L^p(0, T; B)$. *Ann. Mat. Pura Appl. (4)*, 146:65–96, 1987.

[135] S. Svedlund, L.M. Gan. Longitudinal wall motion of the common carotid artery can be assessed by velocity vector imaging. *Clin. Physiol. Funct. Imaging* 31(1):32–38, 2011.

[136] J. Tambača. Notes on the derivation of the cylindrical Koiter shell. Private communication 2004.

[137] R. Temam. Sur la résolution exacte et approchée d'un problème hyperbolique non linéaire de T. Carleman. *Arch. Rational Mech. Anal.*, 35:351–362, 1969.

[138] R. Temam. *Navier-Stokes equations. Theory and numerical analysis.* North-Holland Publishing Co., Amsterdam, 1977. Studies in Mathematics and its Applications, Vol. 2.

[139] A. Quaini. Algorithms for fluid-structure interaction problems arising in hemodynamics. *PhD Thesis, EPFL Switzerland, 2009.*

[140] A. Quarteroni, M. Tuveri and A. Veneziani. Computational vascular fluid dynamics: problems, models and methods. Survey article, *Comput. Visual. Sci.* **2** (2000), 163-197.

[141] I. Velčić. Nonlinear weakly curved rod by Γ-convergence. *J. Elasticity*, 108(2):125–150, 2012.

[142] S.Z. Zhao, X.Y. Xu, M.W. Collins, The numerical analysis of fluid-solid interactions for blood flow in arterial structures Part 2: development of coupled fluid-solid algorithms, *Proc. Instn. Mech. Engrs. Part H*, 212 (1998), 241–252.

[143] X. Zhang and E. Zuazua. Long-time behavior of a coupled heat-wave system arising in fluid-structure interaction. *Arch. Ration. Mech. Anal.*, 184(1):49–120, 2007.

Acknowledgment